OPTIMIZING NEUROMODULATION FOR TEMPORAL LOBE EPILEPSY TREATMENT BASED ON A SURROGATE NEURAL STATE MODEL

A Dissertation
Presented to
The Academic Faculty

by

Sang-Eon Park

In Partial Fulfillment
of the Requirements for the Degree
Doctor of Philosophy in the
Bioengineering program

Georgia Institute of Technology
December 2019

OPTIMIZING NEUROMODULATION FOR TEMPORAL LOBE EPILEPSY TREATMENT BASED ON A SURROGATE NEURAL STATE MODEL

Approved by:

Dr. Robert E. Gross, Advisor
Department of Neurosurgery
Emory University
School of Biomedical Engineering
Georgia Institute of Technology

Dr. John T. Gale
Department of Neurosurgery
Emory University

Dr. Babak Mahmoudi
Department of Biomedical Informatics
Emory University
School of Biomedical Engineering
Georgia Institute of Technology

Dr. Joseph R. Manns
Department of Psychology
Emory University

Dr. Christopher J. Rozell
School of Electrical Engineering
Georgia Institute of Technology

Date Approved: October 25, 2019

To my family and friends

ACKNOWLEDGEMENTS

I am forever indebted to my mentor, Dr. Robert Gross. For welcoming me into the lab; for providing the opportunities for which I could never have dreamed; for giving me the freedom and independence to make many, many mistakes; for supporting my ideas and project; and for the advice that has made me a better person; I thank you.

I also must express my great appreciation for my committee members, Dr. Chris Rozell, Dr. Joe Manns, Dr. John Gale, and Dr.Babak Mahmoudi, who have watched over and guided me from the beginning, and whose advice, collaborations, and support have greatly improved the quality of this work.

I am immensely grateful to my wonderful lab mates. First is Mark Connolly who shares most of my research experience from the beginning to the end. I appreciate all the training, encouraging and advices that you gave to me. Claire-Anne Gutekunst and Alejandra Fernandez always taught me something and contributed to this work. I also appreciate Ken Berglund, Ioannis Exarchos, Angle Santiago-Lopez, Matt Stern, and Thomas Shiu for always teaching something or helping me physically and mentally.

I owe a great debt and am immensely thankful for the mentorship, training, and friendship of Candace Fleischer, who started me on this wonderful path. I would like to thank the students, faculty, and administrators of the Georgia Tech Bioengineering program who have been wonderfully supportive in both the best and worst times. I'd like to especially thank Kiseung Choi, for his scientific insights and immeasurable friendship.

I am forever grateful to my tennis team TM-Hudlow. They have kept me healthy and sane, taught me immeasurably about leadership, teamwork, strength, and love. My greatest friends, GH, NR, JH, YK, SH, SJ – all the best wishes to you and thanks for everything you have done for me.

Finally, to my Mom, Dad, and Sister: Thank you for always being there for me, for your insight and perspective, and for your steadfast belief. I love you all very, very much. I am better than I was, and in large part that is because of all of you.

This work was supported by funding from Kwanjeong Educational Foundation, U.S. National Institutes of Health grants NS085568, NS079268, NS079757, NSF CBET-1512826, and the Mirowski Family Foundation.

TABLE OF CONTENTS

LIST OF TABLES

LIST OF FIGURES

LIST OF SYMBOLS AND ABBREVIATIONS

AAV	adeno-associated viral
ANT	anterior nucleus of thalamus
AUC	averaged area under curve
BaO	Bayesian optimization
CamKIIα	the letter D
ChAT	cholinergic choline acetyltransferase
ChR2	channelrhodopsin-2
CNN	convolutional neural network
Coh	coherence
CV	cross validation
DBS	deep brain stimulation
EF1a	elongation factor 1α
Eff	effective
EGM	Epileptogenesis model
EI	Expected improvement
eNpHR3.0	enhanced halorhodopsin chloride pump 3.0
ENR	elastic net regularization
ETM	expected theta modulation
EYFP	enhanced yellow fluorescent protein
GP	Gaussian process
HFO	high frequency oscillation
hSyn	human synapsin

IIS	Inter-ictal spike
LARS	least angle regression
LFP	local field potential
LnR	linear regression
LR	logistic regression
mCherry	monomeric Cherry
MEA	multielectrode arrays
MRE	medication-resistant epilepsy
MS	medial septum
MSE	mean squared error
MTLE	medication-resistant epilepsy
Neff	ineffective
OLS	ordinary least square
PC	principal component
Phase	phase coherence
PiSM	pre-ictal state model
PSD	power spectral density
PU	positive and unlabeled
RNS	responsive neurostimulation
ROC	receiver operation characteristic
SDBaO	state-dependent Bayesian optimization
SMSE	standardized mean squared error
Std	standard deviation
SVM	support vector machine
TeNT	tetanus toxin

TLM	theta power linear model
UCB	upper confidence bound
VNS	vagus nerve stimulation

SUMMARY

Temporal lobe epilepsy is the most prevalent form of medication-resistant epilepsy, and current electrical stimulation therapy has not been able to accomplish the goal of seizure-freedom. This underscores the need for a new target and a different approach with more effective neuromodulation for epilepsy treatment. The projections from the medial septum (MS) and its regulatory role on the hippocampus make it an attractive neuromodulation target. Optogenetics enables selective excitation or inhibition of individual genetically-defined neuronal subpopulations, and thus provides a chance to find a better target among neuronal subpopulations for inducing a greater therapeutic effect. I have exhaustively explored the effect of exciting or inhibiting different neuronal subpopulations in the normal rat medial septum by using optogenetic stimulation. As a result, MS optogenetic stimulation using hSynapsin promoter in combination with Channelrhodopsin-2 was well suited for modulating electrophysiological activity of the hippocampus.

The conventional approach for preclinical studies requires a large amount of time and resources to find effective stimulation parameters and often fails due to the inter-subject variability in stimulation effect. As an alternative, I presented a novel data-driven approach which can optimize the neuromodulation more effectively and efficiently by investigating the stimulation effect on the surrogate neural state model. For the new approach, I implemented and demonstrated a variety of machine learning techniques to explore the stimulation effect, to describe the pathological neural states and to optimize the stimulation parameters. Specifically, first, I built a data-driven neural state model to

estimate a seizure susceptibility based on electrophysiological recordings. The output of the model played a surrogate role by providing a metric which was regulated via the MS optogenetic stimulation. Second, I further increased the effectiveness of the stimulation by implementing *in vivo* Bayesian optimization which quickly finds the subject-specific optimal stimulation parameters. Finally, I tested whether modulating the surrogate neural state model affected the symptom of epilepsy (i.e. seizure). The treatment efficacy of the data-driven surrogate approach was compared to the stimulation with an empirically selected parameter set. The stimulation parameters to maximize the hippocampal theta (4-10Hz) power, which was a surrogate of the epileptic symptom, was more effective than the empirically selected parameter (7Hz) for the seizure suppression.

CHAPTER 1. INTRODUCTION

1.1 Epilepsy and deep brain stimulation

There is a great need for therapies for epilepsy that lead to high rates of patients becoming seizure-free. Epilepsy affects 1% of the world's population, accounting for a large amount of disability and socioeconomic burden [1]. Decades of targeted drug discovery have improved side effects but have not changed the fact that 30% - or >1 million Americans – continue to suffer from seizures despite optimized medication regimes. For some patients with medication-resistant epilepsy (MRE), especially those with involvement of the medial temporal lobe epilepsy (MTLE), surgical resection may be an effective treatment - leading to ~75% of patients becoming seizure free[2]. Unfortunately, risk of neurological deficit, inability to localize the seizures, and/or multifocal seizure onsets excludes many patients from surgical consideration. For these patients, electrical brain stimulation may provide an effective surgical alternative. There are three types of neurostimulation available at this time. The first approved neurostimulation technique was vagus nerve stimulation (VNS), which stimulates the cervical vagus nerve projecting modulatory effects into the brain. VNS has been shown to decrease seizures in several randomized clinical trials (RCTs) by 16-22% (median seizure reduction), increasing to 40-44% in 3-year open label studies[3]. The second approved technique is responsive neurostimulation (RNS, Neuropace, Mountainview, CA), which decreased seizures by median 37.9%[4]. The third neurostimulation technique is deep brain stimulation (DBS) of the anterior nucleus of thalamus (ANT) which demonstrated 40.4% median reduction in seizure frequency after 3 months vs. 14.5% in sham-stimulation controls, increasing to

57% at 3 years in open-label extension[5]. However, only few (VNS) and 0 of 247 (RNS) patients were seizure-free over the entire 6-year follow-up period. It was also reported that only 5.5% (6/109) had a seizure free interval of at least 2 continuous years during the trial with ANT-DBS. While MRE patients and their clinicians are very grateful for the availability of these treatment alternatives with fewer adverse effects, no such modality has yet to achieve the goal of complete seizure freedom.

1.2 Mesial temporal lobe epilepsy

We focused our efforts on mesial temporal lobe (hippocampal onset) epilepsy (MTLE), for three reasons: 1) MTLE is the most common cause of medication resistant epilepsy[6]. While it is true that there exists effective surgical treatments for MTLE (e.g. temporal lobectomy[2] or stereotactic ablative procedures[7,8]), many patients are not candidates for destructive surgery due to risks to episodic memory[9], or due to bilateral onsets. MTLE remains, therefore, a major target population for novel, advanced treatments. 2) We understand the network involving the limbic structures much better than other brain regions[10], and, as will become clear, we are taking a *network or circuit approach* to advanced therapy. 3) The results from advances in treating limbic epilepsy will likely be transferrable to neocortical epilepsy, as the results in the neurostimulation trials were similar in those patients with MTLE and those with extra-MTLE[4,5].

1.3 Optogenetic modulation of septo-hippocampal pathway

Medial septum (MS) provides an attractive target to modulate activities of a larger hippocampal volume. Successful amygdalohippocampectomy involves resecting a large volume of hippocampus to remove the epileptic foci[11]. However, the volume of neural

tissue modulated by electrical stimulation is much smaller than this resected volume[12]. This may be one reason that direct hippocampal electrical stimulation is insufficient to completely control seizures. Stimulation of an upstream target which projects to a large hippocampal volume is an alternative rational approach. MS in the basal forebrain is highly connected to the hippocampus via the fimbria/fornix, thus providing a potential target for neuromodulation of hippocampal activity[13].

Electrical stimulation is non-specific, affecting all neurons within the volume of tissue activated while inducing both excitatory[14–16] and inhibitory[17,18] effects. Optogenetics enables selective excitation or inhibition of individual genetically-defined neuronal subpopulations[19–22], and thus provides a chance to find a better target among neuronal subpopulations for inducing a greater therapeutic effect. In a few studies, MS optogenetic stimulation successfully modulated hippocampal activity as well as induced behavioral change in rodents. Excitation and inhibition of MS GABAergic neurons affected hippocampal theta oscillation (type 2 theta) in anesthetized mice, and led to increased and decreased object exploration, respectively, in awake animals[23]. Excitation of MS glutamatergic neurons had a stimulation frequency dependent effect on the peak frequency of the theta oscillation, and increased locomotion in awake and behaving mice[24]. In another study, excitation of cholinergic neurons slightly suppressed the theta power in freely behaving mice while enhancing it under anesthesia[25]. However, a deeper exploration of the effect of MS optogenetic stimulation is required as previous studies focused on a specific neural feature (e.g. theta power) and a stimulation parameter which was empirically selected. Especially, a comparison of different target neuronal subpopulations combined

with various stimulation parameters is required to better understand the septo-hippocampal modulation and to induce a desired hippocampal neural activity.

1.4 Limitation of conventional approach for preclinical studies

The conventional approach for preclinical studies for epilepsy treatment has a few disadvantages. First, arbitrarily selected stimulation parameters may cause ineffective treatment[26–29]. This leads to the second disadvantage, namely that a tremendous amount of resources and time is required to find the right parameter. Third, variability of the stimulation effect exists between subjects due to a variation in inherent neural structures and the surgical implants, and even within subjects due to non-stationarity of the stimulated brain's neural state. Therefore, the successful neuromodulation treatment in one subject does not guarantee another successful one in the other subjects; and subject's response to stimulation can and does vary from time to time.

1.5 A novel data-driven approach

We established a novel data-driven approach using surrogate neural features to alleviate the disadvantages listed above. The key components of this method are *surrogate neural features* and *intelligent parameter search*. First, surrogate neural features allow reductions of time and resources required for evaluating the effectiveness of stimulation parameters, as observing an immediate response in neural features induced by the stimulation is possible. Second, the intelligent parameter search quickly provides the subject- and state-specific optimal parameter sets even in a vast parameter space, and thus effectively addresses the issue of the variability between and within subjects.

- ***Surrogate neural features*: <u>What</u> do we modulate?**

We modulate epileptic hippocampal neural features as a surrogate of the pathophysiological feature (seizure). Investigating neural features offers a few advantages: 1) a rapid turnaround to evaluate the stimulation effect, 2) early stage disease detection (epileptogenesis), 3) a high generalizability as it provides more objective criteria, 4) the possibility for prediction of seizures, and 5) a potential to provide insights into underlying mechanisms of the disease. Theta power[13,30,31] and high frequency oscillations (HFOs)[32,33] are examples of hippocampal neural features well known for their relationship to epilepsy. Regardless of decades of research, however, the activity of these neural features has not been fully characterized. In addition, a relationship between different neural features has not been well explored and we do not know if there exist other neural features which are correlated with the pathophysiological feature (seizure). In this project: first, we found neural features related to seizures from the hippocampal local field potential (LFP). These neural features show how the pathology manifests in neural activity. Second, we built a model which provides an output to describe a pathological neural state by using the hippocampal LFP. This model translates the activity of epileptic neural features into the pathological neural state, so the output of the model plays the role of the surrogate of the epileptic symptom, as well as provide a metric (i.e. objective function) which can be regulated through MS optogenetic stimulation. With this data-driven approach, therefore, we aim to tune the malfunctioning brain region by adjusting its electrophysical activity. This approach, which provides a guide to find an effective stimulation method, is valuable especially given that the mechanism of epilepsy is not clearly elucidated.

- ***Intelligent parameter search*: <u>How</u> do we modulate?**

The selection of parameters is of obvious critical importance for neuromodulation as many studies have shown that the modulation of neural features and behavioral change are highly parameter dependent[29]. However, parameter selection has been done empirically and even sometimes arbitrarily in many of the preclinical studies and clinical trials[26–28]. Applying stimulation with the optimal parameters can improve the effectiveness of neural feature modulation, but the optimal stimulation parameters are subject-specific due to a variability in the stimulation effect between subjects. Exhaustive parameter search methods such as a grid search or a random search require a tremendous amount of resource and time which also increases the chance of inducing side effects. Therefore, the exhaustive search methods are especially not suitable for translational applications which usually demand a fast and safe algorithm. In this project, we demonstrated an intelligent parameter search algorithm to find the optimal parameters for neural feature modulation. We have demonstrated that Bayesian optimization, one of the black-box optimization methods, is suitable for finding the optimal parameters for neuromodulation. The optimal stimulation parameter was found quickly by applying the Bayesian optimization toolbox, and we were able to more effectively regulate the neural features toward desirable.

1.6 Thesis organization

Chapter 2: Characterization of the effect of MS optogenetic stimulation in the hippocampal rhythms. Machine learning techniques were applied to explore how activating or inhibiting multiple MS neuronal subpopulations using different stimulation parameters affects hippocampal activities. Methods and results of analyses for finding effective stimulation parameters, predominantly modulated neural features and optimizable stimulation parameters are presented.

Chapter 3: Development of a tool for *in vivo* neuromodulation parameter optimization. *In vivo* Bayesian optimization was implemented to find the optimal MS stimulation parameters to effectively modulate hippocampal neural features. It was demonstrated that the optimal stimulation parameters found by the optimization increased hippocampal theta and gamma power more effectively than the other stimulation parameters.

Chapter 4: Development of data-driven surrogate models by characterizing epileptic neural features from the hippocampal LFP. A regression and a classifier models were built to characterize the neural features during two epileptic neural state transitions: (1) a long-term change during epileptogenesis and (2) a short-term change during the pre-ictal period. The output of the models which estimates the seizure susceptibility can play a role of the surrogates for evaluating the effectiveness of stimulation parameters.

Chapter 5: Modification of *in vivo* Bayesian optimization for effectively modulating epileptic neural states with MS optogenetic stimulation. The modified Bayesian optimization was applied to find the optimal stimulation parameters to effectively modulate the hippocampal theta power and the output of the surrogate model introduced in Chapter 4.

Chapter 6: Identification of a causal link between epileptic neural feature modulation and seizure characteristics. The treatment efficacy of stimulation parameters found by the data-driven surrogate approach was compared to an empirically selected stimulation parameter set. The optimal stimulation parameters for modulating the surrogate neural features were found as described in Chapter 5.

CHAPTER 2. CHARACTERIZATION OF THE EFFECT OF MEDIAL SEPTUM OPTOGENETIC MODULATION IN THE HIPPOCAMPAL RHYTHMS

2.1 Introduction

Given its position within the septo-hipocampal pathway the medial septum (MS) has the potential to modulate a large volume of the hippocampus. Thus, understanding the functional connectivity of the neurons of the septo-hippocampal pathway can inform future stimulation paradigms, similar to how hippocampal deep brain stimulation (DBS) is applied to reduce epileptic seizures and enhance memory function[5,14,34]. However, the different neuronal phenotypes, and associated differences in firing patterns and neural coding of the various MS neuronal subpopulations, together with a complex network connectivity, make the effects of stimulation difficult to predict[35]. MS has three distinctive neuronal subpopulations[36–39] that form intricate connections with one another as well as their hippocampal targets. The GABAergic MS population selectively innervates most of the GABAergic interneurons throughout the hippocampus and thus acts to primarily disinhibit hippocampal pyramidal neurons[40,41]. The glutamatergic MS population innervates local MS GABAergic and cholinergic neurons and also directly projects to the hippocampal interneurons and pyramidal neurons[42–44]. Similarly, cholinergic MS neurons interact with both MS local neurons[45] and hippocampal pyramidal and inhibitory neurons in both direct and indirect fashion[36,46].

Despite initial investigations of MS optogenetic stimulation[23–25,47–51], the effect of the stimulation on hippocampal activity, particularly in regard to the parameters of

stimulation, remains poorly understood and warrants further investigation. Especially, there are a lack of studies comparing the effects on the hippocampal local field potential (LFP) activities induced by stimulating different MS neuronal subpopulations. Given the varied intrinsic characteristics of MS neuronal subpopulations as well as their complex connections, it is expected that the effects and effectiveness of optogenetic stimulation will depend in large part on the targeted subpopulation as well as the optical stimulation parameters. In addition, understanding the relationship between the parameter space and the effects in the hippocampal LFP is essential to identify the optimal parameters for purposeful modulation.

This chapter mainly describes the methods and results of analyses for characterizing the MS optogenetic stimulation effect which were introduced by Park-et-al[52]. Various MS neuronal subpopulations as well as optical stimulation intensities, frequencies and pulse widths were explored. A wide range of frequency domain features were extracted from the hippocampal LFP for analysis, including power spectral density, coherence and phase coherence – the delay of the signal transfer between regions. In a data driven fashion, we created a framework to characterize the hippocampal LFP modulated by MS optogenetic stimulation. Machine learning techniques were leveraged to analyze large sets of data[53,54] in complex parameter and feature spaces and to provide an objective decision making[55–57]. In order to measure stimulation effectiveness, find predominantly modulated neural features, and measure the sensitivity of features to parameter changes, we applied classifiers combined with feature analysis and reduction techniques. We also applied a regression model which describes a relationship between stimulation parameters and a specific feature's activity. Through this framework, we first quantified the degree of

stimulation effectiveness and identified a subset of parameters which induced a substantial change in the hippocampal LFP activity. Second, we identified predominantly modulated hippocampal neural features through a feature reduction technique. Third, we used sensitivity analysis to identify the subset of parameters which can potentially contribute to a maximization or minimization of neural features. Lastly, we built a regression model to predict the hippocampal theta power change based on the stimulation parameters as a model input. Hippocampal theta was chosen based on its well-known relationship with a pathological brain state[31,58] and cognitive function[59] as well as locomotion[60]. This model performed better than the standard linear regression model in describing the non-linear relationship between theta power changes and the stimulation parameters.

2.2 Methods

2.2.1 Surgical procedures

Adult male Sprague-Dawley rats (2-3 month old; 250-300g) from Charles River Laboratories (Wilmington, MA, USA) as well as adult male Long-Evans strain rats that express the bacterial Cre recombinase under control of the cholinergic choline acetyltransferase (ChAT) promoter were used in this study. ChAT rats were bred with wildtype animals in-house. Genotyping was performed on tail tissue from 3-week old pups using a primer pair according to RRRC (Columbia, MO). Animals from different strains were grouped for all analyses. All animals were maintained within a 12/12 light/dark cycle vivarium with unlimited access to food and water. All procedures were conducted in accordance with Emory University's Institute for Animal Care and Use committee.

Two surgical procedures were conducted for each subject as described by Laxpati et al[47]. The first survival surgery was for the viral vector injection to MS. A craniectomy (0.40 mm anterior and 2.00 mm lateral to bregma) was made while rats were anesthetized with 1.5-4% inhaled isoflurane. Injection of viral vector to MS was made at a 20° angle to the dorsal-ventral axis (0.40 mm anterior, 2.12 mm lateral at the 20° angle, 5.80 mm ventral to pia along the rotated axis). Once the pipette was withdrawn, the scalp was stapled closed, and ketofen was administered as an analgesic (3-5 mg/kg). For every viral vector, 1.8 µL containing ~2×10^9 viral particles based on qPCR of viral genome was injected using a pulled-glass pipette attached to a stereotactically mounted injector (Nanoject, Drummond Scientific Co., Broomall, PA, USA).

The second survival surgery was conducted after two weeks for recovery and optogenetic channel expression. The rats were anesthetized with 1.5-4% inhaled isoflurane during the whole surgery. Another craniectomy was made for electrode implantation at the right dorsal hippocampus (centered at 3.50 mm posterior and 2.80 mm lateral to bregma). Five 2 mm stainless steel screws (Plastics One, Roanoke, VA) were mounted on the skull for electrode's ground and reference wires as well as for structural support. To record from both CA1 and CA3, 16-channel multielectrode arrays (MEA; Tucker Davis Technologies (TDT), Alachua, FL., USA) were constructed with sixteen 33 µm diameter tungsten microwires spaced with 175 µm gap between two wires arranged in two rows offset by 1 mm. Each row had different length, 4.0 mm and 3.0 mm to target hippocampal CA3 and CA1, respectively. The MEA was lowered ventrally into the brain until single unit activity was observed from both the CA1 and CA3 regions. After the MEA was placed in the desired location, the ferrule was driven into the reopened original virus injection

craniectomy at a 20° angle to the dorsal-ventral axis. The fiber was placed where a strong stimulus-response signal was observed in the coincident spectrogram at the stimulation frequency as well as in the evoked potential, or a depth of 5.80 mm from pia along the rotated axis if no response was seen. Finally, the craniectomy was sealed with dental acrylic to secure the electrode and the optic fiber with the ferrule in place in the targets. The rats were administered ketofen (3-5mg/kg) and given 3-5 days for recovery before starting experimentation.

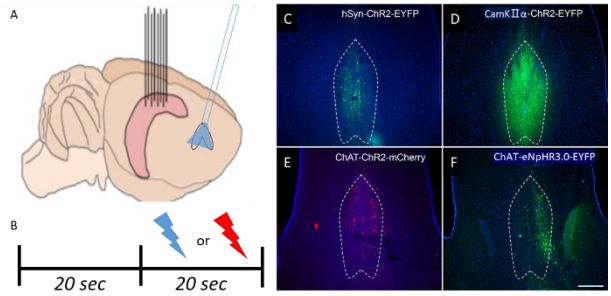

Figure 1. A. 16 channel multi-electrode-array was implanted in the hippocampus. Optic fiber with ferrule was implanted in the medial septum. B. Experimental diagram which includes 20 second baseline followed by 20 second stimulation (blue: excitation or red: inhibition). C-F. Microscope images of the medial septum to check expression of target specific virus (C: hSyn, D: CamKIIα, E: EF1a-DIO-ChR2 in a ChAT-Cre rat and F: EF1a-DIO-eNpHR3.0 in a ChAT-Cre rat). A dotted line indicated the area of MS. The scale bar (1μm) was plotted at the bottom right of F.

2.2.2 Stimulation and recording protocol

Hippocampal LFPs were recorded at 25 kHz using the NeuroRighter system[61,62]. Square-wave optical stimulation pulses were applied from the NeuroRighter system to an implanted ferrule in the medial septum via armored patch fiber cables (200 μm core diameter, 0.67 NA, Plexon). Ferrules were calibrated before implanted to have a range between 0-100I (1I = 1mW/mm^2, 50I equals to 1.57mW). A 465 nm blue LED module was used for the excitation and a 620 nm orange LED module was used for the inhibition. The

whole parameter sets were tested across 3 different days in each animal. As shown in the experimental diagram (Figure 1B), one trial consisted of 20 seconds of excitation with the blue light or inhibition with the orange light following 20 seconds of baseline period. During the trials, the animals were freely exploring a large open plexiglass enclosure, without specific behavioral restrictions or limitations. Between trials, adequate amount of time was placed to wash out the post-stimulation effect.

2.2.3 Description of optogenetic viral vectors and optical stimulation parameters

The stimulation parameters that were tested in our experiments are described in Table 1. To target different neuronal subpopulation in MS, we used recombinant adeno-associated viral (AAV) vectors incorporating three different types of promoters (UNC Vector Core Services, Chapel Hill, NC, USA): the human synapsin (hSyn) promoter pseudotyped with AAV5 is expressed in neurons non-selectively[48,63,64], whereas the calcium/calmodulin-dependent protein kinase IIα (CamKIIα) promoter serotyped with AAV2 is expressed in glutamatergic neurons;[63,64] The Cre-dependent double inverted open-frame (DIO) under control of the constitutively active human elongation factor 1α (EF1a) promoter pseudotyped with AAV5 was used to produce expression in cholinergic neurons in ChAT-Cre transgenic rats[65]. All viruses were used with either codon-optimized channelrhodopsin-2 (ChR2) or an enhanced halorhodopsin chloride pump 3.0 (eNpHR3.0), both of which were with a fluorescent tag of enhanced yellow fluorescent protein (EYFP) or monomeric Cherry (mCherry). As control for optical stimulation and virally mediated transgene expression, EYFP alone was used with the hSyn promoter.

All combinations of promoters and opsins composed biological parameters (Table 1). All seven biological parameters were tested with various optical stimulation parameters.

Three different light intensities, seven frequencies ranging from theta to low gamma and three pulse widths constituted total 63 stimulation parameters.

Table 1. A list of optogenetic viruses (biological parameters) for specific target subpopulation in MS, stimulation parameters and the number of animals used in the experimentation.

		Effect							
		Activation			*Inhibition*			*Control*	
		Virus	Stim Param.*	No. of animals	Virus	Stim Param.*	No. of animals	Virus	Stim Param.*	No. of animals
	Non-selective	AAV5-hSyn-ChR2-EYFP	10,30,50I** 5,7,11,17,23,35,42 Hz 2,5,10 ms	3	AAV5-hSyn-eNpHR3.0-EYFP	50,70,90I 5,7,11,17,23,35,42 Hz 5,10,20 ms	3	AAV5-hSyn-EYFP	10,30,50I 5,7,11,17,23,35,42 Hz 2,5,10 ms	2
Target	*Glutamatergic*	AAV2-CamKIIα -ChR2-EYFP	10,30,50I 5,7,11,17,23,35,42 Hz 2,5,10 ms	4	AAV2-CamKIIα-eNpHR3.0-EYFP	30,50,70I 5,7,11,17,23,35,42 Hz 2,5,10 ms	3	-		
	Cholinergic	AAV5-EF1a-DIO-ChR2-mCherry (ChAT-Cre)	10,30,50I 5,7,11,17,23,35,42 Hz 2,5,10 ms	3	AAV5-EF1a-DIO-eNpHR3.0-EYFP (ChAT-Cre)	50,70,90I 5,7,11,17,23,35,42 Hz 5,10,20 ms	3	-		

Notes: * 1st Row: intensity, 2nd: frequency and 3rd: pulse width. **1I = 1mW/mm^2.

2.2.4 Hippocampal neural features

Frequency domain features were calculated from 16-channel hippocampal LFP recordings. Data were segmented into 20 second baseline and 20 second stimulation epochs and down-sampled to 2000Hz. A multi-taper algorithm from MATLAB Chronux toolbox[66] was used for the feature calculation. A detailed description of neural features follows.

(i) Power spectral density (PSD) – PSD with 1Hz resolution was calculated in 0.1-300Hz range. Then the PSD change from the baseline during the stimulation period was measured in dB unit. 300 features of PSD change were calculated and averaged for the CA1 (Channel 1-8) and the CA3 (Channel 9-16) electrodes separately to generate a total of 600 PSD features.

(ii) Coherence (Coh) – Coh between CA1 and CA3 was measured in 0.1-300Hz range and collapsed into 1Hz bins. Coh was calculated between two facing channels, one in CA1 and the other in CA3 (e.g. Channel 1 in CA1 and channel 9 in CA3), and was averaged from eight different pairs. The difference of Coh between baseline and stimulation period comprised 300 Coh features.

(iii) Phase coherence (Phase) – Phase between CA1 and CA3 was measured in 0.1-300Hz range and collapsed into 1Hz bins. Phase was calculated between two facing channels, one in CA1 and the other in CA3, and was averaged from eight different pairs. The difference of Phase between baseline and stimulation period comprised 300 Phase features.

As a result, CA1 and CA3 PSD, Coh and Phase between CA1 and CA3 in 0.1-300Hz range made up a total of 1200 features.

2.2.5 Histology

Histology was performed after experimentation to verify the location of the electrode and viral vector expression. Rats were transcardially perfused with 0.9% saline followed by 4% paraformaldehyde in 0.1M phosphate buffer after they were deeply anesthetized with an overdose of Euthasol (5ml/kg, Virbac, Fort Worth, Tx, USA). The brain was dissected out and removed after one night being post-fixed with the electrodes and ferrules remaining in the head. Then, 50 µm coronal sections were made on a sliding microtome and mounted on glass slides with Vectashield DAPI (Burlingame, CA, USA) medium for visualization of nuclei. Slides were imaged to visualize the fluorescent tags in the opsins with Nikon DS-fil color digital camera on a Nikon E400 microscope using NIS-Elements software (Nikon Instruments, Inc., Melvile, NY, USA).

2.3 Results

2.3.1 Overview of analyses

Figure 2 demonstrates the main components of our machine learning framework that we developed for characterizing the effect of MS optogenetic stimulation on the hippocampal LFP activity. First, controllability was defined by the degree of stimulation effectiveness in hippocampal LFP and measured by probing the neural feature activity that was distinguishable from the baseline. We used a one-class classification method – positive and unlabeled (PU) learning – to compare neural recordings between the effective and ineffective trials[67]. After the classification, the parameter sets were labeled as effective (Eff) if they were clearly separable from the baseline; otherwise they were labelled as ineffective (Neff). Second, we identified predominantly modulated features by classifying Eff and Neff parameters using logistic regression (LR) model classifier with elastic net

regularization (ENR, Figure 2C). The regularization with combined L1 (LASSO) and L2 (Ridge) penalties was used to identify a sparse sub-set of neural features that were important for the classification by forcing the coefficients associated with non-significant features to be zero[68]. Selected features by ENR were regarded as predominantly modulated features. Third, optimizability of the parameters was defined as how sensitive the modulation of neural feature activity was to the change of parameters. A sensitivity was measured by an inverse prediction of a modulation parameter from the observed neural feature activity, and a higher prediction accuracy indicated a higher optimizability of the parameter (Figure 2D). A naïve Bayes Gaussian classifier was applicable for multi-label and a categorical variable classification[69,70]. Fourth, we modeled neural feature activity as a function of the optical stimulation parameters with a Gaussian process regression (GPR) model, a supervised learning to predict the output by interpolating the observations[71]. A GPR model was selected upon consideration of its ability to describe the non-linear relationship and its flexibility as a non-parametric model.

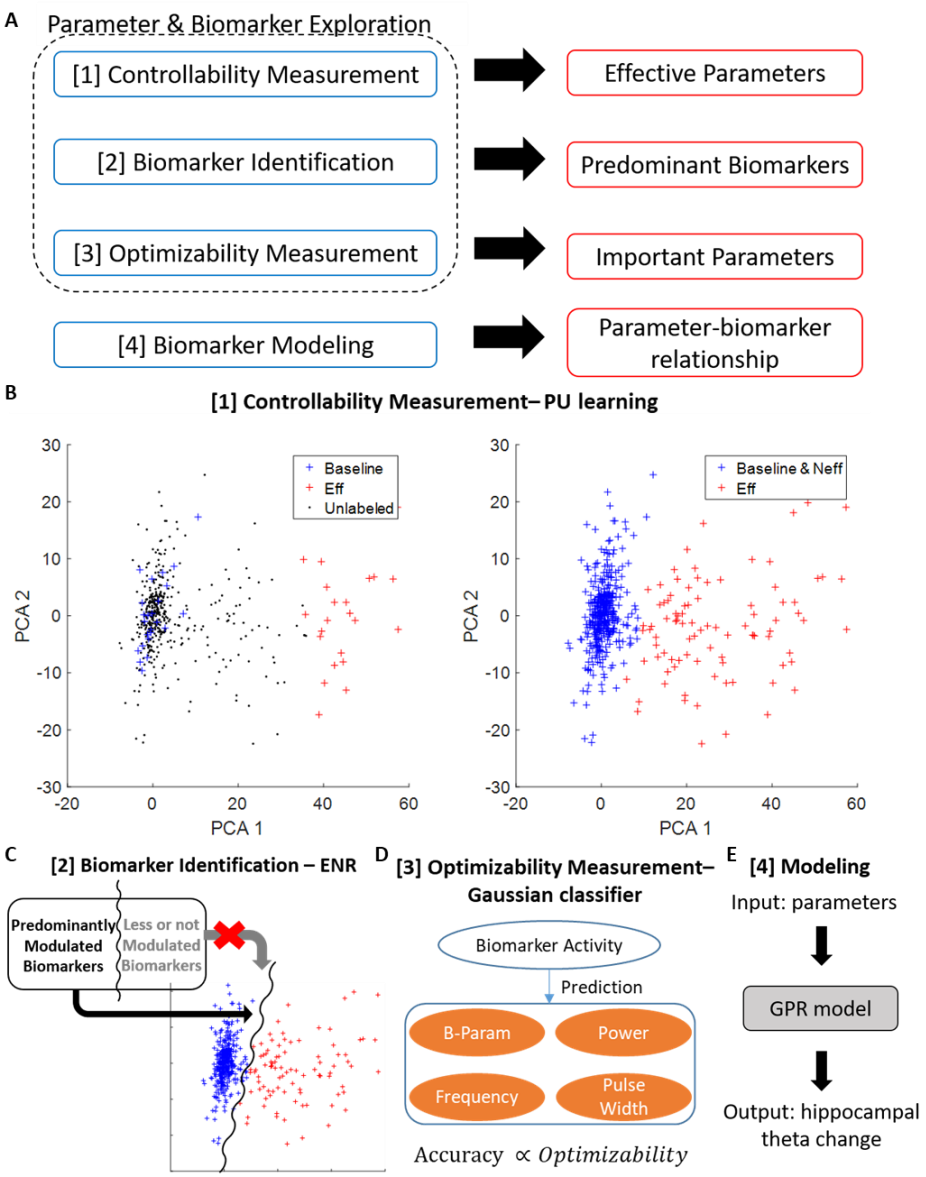

Figure 2. A. A flow chart of analyses introduced in this study. B. The final labels given to each modulation parameter after PU learning classification (right), and the initial labels before classification (left). After the classification, all points were labeled as effective (Eff) or non-effective (Neff). Although the classification was performed in ten-dimensional space, only the first and second principal components are plotted for better visualization. C. How ENR was utilized to find a subset of neural features which contributed to draw the hyperplane separating Eff and Neff. These features were predominantly modulated by the stimulation. D. The scheme of the inverse parameter prediction to evaluate the neural feature's sensitivity toward each parameter. Accurately predicted parameters were regarded as having a higher optimizability as features were sensitive to their change. E. A GPR model was built

to describe a relationship between parameters (input) and neural feature activity (output).

2.3.2 Controllability

2.3.2.1 Building a classifier for controllability measurement

Using the controllability test, we identified the stimulation parameters that effectively modulated the hippocampal neural features using the PU learning one-class classification[67] with a support vector machine (SVM). A SVM was selected to avoid the overfitting by controlling the margin of the hyperplane (i.e. support vectors). This characteristic of a SVM can contribute to a high performance in a classification problem with a moderate number of samples[72,73]. The classification procedure is described in Figure 3. One single point was constituted by averaging the feature sets from multiple trials of the same parameter set. Likewise, 10 trials of the 40-second baseline recording without stimulation constituted one single point by averaging the features. To avoid inaccurate classification and a high computational burden caused by the high dimensionality of the feature space, principal component (PC) analysis was applied to reduce the dimension of the features. Ten PCs were used as features for the classification. At the beginning of the classification, the baseline recording exemplars were assigned to the P class. The rest of the data set that contained the stimulation exemplars were kept as unlabeled (U). The Euclidean distance from the center of P in the reduced feature space was measured for every point in U. Points among U which were distant from the center of P were assigned as initial negative class labels (N) to initialize the classification process. A SVM classifier with a linear kernel was trained with the points from P and N classes. Then, the classifier was applied to U, and the points classified as negative were newly assigned to N (Figure

3B). A new SVM classifier was trained and applied to the unlabeled points iteratively until no new assignments to N were made (Figure 3A). After the last iteration, points remaining as unlabeled were assigned to P class (Figure 3C).

The final labels for the controllability test, either Eff or Neff, were identified according to the result of repeated PU learning classifications. As iteration went on during the PU learning, N class outnumbered P class, which resulted in an unbalanced dataset for classification. To address this issue, we subsampled the points from the outnumbered class (N) through a random selection. The whole classification was repeated 100 times so that the points from the outnumbered class can be further exploited and thus the loss of information caused by subsampling is minimized[74]. During the repetition, each point was classified to the baseline class (P, Figure 3 blue) or the stimulation class (N, Figure 3 red). The final label of either Eff or Neff was decided by thresholding. Eff was assigned to a parameter classified to the stimulation class more than 60 times out of 100 classification (0.6017, 95% upper confidence bound based on the binomial distribution).

Other points that could not reach the threshold were labeled as Neff. After all the points were labeled, we validated the labels by testing if two classes were separable through a cross validation (CV) with a SVM classifier. In addition, various numbers of PCs were tested to minimize the error, and the selection of ten PCs for the features was finally determined.

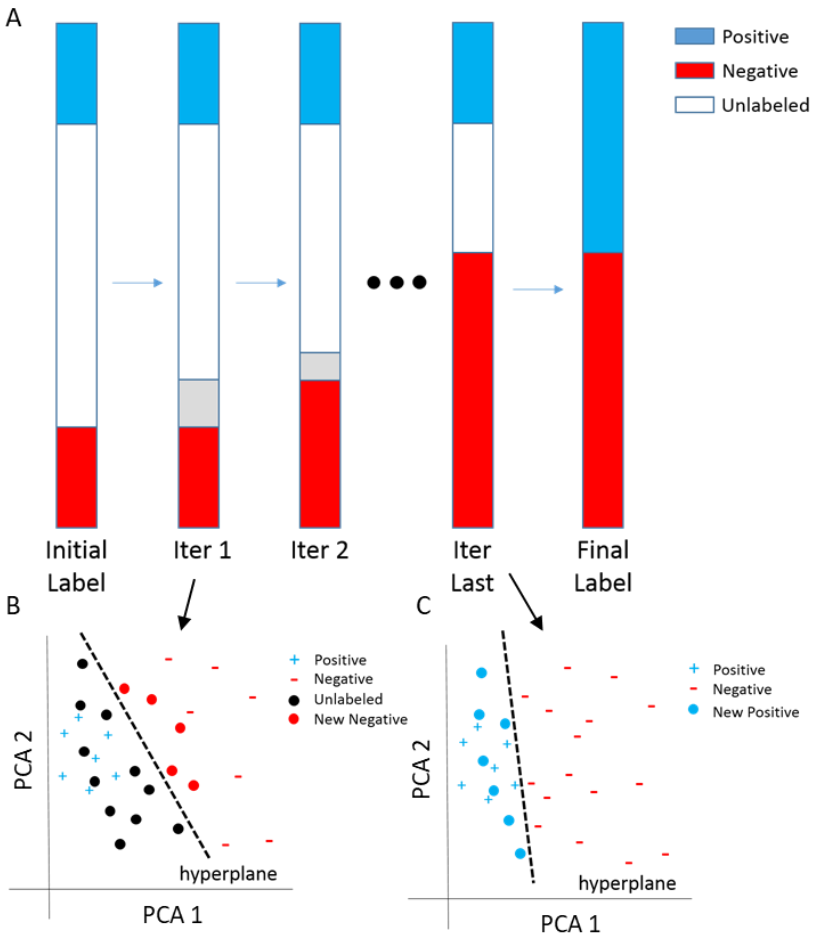

Figure 3. Parameter labeling using the PU learning. A. The portion of positive, negative and unlabeled points as the iteration goes on. A SVM classifier is trained with the labeled points every iteration (Iter) and applied to the unlabeled points. Iteration ends when the SVM classifier does not find a new negative point. B. An example of a hyperplane separating the positive and negative labeled points after the first iteration. The unlabeled points belonging to the same side with the negatives are newly assigned as negative. C. An example of a hyperplane at the last iteration when there are no new negative points detected. The unlabeled points belonging to the same side with the positives are assigned as positive.

2.3.2.2 Neurological frequency band power statistical test

We measured the power change in the neurophysiological frequency bands (Delta: 1–3Hz, theta: 4–10Hz, alpha: 10–16Hz, beta: 16–31Hz, low gamma: 32–60Hz and high gamma: 60–100Hz) induced by the stimulation to validate the controllability test result.

The difference of the power in each band between the stimulation and the pre-stimulation period was calculated in dB scale. The power change in the baseline activity without the stimulation was also calculated in the same way. A two-sample t-test without assuming the equal variances of the populations was performed between the power change from the recordings without the stimulation and recordings belonging to each parameter set. Parameter sets which rejected the null hypothesis were identified for each frequency band ($p < 0.05$, Bonferroni corrected for multiple comparisons).

2.3.2.3 Controllability test results

We first performed a controllability test to measure the degree of stimulation effectiveness for all parameter sets and validated the results with the statistically tested change in the neurophysiological frequency band powers. The outcome of the controllability test showed that of a total of 441 parameter sets, 91 were labeled as Eff and the other 350 were labeled as Neff (Figure 2B, Figure 4A). We found that two biological parameters provided the most effective hippocampal modulation. Specifically, hSyn-ChR2 and CamKIIα-ChR2 exhibited 55 and 36 Eff parameter sets respectively (Figure 4A) of 63 total parameters in the controllability test. The frequency band statistical test also revealed that hSyn-ChR2 and CamKIIα-ChR2 showed the biggest stimulation effect (Figure 4A). The other biological parameters did not induce any substantial stimulation effect. The high accuracy (99.1%) of the cross-validated classification between the neural feature activity induced by Eff and Neff further supported the controllability test results as well as the methods including the selection of the SVM classifier.

In addition, we observed that the stimulation intensity was the dominant factor in modulating neural state, and the frequency and the pulse width affected activity of neural feature only when the intensity was low. In hSyn-ChR2 trials, every stimulation parameter effectively modulated the hippocampal activity when the intensity was above 30I (Figure 4B). When the stimulation intensity was low (=10I), low frequencies (5, 7 and 11Hz) did not show any substantial effect (Figure 4B). This was even more pronounced when the pulse width was shorter (=2ms) (Figure 4B). Moreover, high frequency stimulation (>17Hz) was always effective regardless of the intensity or pulse width. In contrast, in CamKIIα-ChR2 animals, lower intensity (=10I) was always ineffectual (Figure 4B). However, when the intensity was 30I, all the frequencies above 11Hz effectively modulated neural features while low frequency parameter sets (5–11Hz) did not (Figure 4B).

LFP traces were shown to illustrate the effect of the stimulation (Figure 4C and D). Two stimulation parameters identified as Eff (hSyn-ChR2 7 and 42Hz with 50I-10ms, Figure 4C) were contrasted with two Neff parameters (hSyn-ChR2 10I-7Hz-10ms and hSyn-eNpHR3.0 50I-7Hz-10ms, Figure 4D). The effect of the stimulation characterized by the evoked potential was noticeable only in the stimulation with Eff parameters.

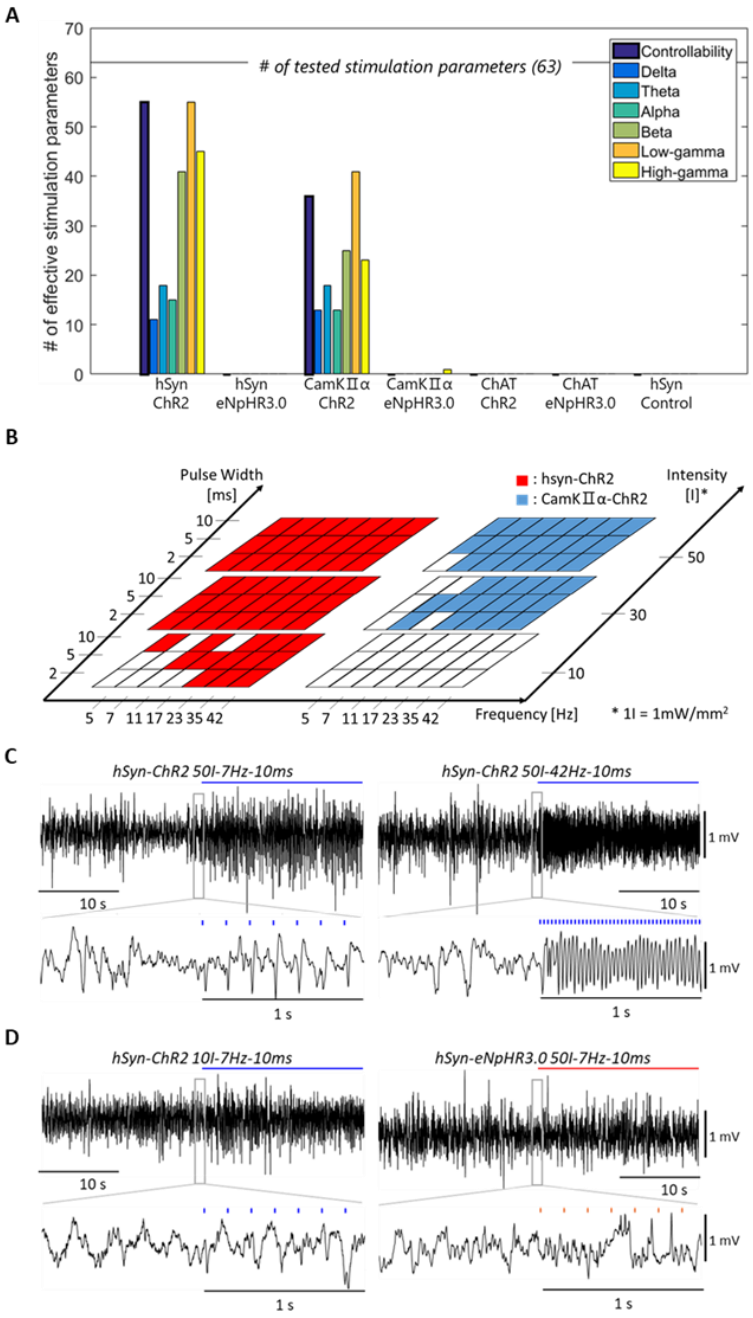

Figure 4. A. Controllability of the hippocampal LFP biomarkers was measured and compared with the t-test (p=0.05, Bonferroni corrected) result of the conventional neurophysiological band power for a validation purpose. The number of stimulation parameters labeled as Eff (controllability) was indicated in the bar graph after grouped by the biological parameter along with the number of stimulation parameters which had significant power change in each frequency band. B. Labels (color: Eff and blank: Neff) for individual stimulation parameter set for hSyn-ChR2 and CamKIIα-ChR2. The other biological parameters were not shown as they did

not have Eff labels. C-D. LFP examples of Eff parameters (C) and Neff parameters (D).

2.3.3 Predominant neural features

2.3.3.1 Identification of predominantly modulated neural features

After labeling the stimulation trials, a LR classification model with ENR was trained to identify predominantly modulated neural features. The model was trained to classify Eff and Neff samples, and ENR forced the model to only select the important features. The model was trained with 80% of the total data and tested with the remaining 20%. Equation 1 shows the cost function that was used for training the classifier. In Equation 1 the alpha determines the ratio between L1 and L2 penalties and the lambda is a weight of the regularization. A nested CV was performed to train and test the classifier (outer layer) after optimizing two hyperparameters of the model (inner layer).

$$\min_{\beta}\left(\frac{1}{N}Deviance + \lambda P_{\alpha}(\beta)\right), \text{where}$$

$$Deviance = -\sum_{i=1}^{N}(y_i \log(\hat{y}_i) + (1-y_i)\log(1-\hat{y}_i))$$

$$y_i\text{: true } and\ \hat{y}_i\text{: predicted value for label}$$

$$\text{and } P_{\alpha}(\beta) = \frac{(1-\alpha)}{2}\|\beta\|_2^2 + \alpha\|\beta\|_1 \qquad (1)$$

In the inner layer, 5-fold CV was conducted and a set of alpha and lambda (Equation 1) that provided the lowest deviance was found through a grid search (alpha: 0-1 and lambda: 0.0001-10). In the outer layer the model was trained with the selected hyperparameters transferred from the inner layer. The coefficients of the model were saved for every 5-fold CV in the outer layer. This nested 5-fold CV was repeated 10 times

resulting in a total of 50 sets of model coefficients. The modulated features were finally identified by the following criterion. Features were selected if their model coefficient was non-zero whereas features with zero coefficient were abandoned. Thus, the selected ratio indicated how often features had the non-zero coefficient. Finally, predominantly modulated neural features were identified if its selected ratio was significantly above the chance.

The most predominant neural feature was compared to the theta band (4-10Hz) PSD regarding their degree of effect and chance of being modulated by Eff parameters. The degree of the effect was defined by measuring the mean of the feature change divided by the feature's baseline variation. The chance of modulation was defined by finding a ratio of parameters which induced a significant feature change among all Eff parameters. A t-test was conducted to identify the significant feature change ($p < 0.05$, Bonferroni corrected for multiple comparisons).

2.3.3.2 Power spectral density was predominantly modulated

We applied ENR to identify the neural features that were predominantly modulated by MS stimulation. The Power Spectral Density (PSD) of the LFPs in CA1 and CA3 were more noticeable than those of coherence (Coh) and phase coherence (Phase) between CA1 and CA3. First, the frequency range of the predominant PSD features was wide-spread for both CA1 and CA3 (Figure 5A-B). In CA1, the PSD for high beta and low-gamma bands were identified as predominantly modulated with the peak of the fitted line observed at 45Hz – a low-gamma wave (Figure 5A). In CA3, the PSD for delta, theta, high-beta and low-gamma bands were predominantly modulated with the peak of the fitted line similar

to the one found in CA1 (45Hz, Figure 5A). Coh and Phase did not show any predominance (Figure 5C-D) and were therefore dropped from further analyses.

Differences of predominantly modulated neural features between stimulation in hSyn-ChR2 and CamKIIα-ChR2 animals were observed (Figure 5A-B) when we applied ENR to each group separately. The stimulation with CamKIIα-ChR2 induced significantly more effect in the high beta band (28-33Hz) PSD in CA1. In contrast, the low-gamma band (38-50Hz) PSD in CA1 and the mid-gamma band (63-73Hz) PSD in both CA1 and CA3 showed higher predominance in hSyn-ChR2 animals.

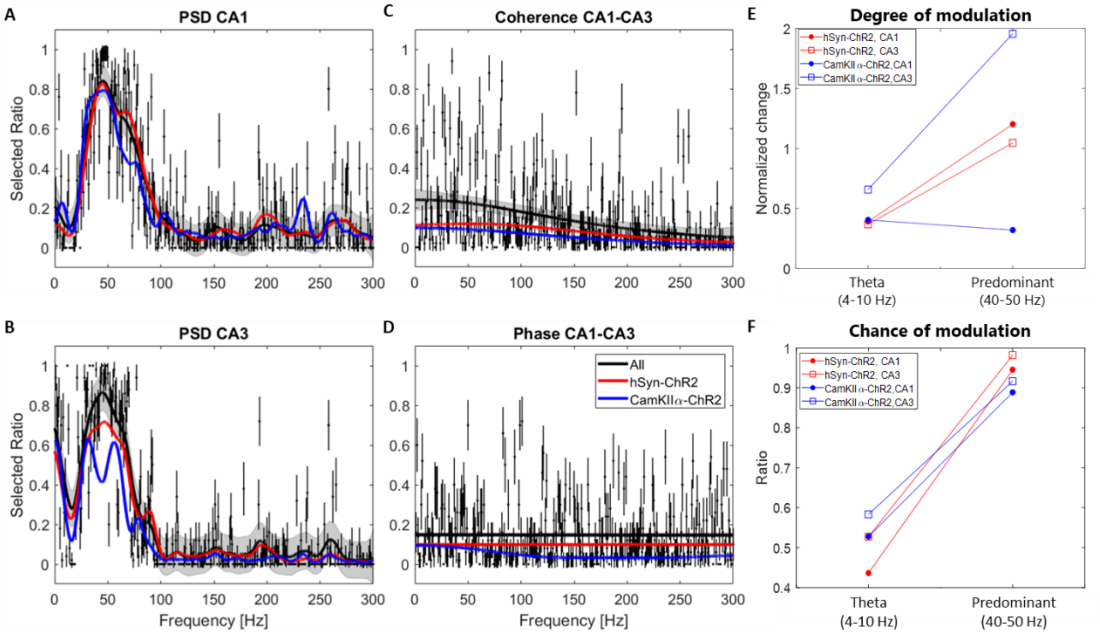

Figure 5. Predominantly modulated neural features. A-D. Selected ratio from repeated ENR (0.1–300Hz, a black dot indicates the mean value and the error bar indicates 95% confidence interval) with a fitting line and the 95% confidence interval (black, the confidence interval was indicated by the shaded area) was plotted. The result of separately applying ENR to hSyn-ChR2 (red) and CamKIIα-ChR2 (blue) was superimposed. E-F. Comparison of stimulation effect in theta (4-10Hz) and predominantly modulated (40-50 Hz) band PSD in CA1 and CA3. The predominant band PSD was largely affected by the stimulation except CamKIIα-

ChR2 in CA1 (E), and more stimulation parameters induced a substantial change in the predominant band PSD than theta (F).

The predominant neural feature (40-50Hz – low gamma band PSD) was largely affected by a higher number of stimulation parameters compared to the theta band (4-10Hz) PSD (Figure 5E-F). The predominant neural feature was selected to be centered at 45Hz – the most predominant both in CA1 and CA3 PSD. The degree of modulation effect, measured by the normalized mean of the feature changes, showed that the stimulation induced a larger change in the predominant neural feature than the theta band except CamKIIα-ChR2 in CA1 (Figure 5E). More Eff parameters induced a significant change in the predominant neural feature than in the theta band PSD (Figure 5F). The high ratio (>0.88) showed that almost every Eff parameters induced a significant change in the predominant neural feature.

2.3.4 Optimizability

2.3.4.1 Optimizability measurement

Optimizability of the stimulation parameters – a sensitivity of neural feature activity toward the parameters – was measured to identify the most useful parameters to modulate the neural feature activity. A Gaussian classifier which is a subtype of the naïve Bayes classifiers was capable of multi-input-multi-output classification for inverse parameter prediction with observed neural feature activity[69,70] (Figure 2D). The process of prediction with the Gaussian classifier was designed to minimize the risk of incorrect prediction (Equation 2). Then, according to Bayes theory, the optimal decision was to select the label which maximized the likelihood (Equation 3, ML: maximum likelihood). The likelihood

of a parameter set with the observed neural activity was calculated based on an underlying assumption that the features followed multivariate Gaussian distribution with the uniform prior (Equation 4). A sparse inverse covariance matrix adapting the L1 regularization[75] technique was used to moderate the problem of an inaccurate prediction caused by the interdependencies in a high dimensional feature space.

$$g^*(x) = \arg\min_{g(x)} \sum_{i=1}^{M} P_{Y|X}(i|x) L[g(x), i],$$

$$g(x): \text{decision function and } g^*(x): \text{optimal decision}$$

$$L[g(x), y] = \begin{cases} 1, g(x) \neq y \\ 0, g(x) = y \end{cases} \quad (2)$$

$$\text{ML: } g^*(x) = \arg\max_{i} P_{X|Y}(x|i) P_Y(i) \quad (3)$$

$$\min_{\beta} \left(\frac{1}{N} Deviance + \lambda P_\alpha(\beta) \right), \text{where}$$

$$P_{X|Y}(x|i) = \frac{1}{\sqrt{(2\pi)^d |\Sigma_i|}} \exp\left\{ -\frac{1}{2} (x - \mu_i)^T \Sigma_i^{-1} (x - \mu_i) \right\}$$

$$where\ P_Y(i) = C\ (Constant) \quad (4)$$

Leave-one-out classification was performed to predict a set of four parameters used in a single trial while the other trials contributed to the probability distribution described in Equation 4. A mean and a covariance matrix were calculated with the training data, and a parameter set for a test trial was predicted by the trained Gaussian classifier. This process was separately performed for two groups ($N_{trial,Eff}$ = 1789, $N_{trial,Neff}$ = 5919) to contrast the prediction availability of Eff and Neff classes. A prediction accuracy was calculated for

individual parameters by checking that a specific parameter was correctly predicted regardless of how the other parameters were predicted.

2.3.4.2 Optimizability test results

Neural features demonstrated sensitivity to biological parameters and stimulation frequency as indicated by their high accuracies of inverse parameter prediction with a Gaussian classifier at 75.91% and 93.8% respectively (Figure 6A). In contrast, neural features showed less sensitivity to intensity and pulse width with prediction accuracies of only 50.64% and 41.25% respectively (Figure 6A). These results contrasted with the predictions obtained with the Neff parameters which demonstrated a low prediction accuracy for all parameters (<30%, Figure 6A).

The prediction accuracies of hSyn-ChR2 and CamKIIα-ChR2 suggested that both biological parameters induced clearly distinguishable effects on neural features (Figure 6B). Similarly, the high prediction accuracies for all frequencies showed that frequencies also induced strongly distinguishable effects on neural features (Figure 6B). Moreover, the lower prediction accuracies of intensity and pulse width showed that neither of these parameters induced noticeably different modulation effects on neural features. This implies that neural features were only sensitive to biological and frequency parameters, so they are useful parameters to control neural activity.

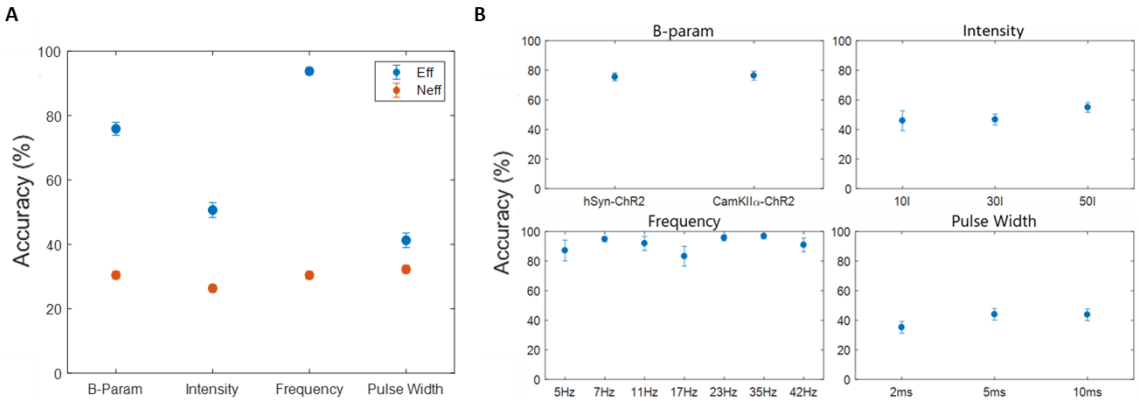

Figure 6. Inverse parameter prediction accuracies in optimizability test. A. The mean and the confidence interval of the accuracy of the prediction grouped by each parameter (blue). The prediction result of parameters from Neff class was shown for a comparison purpose (red). The higher accuracy of biological parameter (B-param) and frequency prediction indicates that neural features are sensitive to these parameters. B. The accuracy for individual component of the parameter groups.

2.3.5 Stimulation parameter - hippocampal theta modeling

2.3.5.1 GPR modeling

We used regression modeling to describe the hippocampal theta activity as a function of the MS stimulation parameters. We modeled the change in the hippocampal theta power in CA1 and CA3 from the baseline as a function of the stimulation parameters using the three-dimensional GPR model for each biological parameter. The theta band (4-10Hz) power was calculated by the sum of the area under PSD curve, and its change from the baseline to the stimulation period was calculated in dB level. We used a constant zero mean and a third order Matern kernel covariance function with automatic relevance detection[76] to train the GPR model (Equation 5).

$$k(x_p, x_q) = \sigma_f^2\left(1 + \sqrt{3}r\right)\exp\left(-\sqrt{3}r\right) \quad (5)$$

$$r = \sqrt{\sum_{m=1}^{d} \frac{(x_{pm} - x_{qm})^2}{\sigma_m^2}}$$

The hyperparameters of the covariance and the likelihood function of the GPR model were optimized to minimize the negative log-marginal-likelihood of the observations. The model was trained with 90% of the whole data and tested through 10-fold CV with 10 repetitions. A standardized mean squared error (SMSE) between the model output and the observed theta power change was calculated to measure the goodness-of-fit (Equation 6) with the test data.

$$\text{SMSE} = \frac{\sum_{j=1}^{N} (y_j - \hat{y}_j)^2}{N} \frac{1}{var(y)}, \text{ where}$$

$$y_j\text{: observed value and } \hat{y}_j\text{: model output} \tag{6}$$

Also, the variance of the model output was calculated to measure the variability of the model with the test data. The learning curve of the model was calculated by repeatedly measuring SMSE while increasing the number of training data to monitor the improvement of the model. The convergence criterion was defined as when the SMSE value was confined within the 1% range of the final value at the end of the training. The performance of the GPR model was compared to a linear regression (LnR) model to test the non-linearity of the relationship between the stimulation parameters and the change in the hippocampal theta power.

2.3.5.2 Hippocampal theta power changes as function of stimulation parameters

The GPR model for hSyn-ChR2 and CamKIIα-ChR2 described the non-linear relationship between the stimulation parameters and changes in theta power. The higher output variance and the lower SMSE of the hSyn-ChR2 and CamKIIα-ChR2 models

indicates their good performance in predicting the change in theta power in CA3 (Figure 7A-B). In contrast, hSyn-eNpHR3.0, CamKIIα-eNpHR3.0, ChAT-ChR2 and ChAT-eNpHR3.0 models resulted in a variance of 0 and SMSE of 1 (Figure 7A-B) indicating that these latter models were unable to describe the relationship between the parameters and theta power (Figure 7A-B).

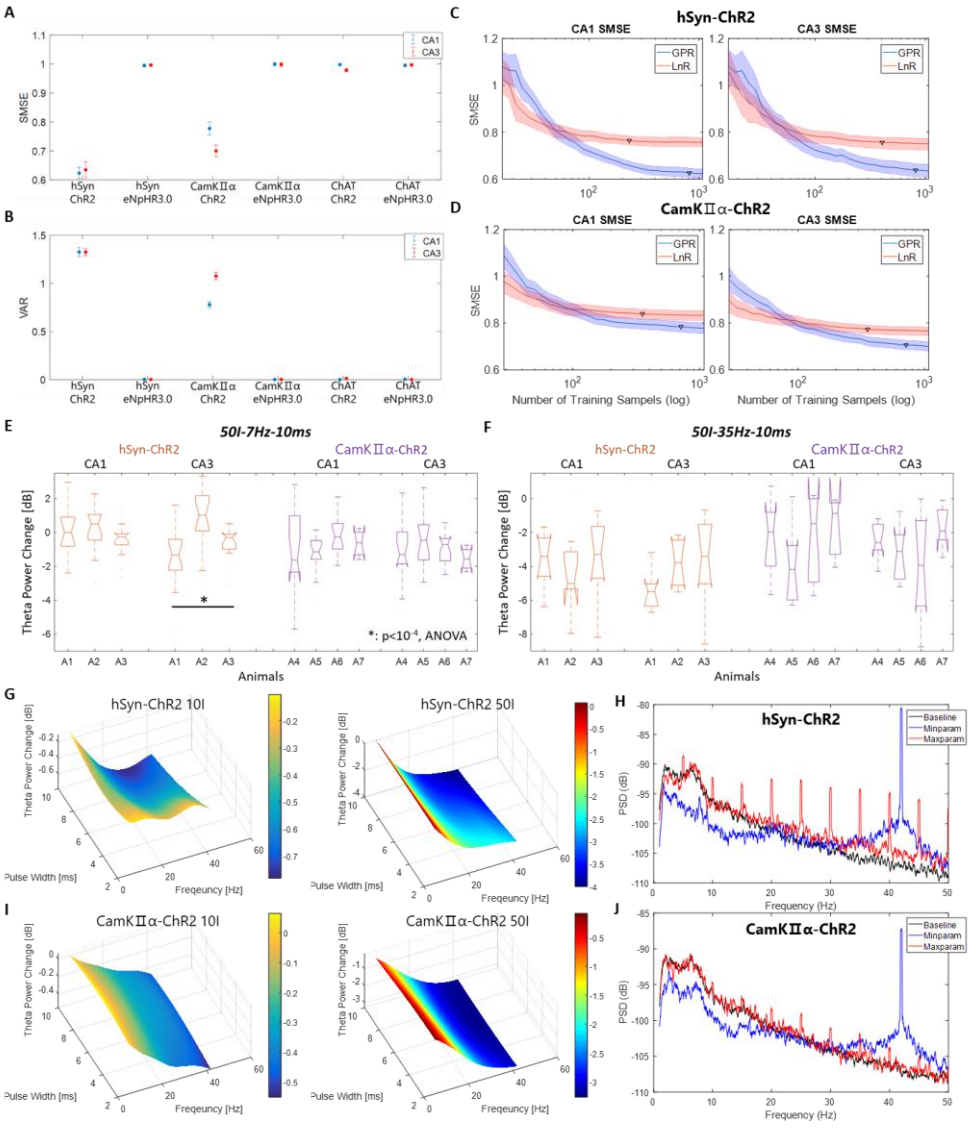

Figure 7. The validation of GPR model and examples of an application for finding the optimal parameters. The model describes the relationship between stimulation parameters and changes in hippocampal theta power (4–10Hz) A-B. SMSE and the variance of the GPR model output for every biological parameter in CA1 and CA3.

C-D. Learning curves of the GPR model with the growth in the number of training data. The learning curves of LnR model plotted for a comparison purpose. The black triangles indicate the converged points. E-F. Theta power change for two stimulation parameters to tract the origin of SMSE by comparing the variability between trials and animals. G. Theta power in CA3 GPR model of hSyn-ChR2 on the frequency-pulse width plane. H. PSD of hSyn-ChR2 when stimulated with maxparam (*50I-5Hz-2ms*, red) and minparam (*50I-42Hz-10ms*, blue) compared to the baseline (black). I. Theta power in CA3 GPR model of CamKIIα-ChR2 on the frequency-pulse width plane. J. PSD in 0.1–50Hz of CamKIIα-ChR2 when stimulated with maxparam (*10I-5HZ-5ms*, red) and minparam (*50I-42Hz-10ms*, blue) compared to baseline (black).

A comparison between the learning curves of the linear and non-linear models for the hSyn-ChR2 and CamKIIα-ChR2 showed that the GPR model captured the non-linear relationship between the activity of neural features and the stimulation parameters (Figure 7C and D). Following a certain amount of training data (>100 samples), GPR models performed better compared to LnR models, and such difference in performance can be attributed to the GPR model's ability to describe non-linear relationships. For example, a GPR model was able to demonstrate the non-linear relationship between changes in theta power in response to varying frequencies at lower intensity (Figure 7G, left). The convergence points in the learning curves indicated that the GPR models required more training data compared to the LnR models (Figure 7C and D).

A variability of the stimulation effect on the theta power in CA1 and CA3 was compared to tract the origin of the error of the GPR model represented by SMSE. The theta power change in CA1 and CA3 induced by four Eff parameters (hSyn-ChR2 & CamKIIα -ChR2 combined with 50I-7Hz & 35Hz-10ms) is shown in the box plot for every animal (Figure 7E-F). The box and whisker plots indicated a high variance between trials within the same animal (Figure 7E-F). The variability between animals was significant only in

one (hSyn-ChR2, 50I-7Hz-10ms in CA3) out of 8 parameters according to ANOVA test ($F_{2,46} = 13.3$, $P<0.0001$).

2.4 Discussion

Despite extensive studies describing the involvement of MS in the septo-hippocampal pathway, the precise mechanisms by which subpopulations of neurons in the MS modulate hippocampal LFP activity remains largely unknown. The lack of this cell-type specific exploratory analysis of the septo-hippocampal pathway modulation hinders the selection of optimal stimulation parameters for neural feature and potentially behavioral modulation. In the present study, we exhaustively tested combinations of MS stimulation parameters, including seven different biological parameters, and applied machine learning techniques to characterize their effects on neural features from hippocampal LFPs. The results demonstrate that only two of the MS biological parameters in combination with sets of optical stimulation parameters induced significant changes in LFP (Figure 4). Further analysis identified low-gamma frequency PSD as the predominantly modulated neural features in LFPs while coherence and phase coherence were only marginally modulated (Figure 5). Manipulation of the biological parameters and stimulation frequency were revealed to be most useful when optimizing the neural feature modulation (Figure 6). Lastly, the GPR model performed better than the linear model in describing the relationship between neural features and parameters and was consistent with the previous analyses (Figure 7). As a conclusion, these results emphasized that a selection of an optogenetic virus as well as stimulation parameters is important to induce a desired neural activity.

The results and techniques developed in this chapter were leveraged in the following chapters. First, as a result of the controllability test we used hSyn-ChR2 for the

further studies as it provides the maximum controllability on the hippocampal activities. Second, we will explore a broad space to find epileptic neural features as MS optogenetic stimulation modulates not only the hippocampal theta power but also the other frequency band power. Third, the frequency axis will be mainly explored to find the optimal parameters as it provided the highest optimizability. Fourth, the parameter space explored in this chapter did not provide the effective theta power increase so a broader parameter space will be tested.

2.4.1 Origin of variations in controllability

Variation in controllability can stem from the diverse characteristics of light-driven ion channels and MS subpopulations. In animals injected with hSyn-ChR2, intensity was the most dominant factor for controllability, and frequency and pulse width contributed only when intensity was low. Raising light intensity increased not only the number of neurons stimulated but strength of the induced current of each neuron, likely accounting for the intensity being a major factor for controllability. Higher intensity can penetrate deeper within the tissue, potentially recruiting more of the transduced MS neurons to fire[22]. Higher intensity also likely increases the percentage of channels recruited within a given volume. In addition, according to an *in-vitro* study of neurons expressing ChR2, a positive relationship was found between intensity and the peak amplitude of the induced current at the channel level[77]. The fast firing rate of GABAergic and glutamatergic neurons that were transduced with the hSyn promoter may allow for a robust response from the high frequency stimulation. Previous studies have shown that GABAergic neurons[78] (12–39Hz) and glutamatergic neurons[79] (12–17Hz) have a faster firing rate than cholinergic neurons[78] (0.3–0.5Hz) in MS. We also showed that pulse width, which is also positively related to

the peak amplitude of the induced current at the channel[77], significantly affected the controllability of the neural features when the intensity of the stimulation pulse was low. In this study, the inhibition with using short pulses with eNpHR3.0 did not affect the hippocampal LFP substantially even at the longest pulse width (20ms) and the highest frequency (42Hz) that we tested. Several studies including a lesion and a pharmacological block of MS attenuated or completely disrupted the hippocampal theta power[24,80,81]. These studies taken together with ours suggest that inhibition in the MS needs to be prolonged or chronic to affect the hippocampal oscillations in the hippocampus.

In the case of CamKIIα-ChR2, in accordance with the results from hSyn-ChR2, intensity was the most important factor for controllability, likely involving similar mechanisms. In CamKIIα-ChR2 experiments, the frequency also affected the controllability when the intensity was low; high frequency stimulation demonstrated higher controllability. We suspect that the specific activation of fast firing glutamatergic neurons in MS was responsible for this, although it is unclear if they are primarily acting through direct projections to the hippocampus, or via local synapses on GABAergic MS projections.

In our studies using the cholinergic specific expression of both ChR2 and eNpHR3.0, we observed only a marginal stimulation effect on hippocampal LFPs with MS modulation. MS cholinergic neurons are characterized by their low spontaneous firing rate which may explain their negligible stimuli response[78]. In addition, several studies suggest the cholinergic projections are largely acting through muscarinic receptors, which would not demonstrate the same frequency-specific stimulation response as seen with GABAergic and glutamatergic neurons[82].

2.4.2 Hippocampal low-gamma power as predominantly modulated neural feature

The low-gamma spectral band power in CA1 and CA3 was predominantly modulated by the MS optogenetic stimulation. This was in contrast with previous studies which have proposed a correlation between MS and hippocampal theta power. Previous lesion studies and electrophysiological findings[40,45,80,83,84] suggested a role of MS as a pacemaker for the hippocampal theta rhythm. However, within our parameter space, both hSyn-ChR2 and CamKIIα-ChR2 stimulation more predominantly modulated the low-gamma band power. This suggests that the effect induced by the external brain stimulation is different from the one expected based on the lesion study and the natural brain dynamics. Together with a previous study which showed that a pharmacological block of MS suppressed post-ictal hippocampal gamma wave[85], our study emphasizes the role of MS in the modulation of hippocampal gamma rhythm. These results also suggest a gamma-related mechanism by which MS stimulation may be able to affect memory performance given their well-known relationship[86,87].

2.4.3 Optimizable MS stimulation parameters for modulating the hippocampal neural features

Measuring optimizability – the sensitivity of neural feature activity toward the change of parameters – can provide an efficient way to optimize the modulation of neural feature activity. The complex anatomical structure of the septo-hippocampal system makes the effects of stimulation hard to anticipate. Finding a desired parameter set therefore requires a tremendous amount of resources exploring an infinite parameter space. By utilizing optimizability tests, we can identify sub-regions of the stimulation parameter

space for targeted exploration by identifying unimportant parameters, such as intensity and pulse width.

In our studies, results from the optimizability test were somewhat different than those from the controllability test. For example, although the stimulation intensity highly affected the controllability, it did not impact optimizability in the neural feature activity. One possibility is that intensity plays a thresholding role (like a switch) in the induction of the stimulation effect. On the other hand, frequency played a secondary role in the controllability, but was highly useful for inducing various neural feature activities. Therefore, to optimize neural feature modulation it is best to explore the stimulation frequency space while setting the intensity at a high level.

2.4.4 Modeling relationships between stimulation parameters and the hippocampal neural features

The stimulation parameter-neural feature relationship revealed by the GPR model was consistent with the controllability and optimizability results. In addition, the variation of neural feature activity along the frequency axis was much higher than along the pulse width axis (Figure 7G and I) which agrees with the optimizability test result.

The variability in the neural feature modulation represented by SMSE (Figure 7A, C and D) suggested a state dependency of the stimulation effect. The theta power change induced by the stimulation was different for every trial, and this variance was more noticeable than the variance between animals (Figure 7E-F). This is in line with several studies indicating that a variation in stimulation effect can come from the internal brain state as well as from the behavioral state. We have previously shown that the impact of local hippocampal stimulation[88] and MS optogenetic stimulation[89] can be predicted by

hippocampal LFP activity. Moreover, Vandecasteele et al. also described that MS stimulation effect can be modulated by ripple events in the hippocampus[25]. The behavioral state such as the locomotor activity was also reported to affect the effect of MS optogenetic stimulation[25]. In this study, we characterized the stimulation effect by repeatedly testing the same parameters in a random fashion in an attempt to cancel out influence from behavioral states. Performing stimulation simultaneously with behavioral tasks or internal brain states measured by electrographic recording from MS may better clarify the potential participation of such states on hippocampal stimulation.

2.4.5 Study Limitations

Although we have tested a large number of parameters, there is still a broad space which has not been explored, and it is unclear whether the results within our experimental parameter space will extrapolate to the broader space. Since frequency exhibited the highest optimizability in neural activity, it will be worth exploring a broader frequency range, within the biological limitations of the optogenetic channels. There is a possibility that a different predominantly modulated hippocampal neural feature (45Hz PSD in CA1 and CA3) is observed if a different stimulation frequency range is applied.

In addition, the stimulation effect of MS GABAergic neurons was not identified as they were modulated together with some glutamatergic and cholinergic neurons when hSyn promoter was used. Such specific stimulation could be further explored with the use of transgenic animals. Selective modulation of GABAergic neurons may identify that the stimulation effect presented in hSyn-ChR2 animals is mainly induced by MS GABAergic neurons or by an interaction with the other neuronal subpopulations.

CHAPTER 3. DEVELOPMENT OF *IN-VIVO* OPTOGENETIC STIMULATION PARAMETER OPTIMIZATION

3.1 Introduction

Neuromodulation is becoming a fundamental tool for understanding and treating neurological and psychiatric diseases. The selection of parameters is of obvious critical importance for neuromodulation as many studies have shown that the modulation of neural feature activity and behavioral change is highly parameter dependent[29]. However, parameter selection has been done empirically and even sometimes arbitrarily in many of the preclinical studies and clinical trials[26–28]. Applying stimulation with the optimal parameters can improve the effectiveness of biomarker modulation. Moreover, optimal stimulation parameters are subject-specific, and further, the stimulation effect depends on the pre-stimulation neural state[88–90] which implies that the optimal parameter is *non-stationary*. Exhaustive parameter search methods such as a grid search or a random search require a tremendous amount of resource and time which also increases a chance of inducing a side effect. Therefore, the exhaustive search methods are especially not suitable for translational applications which usually demand a fast and safe algorithm.

A Bayesian optimization (BaO), one of black box optimization algorithms, is a well-developed field of engineering that can be applied to the problem of tuning stimulation parameters. The optimization algorithm requires two fundamental components–an objective function and a search space. The objective function is a quantitative measure of optimality, for example the value of an electrophysiological feature. The other component,

the search space, is the range of stimulation parameters that can be tested. This parameter space is typically constrained based on the capabilities of the stimulator, safety considerations, and the goal of the neural modulation intervention. Lorenz et al. demonstrated how BaO could search a parameterized space of audio-visual stimuli to identify the stimulus that maximizes the difference between temporal and occipital activation, as measured by fMRI[91]. Building on the findings from Lorenz et al., our work focused on using related black-box optimization approaches for tuning optogenetic stimulation of the medial septum (MS) based on its effect on hippocampal neural activity.

In this chapter, I detail the validation and utility of BaO for MS optogenetic modulation of the hippocampal neural activity. The goal is to implement an autonomous system that learns a set of stimulation parameters that induce a desired hippocampal activity through iterative interaction with the neural circuit. Specifically, we tested this approach to modulate two different hippocampal neural activities in normal rats. The first test was to increase the low-gamma band power, which was identified as a hippocampal neural feature predominantly modulated by the MS optogenetic stimulation (Chapter 2). The second test was to increase the hippocampal theta band power. It was shown in the previous chapter that the theta power is only marginally or not increased with the tested stimulation parameters, so we expanded the parameter space to find the one which can effectively increase the theta power.

3.2 Methods

3.2.1 Animal preparation

Two survival surgeries for virus injection (1st survival surgery), electrode implantation and optic ferrule/fiber implantation (2nd survival surgery) were conducted as described in 2.2.1. The experiment for this study was performed in total 6 rats. The parameter optimization for gamma power maximization and theta power maximization was performed in two and four rats respectively.

3.2.2 Experimental setup

Electrophysiological recording was performed while a rat was awake and freely behaving. A headstage consisting of 16 recording channels with active impedance matching (Tucker Davis Technoolgies, TDT) was securely connected to the implanted electrode. A patch fiber cable (200μm diameter, 0.67 NA, Plexon) was used to connect to a 465nm blue LED to the implanted ferrule, which had been calibrated prior to the implantation. LFP were sampled at 25kHz and band-pass filtered at 1-200Hz (RZ2, TDT).

3.2.3 Objective function calculation

The hippocampal theta and gamma power were calculated by using MATALB Chronux toolbox with a multi-taper method. Recording channels which contained noise (e.g. motion artifact and 60Hz noise) excluded from the analysis.

3.2.3.1 Hippocampal gamma power

The absolute value of hippocampal low gamma (33-50Hz) power was used as an objective function during the optimization.

3.2.3.2 Hippocampal theta power: expected theta modulation

The hippocampal theta power oscillates based on the behavioral or internal neural state of the rat, and a linear relationship was observed between the theta power in the current time window and the change of the theta power to the subsequent window (Figure 8). We developed a new objective function, the expected theta modulation (ETM, Figure 8) to incorporate this characteristic of the theta power. To calculate ETM, first, theta power was measured on ten overlapping 3s windows moving by 0.6 second during stimulation. A linear model was then used to estimate the relationship between theta power in one window as a predictor of the change in theta power to the next window. The triangular area under this line was then compared to a model generated from the previous baseline window. The difference in these areas was used to calculate the ETM. A positive ETM indicates that the corresponding stimulation parameter tends to increase theta power, while a negative ETM indicates the opposite. From an optimization perspective, the ETM is a scalarized approach to jointly maximizing the theta power in one time-window and the increase in theta power to the subsequent time-window.

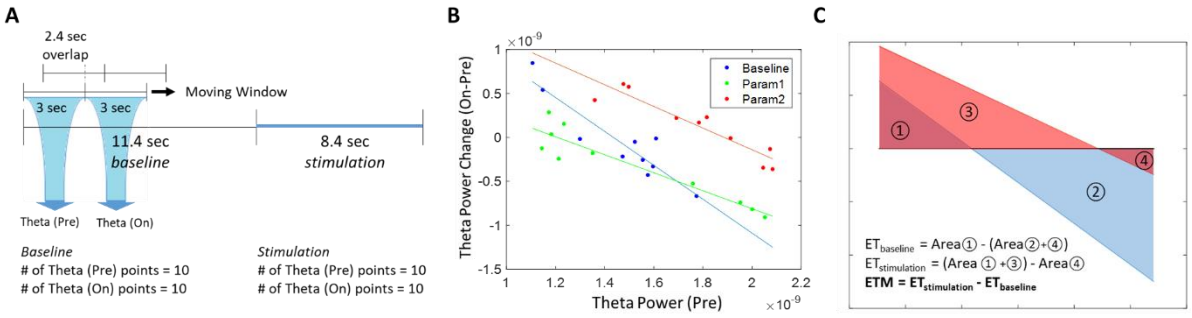

Figure 8. Introduction of theta power linear model (TLM) and expected theta modulation (ETM). A. A schematic of a moving window segmentation to generate TLM. Two consecutive 3-second segments were used for calculating theta (pre) and theta (on), and these windows moved 0.6 seconds each step. Ten pairs of theta (pre) and theta (on) were calculated for both baseline and stimulation period. B. Theta (pre) compromised a linear relationship with the differences between theta (on) and theta (pre). This linear relationship which is characterized by two factors (slope and

y-intercept) was dependent on the stimulation parameters. Three examples of the TLM, one with baseline and the other with two different stimulation parameter sets, are shown. C. Expected theta (ET) is defined by the area of the triangle formed by TLM and y=0 line. ETM is defined as the difference of ET between the baseline and the stimulation TLM.

3.2.4 Bayesian closed-loop optimization

BaO is a model-based optimization that has been used for optimization of expensive cost functions[92]. An overview of the BaO algorithm is shown in Figure 9. As the BaO algorithm queries the cost-function, it iteratively builds a model of the underlying data, which is then used to select which the area of the parameter space is to be subsequently sampled. Gaussian processes (GP) are typically employed as the underlying model, although other models such as random forests have been utilized. In our implementation, we used a GP with a constant mean function and a third order Matern kernel with automatic relevance detection for the covariance (Equation 7).

$$k(x_i, x_j|\theta) = \sigma_f^2(1+\sqrt{3}r)\exp(-\sqrt{3}r)$$
$$r = \sqrt{\sum_{m=1}^{d} \frac{(x_{im} - x_{jm})^2}{\sigma_m^2}} \quad (7)$$

The mechanism for selecting which point to sample is an acquisition function which can evaluate the improvement, or potential for improvement, of each point in the parameter space. While evaluating the objective function can be computationally expensive, the process of maximizing the acquisition function is comparatively cheap. In this analysis, we considered two acquisition functions:

Expected improvement (EI):

$$H_{EI}(x) = \begin{cases} (\mu(x) - f(x^+) - \xi)\Phi(z) + \sigma(x)\phi(z) & if\ \sigma(x) > 0 \\ 0 & if\ \sigma(x) = 0 \end{cases}$$

$$z = \begin{cases} \dfrac{(\mu(x) - f(x^+) - \xi)}{\sigma(x)} & if\ \sigma(x) > 0 \\ 0 & if\ \sigma(x) = 0 \end{cases} \quad (8)$$

Upper confidence bound (UCB):

$$H_{UCB} = \mu(x) + \sqrt{\kappa_t}\sigma(x) \quad (9)$$

where the sequence κ_t was defined as $\kappa_t = 2\log(t^2\pi^2/6)$.

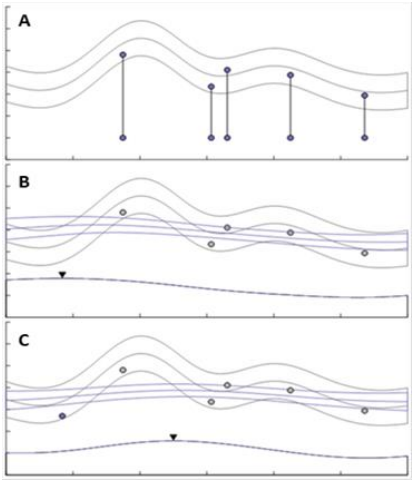

Figure 9. Overview of the Bayesian optimization (BaO) algorithm. A) During an initial phase, sample points are randomly selected from a uniform distribution and evaluated. B) A Gaussian process model is then fit to the existing data. An acquisition function is then used to propose a candidate sample point based on the expectation and uncertainty estimated by the model. C) This proposed sample point is then evaluated, the model is updated with the new data, and the process B-C is repeated.

3.2.5 Stimulation parameters

3.2.5.1 Parameters to maximize hippocampal gamma power

Three parameters of a single-frequency pulse (Figure 10B) were optimized to maximize the hippocampal gamma power: an intensity of light (10-50I, 1I = 1mW/mm^2), a frequency (5-42Hz) and a pulse-width (2-10ms).

3.2.5.2 Parameters to maximize hippocampal theta power

Two different stimulation parameter spaces were used and compared for optimization to maximize the hippocampal theta power. The first parameter space used a fixed intensity (30I or 50I) and pulse-width (8ms) but allowed for nested pulse-trains described by two frequency parameters (slow: 5-11Hz and fast: 35-100Hz, Figure 10A). This stimulation pattern consisted of high frequency pulses delivered in bursts at a lower frequency. The second parameter space was with a fixed intensity (30I or 50I, Figure 10B) single-frequency pulsatile square wave with parameters for pulse-width (1-8ms) and frequency (2-100Hz).

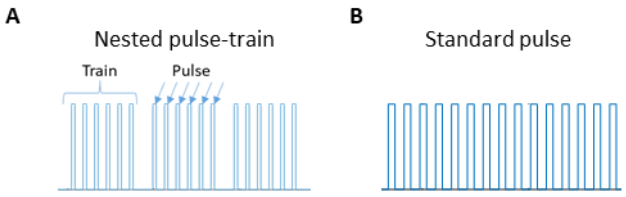

Figure 10. Patterns of MS optogenetic stimulation. A. Nested pulse-train. B. Standard single-frequency pulse.

3.2.6 In silico simulation

3.2.6.1 Modeling the effect of medial septum optogenetic stimulation on hippocampal gamma power

Data from the previous chapter mapping medial septum optogenetic stimulation to hippocampal gamma power was collected from three subjects on three different experimental days for a total of 1267 samples. Subject-specific models mapping the stimulation parameters (intensity, frequency and amplitude) to the hippocampal gamma power were constructed by fitting the samples to a GP regression model that captures the expected hippocampal response to medial septum optogenetic stimulation. Therefore, this GP model can be used as a simulation platform by providing a hippocampal gamma power as an output when the stimulation parameter set was given as an input. The uncertainty of the output caused by adding noise to the output was also defined by the GP model.

3.2.6.2 Simulation to compare random search and Bayesian optimization

The efficiency of BaO to find the optimal stimulation parameter set to maximize the gamma power was compared to the random search method. The models mapping medial septum stimulation parameters to hippocampal gamma power as described above (3.2.6.1) were used to construct a simulation platform. Each simulation trial included 40 samples for BaO and the random search, and the estimated optimal stimulation parameter set was found after every sample. BaO randomly explored the parameter space in first 10 samples and then explored with the UCB acquisition function (Equation 9, mu =0.4) for the last 30 samples. The estimated optimal parameter set was decided by a GP model constructed with the tested samples and observations. Two different methods were used for random search to decide the estimated optimal parameter set: 1) the sample which observed the maximum gamma power and 2) the parameter set which supposedly maximizes the gamma power according to the GP model constructed with the tested samples and observations. An error, a distance between ground truth and estimated

maximum gamma power, during the simulation exploring 40 samples was measured to evaluate each search method. The simulation was performed for three animals with 10 repetitions for each animal.

3.2.7 In vivo optimization

3.2.7.1 Optimization to maximize hippocampal gamma power

Two subjects (R4 and R5) underwent the optimization and test cycle four times over the course of two weeks. During the optimization, each sample consisted of 20s of stimulation and were separated by 100s. Ten initial samples drawn from a uniform random distribution were used for the burn-in period, followed by 20 samples guided by the algorithm. The UCB acquisition function using a value of nu=0.4 (Equation 9) was used for the hyperparameter of the algorithm.

3.2.7.2 Optimization to maximize hippocampal theta power

Four male Sprague Dawley rats underwent the optimization and testing phases. Total of eight and seven trials were performed respectively for optimization of a standard single-frequency pulse and a nested pulse-train. For one of the subjects the optimization phase lasted for 50 samples, while for the other three, the optimization was stopped after 30 samples or shorter if converged.

During the optimization, each sample consisted of 11.4s of baseline and 8.4s of stimulation and were separated by 20s. The objective function, ETM, was calculated as described in Figure 8. Ten initial samples drawn from a uniform random distribution were used for the burn-in period, followed by 20 samples guided by the algorithm. The EI

acquisition function using a value of nu = 0.01 (Equation 8) was used for the hyperparameter of the algorithm.

3.2.8 Post-optimization parameter test

After finishing the learning phase of the optimization, no stimulation was delivered for 15 minutes. During the post-optimization testing phase, 30 stimulations were delivered – randomized between sham stimulation, the optimal stimulation parameters the algorithm identified as inducing the highest gamma or theta power, and the stimulation parameters identified as inducing a minimal change in hippocampal gamma or theta power (sub-optimal). Each stimulation was applied for 5 seconds following 5 second baseline, and the 50 second gap between two trials was placed to wash out the stimulation effect.

3.3 Results

3.3.1 Simulation to compare random search and Bayesian optimization

The simulated results showed that BaO outperformed the random search for finding the optimal stimulation parameter set to maximize the hippocampal gamma power. The efficiency of BaO was compared with two random search methods, one without and another with the GP model to decide the estimated optimal parameter set as described in 3.2.6.2. The trajectory of the error between the ground truth and the estimation of the maximum hippocampal gamma power was compared for each searching method (Figure 11). After 10^{th} sample where the intelligent search begins for BaO, the error at each sample of BaO was lower than the one from the random search methods (Figure 11A). In addition, the final error at the end of search was significantly lower compared to the random search

(Figure 11B). These results demonstrated that BaO can find the optimal stimulation parameter set more quickly and accurately than the random search.

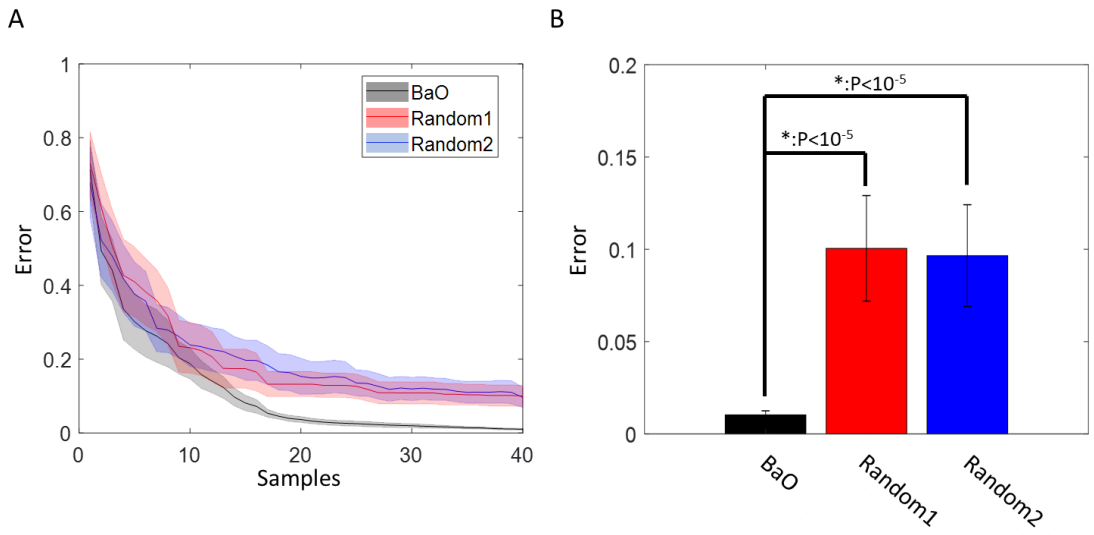

Figure 11. Comparison between Bayesian optimization (BaO) and the random search for finding the optimal medial septum optogenetic stimulation parameter set to maximize the hippocampal gamma power. Random1 and Random2 represent the random search method to GP model (Random2) or not (Random1) for deciding the estimated optimal parameter set. A. The trajectory of the error. B. The final error at the end of the parameter search.

3.3.2 Gamma power in vivo Bayesian optimization

The optimal intensity and frequency of MS optogenetic stimulation to maximize the hippocampal gamma power were quickly found by the BaO algorithm. Figure 12 shows the trajectory of the parameters and the objective function (i.e. gamma power) during the initial random search and the intelligent search phase. At each sample, the estimated optimal stimulation parameters and the predicted hippocampal gamma are shown with solid lines. The actual stimulation parameters sampled are shown with dotted lines. In all

trials, the algorithm rapidly converged on intensity and frequency parameters within 10 samples. The final estimated optimal parameter set was a combination of a high intensity and a high frequency. In contrast, the algorithm's estimate of the pulse-width did not readily converge in all trials, and the final estimate of the optimal pulse-widths was more varied. The 'lack' of convergence and wide range of final values for pulse-width also agrees with the previous results showed the relative lack of influence of pulse-width on hippocampal neural activities above 2ms (Chapter 2, Figure 6).

After the optimization phase and a short delay to allow for the washout of any potential accumulated effects, each subject underwent a prospective validation of the estimated optimal stimulation parameters. Overall, the estimated optimal parameters produced a hippocampal gamma power 2-2.5 times than during sham trials. The sub-optimal stimulation parameters estimated to have the minimal effect on the objective function only marginally increase the gamma power.

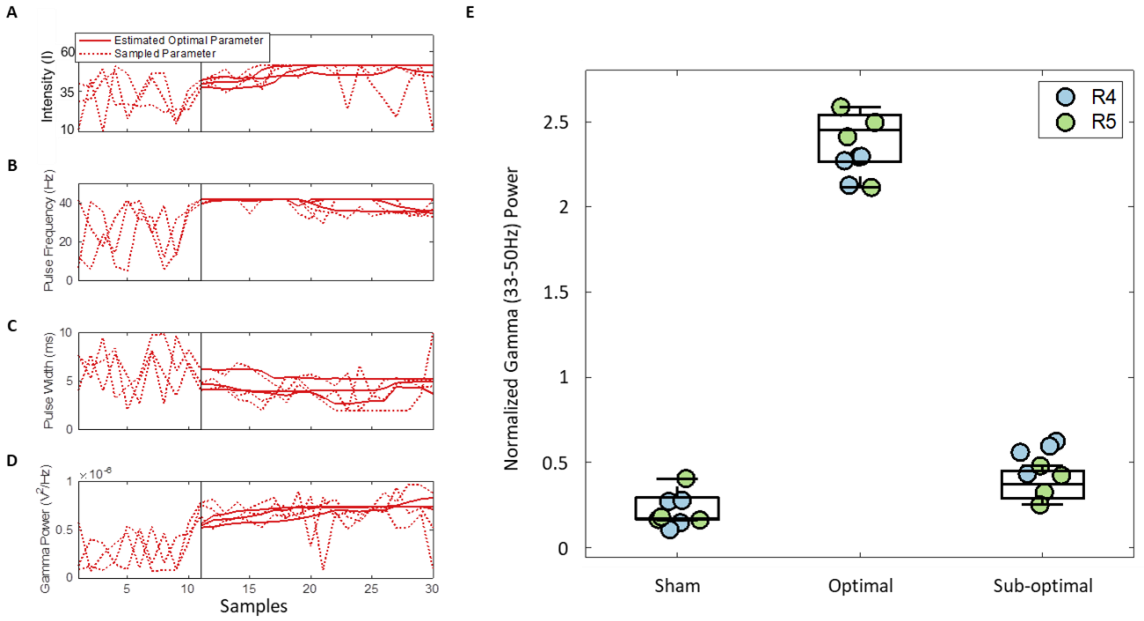

Figure 12. A-C. Trajectory of optimization *in vivo*. Each subplot shows the traces for optimizing stimulation parameters (A-C) and gamma power (D) using the BaO algorithm to maximize the hippocampal gamma power. The solid line indicates the stimulation parameters (A-C) or the gamma power (D) that the optimization algorithm estimated to be optimal, while the dashed line shows the actual stimulation parameters sampled or the measured gamma power. E. The post-optimization test results. Box plots show the normalized quartiles of the hippocampal gamma power using the optimal and sub-optimal subject-specific stimulation parameters along with the sham trials. Circles are the mean hippocampal gamma from each of the post-optimization test trials. The different colors correspond to different animals.

3.3.3 Theta power in vivo Bayesian optimization

3.3.3.1 Standard single-frequency stimulation

Through both optimization and test phases, it was clear that standard pulsatile MS optogenetic stimulation was unable to induce a significant increase in hippocampal theta power. Figure 13A and B show the trajectories of the frequency and pulse-width sampled by the optimization algorithm (dotted line) and the estimate of the optimal (solid line) as additional samples are collected. The two example trials are shown in light vs. dark blue.

When searching for the frequency that maximizes the increase in hippocampal theta, we could see that the algorithm initially searched the range of parameters between 2 and 100Hz. However, in one trial (light blue) after the first 10 random samples were collected, the algorithm immediately converged on 2Hz as the estimated optimal frequency, and only once sampled a different pulse-frequency at sample #33. In the second trial, the algorithm converged on a 2Hz pulse-frequency after sample #19 and similarly only sampled one other pulse-frequency, but without change the estimated optimal. For pulse-width, the two different trials converged on very different parameters: 1ms and 6.3ms, despite sampling the range of potential stimulation parameters during the burn-in phase (i.e. random search) and early in the optimization. This is likely due to the relative flatness of the objective function. In other words, changing the pulse-width of the stimulation has little impact on hippocampal theta power, so the algorithm selected parameters somewhat arbitrarily. Figure 13 shows the change in hippocampal theta power predicted by the model for the current estimate of the optimal stimulation frequency and pulse-width. For both trials, after the 10 burn-in samples were collected, the estimated change in hippocampal theta was negative (i.e. best stimulation decreases hippocampal theta). However, as the algorithm searched for the stimulation frequency and pulse-width that maximized hippocampal theta, it eventually found a set of parameters, specifically a pulse frequency of 2Hz, that minimally decreased the hippocampal theta. The validation results in Figure 13 show that this inability of single-frequency pulsatile MS optogenetic stimulation to increase hippocampal theta power above baseline is robust and generalizes across animals. In comparison to sham stimulation, the best set of stimulation parameters identified by the

optimization algorithm caused a slight, but not significant, decrease in hippocampal theta power.

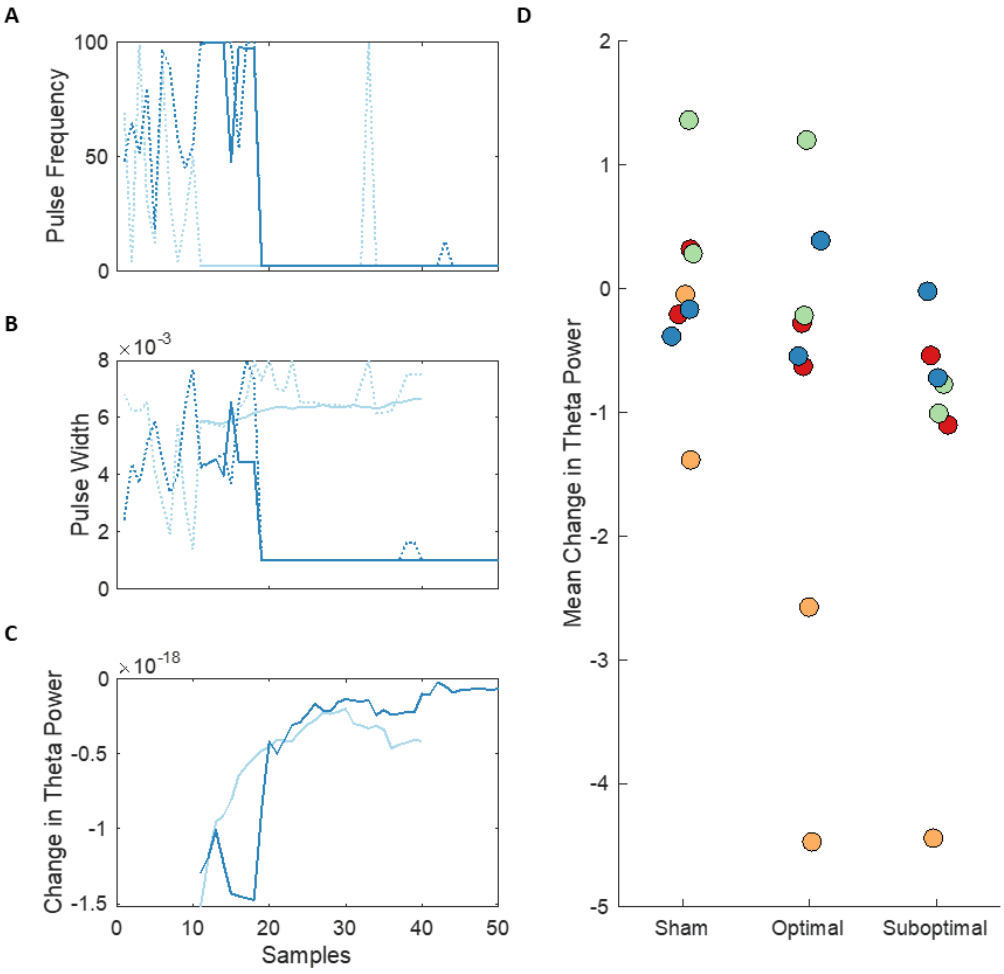

Figure 13. *In vivo* Bayesian optimization and testing of single-frequency pulsatile stimulation to increase the hippocampal theta power. A-B. Stimulation frequency and pulse-width, respectively, sampled by the optimization algorithm (dotted lines), along with estimate of the optimal stimulation parameters (solid line) as each new sample is collected. C. The predicted hippocampal theta power when the optimal stimulation parameters are applied according to the Gaussian process model. The light and dark blue traces indicate the two different trials from the same animal. D. Results of the testing phase. Each circle is the mean of 10 samples from either sham,

optimal, or suboptimal stimulation. The different colors correspond to different animals.

3.3.3.2 Nested pulse-train stimulation

Hippocampal theta power can be increased by applying MS optogenetic stimulation with nested pulse-train stimulation. With the finding that MS optogenetic stimulation using a standard single-frequency pulse could not provide our desired effect of increasing hippocampal theta power, we turned our focus to nested pulse-train stimulation (Figure 10A). The optimization algorithm explored the two-dimensional space of possible parameters which consisted of the pulse-frequency and the train-frequency, while the intensity and pulse-width were fixed. The configuration of the BaO algorithm was the same as in the previous experiment searching the standard single-frequency parameter space. Figure 14 shows the results of using BaO to search the nested pulse-train parameter space to maximize hippocampal theta power. The trajectory for the two representative trials of optimization is shown in Figure 14A**.** We can see that for both trials, after the initial burn-in phase, the algorithm rapidly converged on a pulse-frequency of 100Hz. While each trial sampled one other value, 35Hz, once, this did not change the estimated optimal stimulation parameter. In Figure 14B, we can see that for both trials the algorithm eventually converged on the lowest possible train-frequency (5Hz) as the estimated optimal. However, convergence to this parameter took longer in one trial than the other. In looking at the predicted effect of the current estimated optimal stimulation parameters, we can see that in both trials the optimization algorithm rapidly found stimulation parameters that could increase hippocampal theta above baseline. While in Figure 14B the trial in light blue

shows a late change in the estimated optimal train-frequency parameter, this did not have a substantial effect on the change in hippocampal theta power.

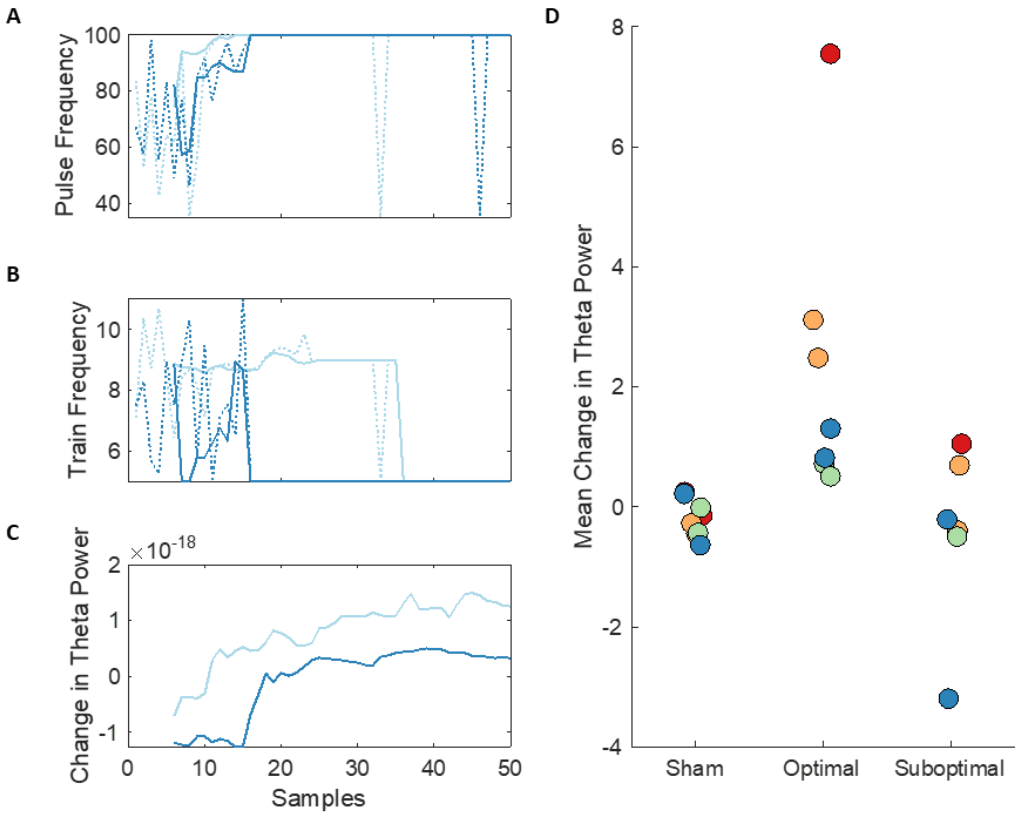

Figure 14. *In vivo* Bayesian optimization and testing of nested pulse-train stimulation to increase hippocampal theta power. A-B. Stimulation pulse-frequency and train-frequency, respectively, sampled by the optimization algorithm (dotted lines), along with estimate of the optimal stimulation parameters (solid line) as each new sample is collected. C. The predicted hippocampal theta power when the optimal stimulation parameters are applied according to the Gaussian process model. The light and dark blue traces indicate the two different trials from the same animal. D. Results of the testing phase. Each circle is the mean of 10 samples from either sham, optimal, or suboptimal stimulation. The different colors correspond to different animals.

When the estimated optimal parameters were compared with sham during the testing phase, it was clear that the BaO algorithm was able to identify a subset of the

parameter space that was able to induce an increase in hippocampal theta power above baseline (Figure 14D). Meanwhile, the sub-optimal parameters estimated to have the minimal effect on the objective function only marginally increase or decrease the theta power.

3.4 Discussion

Selecting neural modulation parameters and policies is a challenge that spans much of neuroscience, neurology, and neurosurgery. While evaluating any neurological intervention is time and resource intensive, the high dimensionality of stimulation parameters makes the problem of finding the optimal set difficult, if not intractable. The optimization framework presented here offers a principled approach to address this problem. As we have shown, BaO outperformed the random search method and can be directly applied in real-time to learn subject-specific optimal stimulation parameters. The simulation results showed that BaO can find the optimal parameter set than the random search. BaO was also able to find the optimal parameter set to maximize the hippocampal gamma power in the *in vivo* experiment. Moreover, with a suitable hypothesis, this algorithm can be used to search novel parameter spaces. We applied BaO to explore the parameter space of the novel nested-pulse train pattern and found the optimal stimulation parameter set to maximize the hippocampal theta power.

The BaO algorithm confirmed that the effect of the standard pulsatile stimulation was limited to decreasing hippocampal theta power. Based on the previous study (Chapter 2, Figure 7), it was likely that any of the stimulation parameters previously tested would decrease hippocampal theta power. However, it was possible that some unsampled

parameter combination in the parameter space would cause the desired increase in the hippocampal theta power. Using the BaO algorithm from the theta maximization experiments we were able to test this hypothesis. The closed-loop optimization approach was unable to find a set of stimulation parameters that increased hippocampal theta power, so it is verified again with a strong evidence that the standard pulsatile stimulation could only decrease the theta power. While the mechanism of *why* standard pulsatile stimulation of the MS could not increase hippocampal theta is beyond the scope of this study, one explanation is that stimulation at these lower frequencies entrains the hippocampal LFP to a very narrow frequency band while decreasing power in the adjacent bands. The net result is an overall decrease in power across the theta band.

Black-box optimization can navigate novel parameter spaces when a suitable hypothesis is provided. While the space of standard pulsatile stimulation parameters was limited to decreasing hippocampal theta, we found that by switching to a space of nested pulse-train stimulation parameters we were able to successfully increase hippocampal theta power overall. The hypothesis that a nested pulse-train stimulation pattern could increase hippocampal theta power was loosely based on recent studies showing that electrical theta-burst nested pulse-train stimulation of the MS/fornix could improve memory in epileptic rodents[93]. While we did not know *a priori* what the objective function mapping nested pulse-train parameters to hippocampal theta power, the BaO algorithm was able to find solutions that significantly increased theta power. This result demonstrated the ability of closed-loop optimization procedures to efficiently investigate unknown objective functions.

There are several factors that can prevent a successful optimization procedure. That nested pulse-train stimulation elicited the desired increase in hippocampal theta was the fortunate product of the specific selection of a parameter space with the correct controllability over the desired neural feature. Without these components the optimization procedure will not be successful regardless of the choice in optimization algorithm. Another critical factor is the correct engagement with the neural tissue and accurate measurement of the objective. One example of the former was shown in the optimization of nested pulse-train stimulation to increase the hippocampal theta. In one of the trials, the ability of MS optogenetic stimulation to modulate hippocampal theta power was substantially limited. This decrease occurred simultaneously, and was likely caused by, an inadvertent shift in the location of the fiber optic ferrule. With the light from the fiber optic no longer completely activating the channel rhodopsin in MS, and therefore modulating the hippocampus, it would be expected that the increase in hippocampal theta power is diminished. In sum, while closed-loop optimization can be a powerful tool, it is only as effective as the combination of parameter space, objective function, and engagement with the neural tissue.

Closed-loop, black-box optimization has the potential to address a wide range of problems in neural modulation. While the framework presented here centered around optogenetic stimulation, which does not have an immediate direct pathway to clinical translation, there is no reason these algorithms cannot be extended to clinical therapy. Several extensions of the standard optimization algorithms may find specific application in the clinical domain. These include: multi-objective optimization where multiple neural features are mutually competitive and need to be addressed simultaneously, safe

optimization where regions of the parameter space may be unsafe but the location of these regions is unknown, and preferential optimization where the objective function is more subjective. Finally, there is state-dependent optimization, where the algorithm learns a stimulation *policy* that depends on the current stat of the neural system. Taken to its logical conclusion and combined with approaches from control theory, state-dependent optimization is a direct pathway to the application of optimal control theory to neural modulation. Ultimately, with the correct use of exploratory data and simulation models, black-box optimization approaches are well-poised to improve the process of tailoring neural modulation therapy to specific patients and therapy-dependent requirements.

CHAPTER 4. DEVELOPMENT OF DATA-DRIVEN MODELS TO DESCRIBE A PATHOPHYSIOLOGICAL HIPPOCAMPAL NEURAL STATE BASED ON ELECTROPHYSIOLOGICAL RECORDINGS IN THE EPILEPTIC RAT.

4.1 Introduction

Identifying therapeutically effective stimulation parameters for epilepsy requires a tremendous amount of time and resources as seizures can be infrequent and the space of possible stimulation parameters is vast. Data-driven models of seizure susceptibility can act as a surrogate for predicting how effective a set of stimulation parameters is. Using these models to guide a selection of the stimulation parameters can save time and resources for ultimately mitigating the seizures.

There has been an effort to identify epileptic neural features from eletrophysiological recording. A few studies have shown that the epileptogenesis is presented in the neural activity in some animal epilepsy models. Bragin-et-al showed that high-frequency oscillations (HFOs) during the development of epilepsy was related to the appearance of spontaneous seizures in rat intrahippocampal kainic acid model[32]. Behr-et-al showed that a significant difference in a type of seizures as well as their onset zone between early stage and late stage in pilocarpine-treated rats[94]. A pattern of interictal spikes and HFOs was changed after rats experienced the first seizure in the same model[33]. In addition, Desai-et-al showed that the peak of local field potential (LFP) in tetanus toxin (TeNT) epileptic rats was at the low-theta band while one in normal rats was at the mid-theta band[30]. A transition

in the wide power spectrum band of LFP was observed as the pathological symptom progressed in the same study. Activities in LFPs in the hippocampus and other brain regions right before the seizure onset (i.e. pre-ictal period) also have been explored. Sedigh-Sarvestani-et-al showed that hippocampal theta and delta power changed during the pre-ictal period[31]. Cadotte-et-al observed that the granger causality of LFPs between CA1 and dentate gyrus was changed prior to the seizure onset[95]. Additionally, the theta synchrony between dorsal hippocampus and medial prefrontal cortex increased during the pre-ictal period[96]. These studies suggest a further investigation to search neural features in a wider space and to characterize their activity during the progression of epileptogenesis and during the pre-ictal period.

In this study, we developed data-driven models by characterizing epileptic neural features from electrophysiological recordings in the hippocampus. Two different data-driven models were constructed to identify neural features and characterize their activities in a rat TeNT mesial temporal lobe epilepsy (MTLE) model. One model was developed to track how a long-term seizure-susceptibility increases over time (epileptogenesis) in rats after the initial injection of TeNT. Another model was constructed to estimate a short-term likelihood of seizure onset (ictogenesis) in TeNT rats by classifying the hippocampal neural features extracted from pre-ictal and inter-ictal periods.

4.2 Methods

4.2.1 Tetanus toxin rat epilepsy model

Tetanus neurotoxin injection into the hippocampus provides a rat model of MTLE in which the hippocampal circuit is primarily perturbed by disruption of GABAergic

neurotransmission[97,98]. It leads to chronic seizures characterized by high excitability without a large hippocampal cell loss or mossy fiber sprouting[99]. After a TeNT injection in the rat hippocampus, there are 10-14 days of the latent period without seizures followed by 14-21 days of the active-seizure period (Figure 15). During the active-seizure period, the rat exhibits 0-6 behavioral or electrographical seizures per hour.

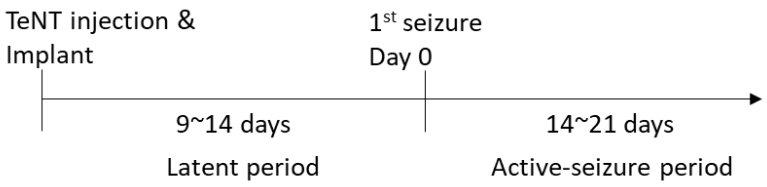

Figure 15. A brief description of two periods observed in a rat tetanus toxin (TeNT) model.

4.2.2 Animal preparation

An adult male Sprague-Dawley rat underwent two surgical procedures as described in Laxpati-et-al [47]. All procedures were approved by the Emory University Institute for Animal Care and Use Committee. The first survival surgery was an injection of a viral vector (AAV5-hSyn-hChR2(H134R), 1.8μL of 10^{13} particles/mL) to transfect the neurons in the medial septum (MS) as a part of another study. To the best of our knowledge, any effect of MS optogenetic virus in intrahippocampal TeNT model has not been reported. A second survival surgery was performed for the injection of TeNT and the implantation of the electrode into the hippocampus, and the implantation of the fiber optic ferrule into the MS. 10-45 ng of TeNT was injected into the dorsal hippocampus centered at 3.50mm posterior and 2.80mm lateral to bregma using a pulled glass pipette attached to an injector. Five 2.0mm stainless steel screws were mounted on the skull for the structural support and

to serve as the reference and ground for a multi electrode array (MEA). The 16-channel MEA (Tucker Davis Technologies, Alachua, FL), consisting of two rows of eight channels offset by 1mm, was advanced ventrally into the brain while single unit activity was observed from both the CA3 and CA1 regions of the hippocampus. After the MEA was placed in the desired location, the ferrule was driven into the MS. The craniotomy was sealed with dental acrylic to secure the electrode and the ferrule.

4.2.3 Data collection

The LFPs from the awake and freely behaving animals were recorded during the latent period and the active-seizure period (Figure 15). The LFPs were recorded from the hippocampus with 8 channels from CA1 and 8 channels from CA3. The data were collected by using TDT RZ2 acquisition system at 24414Hz and down-sampled to 2000Hz after DC-filtered. Only baseline data which were recorded at least after 24-hour of stimulation were used for the entire study. The animals were monitored behaviorally and electrophysiologically every day to detect the 1st seizure. Both data from the latent and active-seizure periods were used for constructing epileptogenesis model, and the data from active-seizure period were used for constructing pre-ictal state model by characterizing LFP activities during the pre-ictal and inter-ictal periods.

4.2.4 Epileptogenesis model construction

4.2.4.1 Feature extraction

Feature and Label: A feature set was calculated from the LFP recordings and labeled as a relative day to the first seizure (-7 to 18, Figure 15) to build a regression model.

Calculation: A pool of educated frequency domain features was calculated by using MATLAB and Chronux toolbox. The feature pool consisted of 4 groups of 3-300Hz frequency domain features – power spectral density (PSD) in CA1 and CA3, coherence (COH) and phase coherence (PHASE) between CA1 and CA3. Two sets of PSDs were calculated and averaged from 8 channels in CA1 as well as 8 channels in CA3 respectively. COH and PHASE was calculated and averaged from 8 different pairs of facing channels, one from CA1 and another from CA3. To reflect that a frequency domain feature shows a similar pattern with nearby frequencies in the high frequency domain, 2Hz and 4Hz bins were used for 100-200Hz and 200-300Hz bands respectively while 1Hz bins were used for 3-100Hz band. This binning method produced 172 features for each group (PSD CA1-CA3, COH and PHASE) and 688 total features. Data having a seizure or a huge motion artifact were excluded from the feature calculation. *Normalization:* Normalization was performed by z-scoring the features from each animal separately. In each animal, values of a mean and a standard deviation (Std) of features were calculated from the latent and the active-seizure periods separately. Then by averaging the values from two periods, the final mean and Std values used for the z-scoring were calculated. Removing outliers was performed at the same time. Outliers of features such as one from an interictal spike accompanied a huge power, so their existence highly affected the calculation of mean and Std values as well as the normalization. Therefore, the outliers of features were excluded when calculating the mean and Std values.

4.2.4.2 LARS-ENR

Least angle regression with elastic net regularization (LARS-ENR) is a linear fitting method which selects only a subset of features to avoid overfitting [68,100,101]. It has an

advantage that the selected sparse feature set makes the model easily interpretable. The relationship between input (X) and output (y), and the solution to build a model are indicated by the following equations:

$$y=X\times\beta+\varepsilon,$$
$$\beta=\arg\min\left[\left\|y-X\times\beta\right\|^2+\text{delta}\times\left\|\beta\right\|^2+\text{lambda}\times\left\|\beta\right\|\right] \quad (10)$$

The solution includes a linearly combined L1 and L2 penalties to avoid the overfitting. The LARS algorithm starts with an empty active feature set and iteratively calculates a new active feature set and adds a feature while following the direction of the model coefficients (β) toward the ordinary least square (OLS) solution. A new feature is collected when its correlation with the residual vector from the OLS is equally important with the active feature set. When a new feature is collected, a new direction toward the OLS with the current active feature set is calculated. The algorithm stops when the OLS is reached with the designated delta and lambda (Equation 10).

4.2.4.3 Model building

Epileptogenesis model (EGM) was built by repeatedly training, validating and testing a LARS-ENR model. 80% of the data was used for the training and validation of the model. To solve the unbalanced sample problem, we subsampled the positive-labeled (day>=0) samples to make its length same with the negative-labeled samples. We repeated the identical model construction process to fully exploit the positive-labeled samples while using the same set of negative-labeled samples for minimizing the information loss caused by the subsampling[74]. As LARS algorithm requires labels placed in the center, the negative

labels were multiplied by 2.285 to make the mean of the whole labels at 0. A nested cross validation was performed to find the best lambda and delta in the inner layer and to train and test the model in the outer layer. In the inner layer, 4-fold CV was performed within the training set only to select the best lambda and delta values which produced a minimum error. The selected lambda and delta were transferred to the outer layer to train the model with the whole training set. The 5-fold cross validation in the outer layer with 20 repetitions resulted in 100 different models. The final model was generated by averaging the coefficients of all trained models. The remained 20% of data were used for testing the final model.

4.2.4.4 Feature analysis

A subset of features informative to epileptogenesis was identified by leveraging a characteristic of ENR which removes unnecessary features. A feature was regarded as selected if it has a non-zero model coefficient. The coefficients of all trained models from CV and repetitions were investigated. A selected ratio of the features and the confidence interval based on binomial distribution were calculated. Features with the selected ratio greater than the chance were identified and grouped together with ones close. Activities of the grouped features were investigated, and those whose activity shows a certain pattern were identified as informative to epileptogenesis.

4.2.5 Pre-ictal state model development

4.2.5.1 Seizure detection

A seizure was defined by detecting a sum of wide band PSD (3-300Hz) above its baseline level (Figure 18A). A time series of the wide band PSD was calculated from 3 second segments of the hippocampal LFP with the 1 second moving window. The thresholding value was calculated by the standard deviation of bottom 70% PSD values multiplied by 3, and a series of segments (>15 sec) with their PSD above the threshold was defined as a seizure.

4.2.5.2 Feature extraction

The same set of frequency domain neural features as described in 4.2.4.1 were extracted from pre-ictal and inter-ictal periods. The pre-ictal period was defined as a 30-second long window right before the seizure onset. Another long window (2-4 minute) placed at least 2-minute away from the end of the seizure and the per-ictal period was defined as the inter-ictal period. It was shown that the activity of the neural features was altered in both a daily basis as described by EGM (please see below section 4.3.1) and a minutely basis (i.e. transition between pre-ictal and inter-ictal). To describe only the transition between pre-ictal and inter-ictal states, the features were normalized by the baseline features extracted from the same day recording to offset the daily changes from epileptogenesis. These baseline features were extracted from LFPs during the inter-ictal period.

4.2.5.3 SVM-ENR

Support vector machine with elastic net regularization (SVM-ENR) is a linear classifier which selects only a subset of features to avoid overfitting[68,100,101]. The

relationship between input (X) and output (y), and the solution to build a model are indicated by the following equations:

$$y = X \times \beta + \varepsilon,$$
$$\beta = \arg\min \left[\| y - X \times \beta \|^2 + \text{lambda} \times \| \beta \|^2 \text{ s.t. delta} \geq \| \beta \| \right] \quad (11)$$

The solution can be viewed as a linear regression with both L1 and L2 penalties to avoid the overfitting. The model coefficients (β) are decided with given regularization parameters (Equation 11, lambda and delta)

4.2.5.4 Model building

Pre-ictal state model (PiSM) was built by repeatedly training, validating and testing a SVM-ENR model which classifies neural feature samples from pre-ictal and inter-ictal periods. A 5-fold nested cross-validation was performed for training and testing the classifier. In outer layer CV, 214 seizures were used for the training set and 53 seizures were used for the test set. By using separate groups of seizures for training and test sets, the overfitting and the generalizability between seizures were tested simultaneously. For the outer layer cross validation, 1284 and 8456 samples were extracted from the pre-ictal and inter-ictal period respectively. The samples from the inter-ictal period outnumbered the ones from the pre-ictal period which resulted in an unbalanced dataset for the classification. To address this issue, we divided the samples from the inter-ictal period to 5 groups through a random selection so that each group has the equal number of samples with the pre-ictal samples. The classification was repeatedly performed for 5 different inter-ictal groups while using the same pre-ictal samples so that the loss of information

caused by subsampling is minimized[74]. During the training, the inner layer CVs were performed to optimize the hyperparameters (Equation 11, lambda and delta). Then the classifier was trained with the optimized hyperparameters in the outer layer and tested with the test set.

4.2.5.5 Feature analysis

As described above in 4.2.2.4, a subset of features which are informative to the pre-ictal period was identified. Features of which selected ratio above the threshold were identified, and then the features close to each other were grouped together. An activity of the feature groups during the pre-ictal period was investigated, and those whose activity was altered during the pre-ictal period were identified as informative.

4.3 Results

4.3.1 Characterization of epileptogenesis

4.3.1.1 Regression for progress of epileptogenesis

EGM successfully described the progress of epileptogenesis in multiple rats with the frequency domain neural features. A goodness of fit measured by R squared with the validation set during the cross validation was consistent ($R^2_{val} = 0.724 \pm 0.025$). The test set, which was never shown to the model, was used for purpose of testing the final model. The test set from day -7 to 18 was given to the final model, and the box plot in Figure 16 shows the output of the model. Overall, the model well predicted the relative day to the 1st seizure as the output of the model was well matched with their ground truth (Mean squared error $(MSE)_{ovr} = 23.1$, $R^2_{ovr} = 0.5090$). The median of the output followed the y=x line until the

day 12th where it started to plateau. In the latent period, the model described the progress of epileptogenesis with a small output variance (MSE_{lat} = 3.16). Meanwhile, the output of the model varied more in the active-seizure period (MSE_{act} = 23.9).

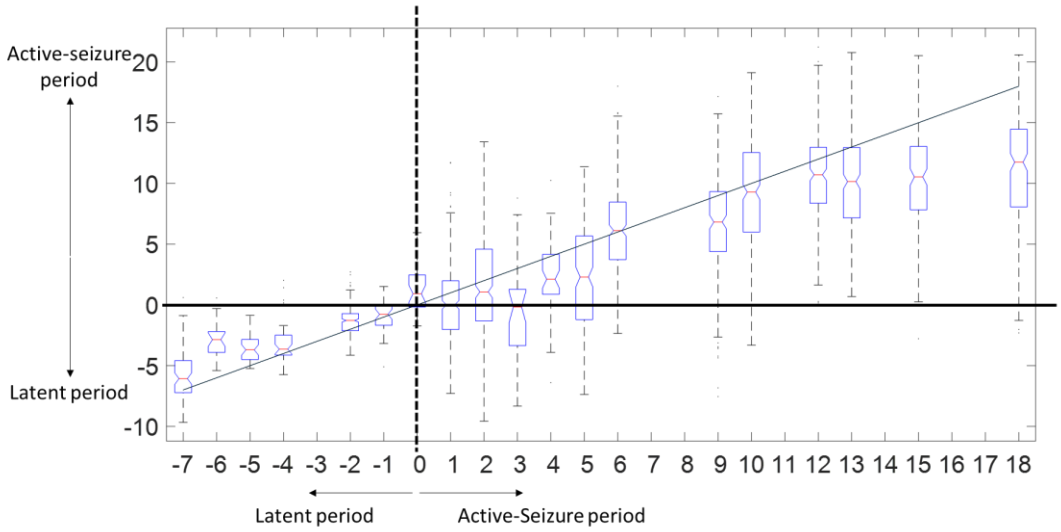

Figure 16. The output of the epileptogenesis regression model (y-axis) with the test set (x-axis: ground truth). In both axes, the values indicate the relative day to Day 0 (1st seizure day, negative: before & positive: after). A y=x line was superimposed to show the desired input output relationship.

4.3.1.2 Informative neural features for epileptogenesis

A few groups of neural features showed an increasing pattern during the pre-ictal period while others showed the opposite pattern (Figure 17). PSD of a low frequency band between 4-60Hz in CA1 gradually increased after the first day of seizure whereas a high frequency band between 70-200Hz in CA1 collapsed at day 0 and bounced back after few days. PSD of CA3 showed a similar pattern with CA1 PSD that a low-frequency band between 4-42Hz gradually increased while a high-frequency band between 230-270Hz decreased at Day 0 and bounced back. A theta band (3-11Hz) COH between CA1 and CA3 showed a complex behavior that it gradually increased between day 0-6 and decreased after

day 6. The linear regression model, which is not available to describe the non-linearity, gave a positive coefficient for this feature group. The beta and low-gamma band (13-47Hz) COH showed a rapid increase after Day 0 and decreased below its latent-period value. Phase difference between CA1 and CA3 showed decrease in the beta (15-42Hz) and high-frequency band (110-252Hz) after Day 0. The decrease of PHASE indicates that the phase of LFP in CA1 became smaller than the phase of LFP in CA3.

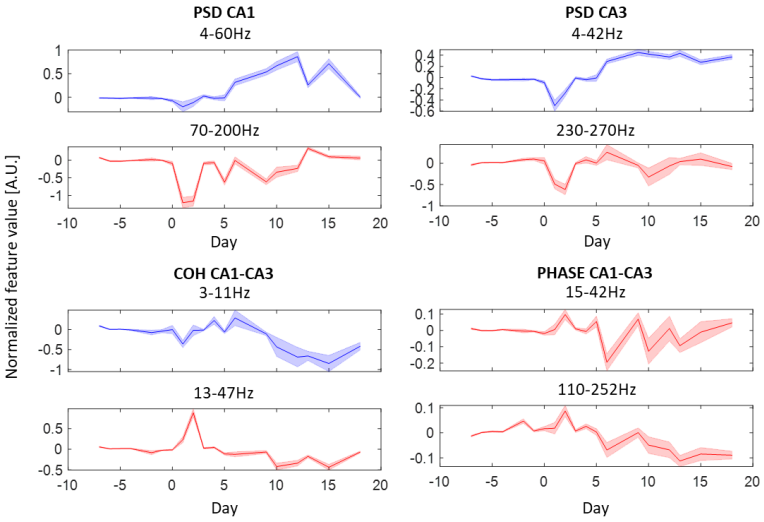

Figure 17. Groups of neural features informative to epileptogenesis. A neural feature's pattern of increase (blue) or decrease (red) during epileptogenesis is shown.

4.3.2 Characterization of pre-ictal state

4.3.2.1 Classification between pre-ictal and inter-ictal period

The classification results show that differences exist in neural activities between pre-ictal and inter-ictal periods. The classifier, PiSM, was tested on the test dataset, and the classification results are plotted in Figure 18B which shows a receiver operation characteristic (ROC) curve with averaged area under curve (AUC, 0.7553) and the

classification accuracy (0.6875) indicated. Then a time series of neural features extracted from 300-second window before the seizure onset was streamed to the classifier. This generated a time series of the classifier output which indicates a likelihood of the seizure onset. The averaged classifier output at each timepoint relative to the seizure onset is plotted in Figure 18C. The classifier output gradually decreased from 120 second before the seizure onset and began to drop rapidly at 60 second before the onset. Then the test dataset was used for measuring the ratio classified as ‘pre-ictal’ at each timepoint (Figure 18D). The ratio began to increase at 80 second before the seizure onset, and around 73% of test set was classified as ‘pre-ictal’ right before the seizure onset (193 of 253 test samples, each sample means one seizure). The averaged ratio classified as ‘pre-ictal’ was around 31% for the samples from inter-ictal period.

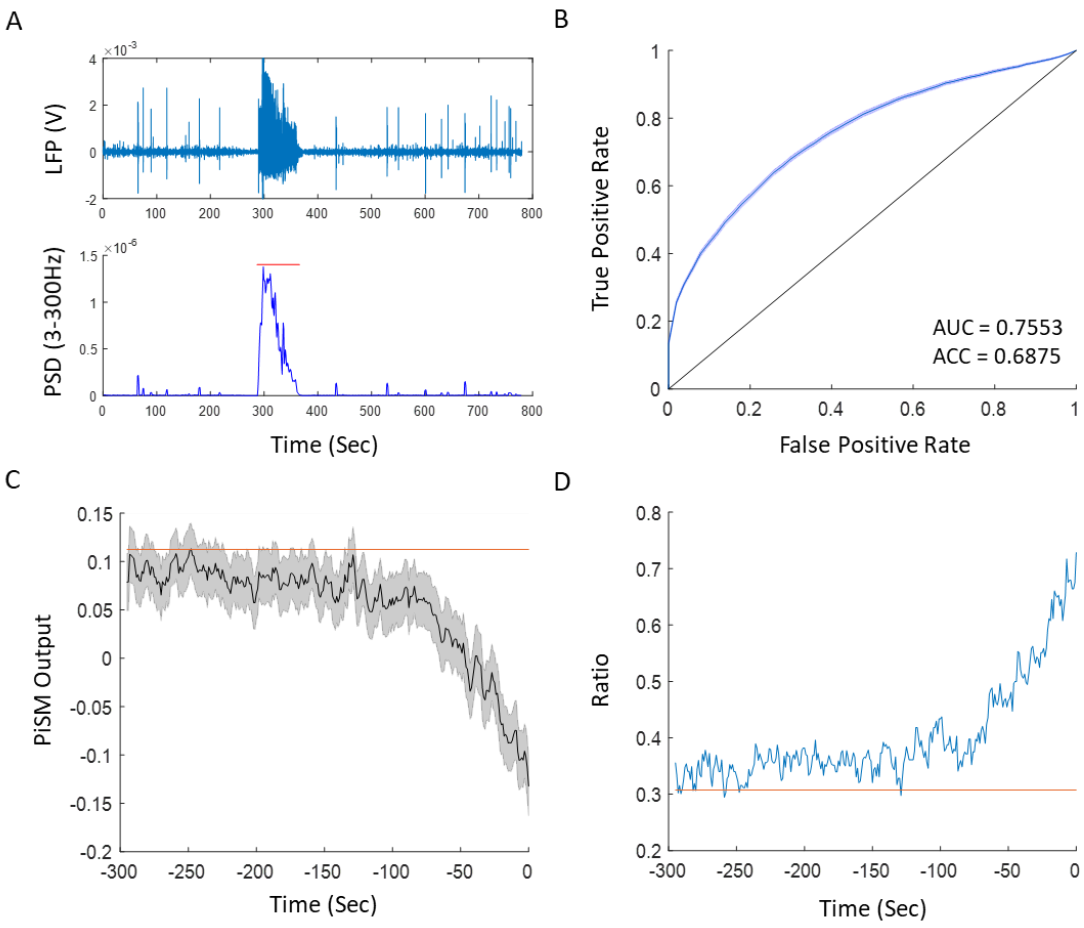

Figure 18. A. An example of hippocampal LFP during a seizure (top) and a seizure detection with the thresholding method (bottom). The seizure is detected and indicated by the red line. B. ROC curve from the classification with the test set. C. Time series of pre-ictal state model (PiSM) output with the confidence interval (shaded area). The average value of the PiSM output during inter-ictal period is indicated by the red line. D. The ratio of classified as pre-ictal for each time point. The average ratio during the inter-ictal period is indicated by a red line.

4.3.2.2 Informative neural features for pre-ictal state

A few groups of neural features showed an increasing pattern during the pre-ictal period while others showed the opposite pattern (Figure 19). A high frequency band PSD between 260-280Hz in CA1 slightly increased during the pre-ictal period. COH between CA1 and CA3 in beta band (25-39Hz) and a high frequency (182Hz) as well as PHASE in

172-174Hz increased during the pre-ictal period. In contrast, low frequency band power in CA1 (4-21Hz) and CA3 (3, 21-33Hz) decreased during the pre-ictal period. Also, low frequency COH (3-7Hz) and phase difference in 53Hz between CA1 and CA3 decreased. Low frequency PSD and COH began to decrease earlier than the other features (~70 seconds before seizure onset). Other features, especially those which increased, started to be altered closer to the seizure onset.

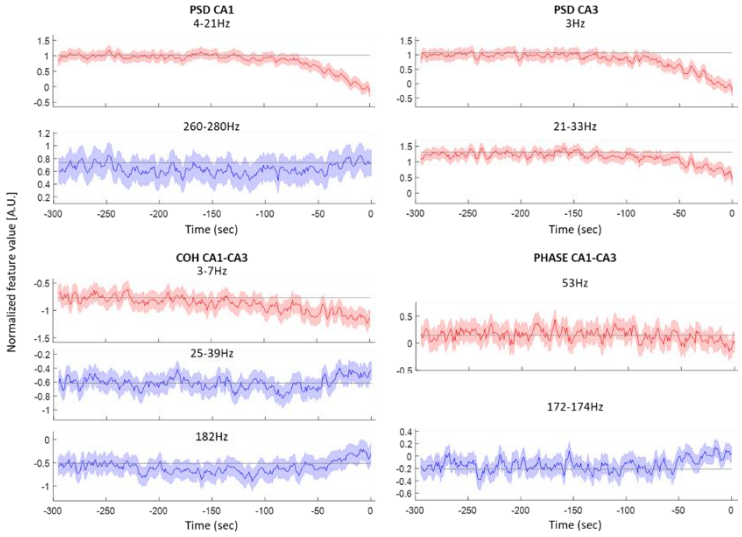

Figure 19. Groups of neural features informative to pre-ictal state. A neural feature's pattern of increase (blue) or decrease (red) during the pre-ictal period is shown.

4.3.3 Hippocampal theta power

It has been repeatedly reported that the hippocampal theta band (4-10Hz) power is related to the epilepsy and seizures, and the theta power was identified as an informative neural feature to a neural state transition during epileptogenesis and the pre-ictal period in our study. In EGM, the theta power showed a pro-seizure characteristic as its level was higher during the active-seizure period than the latent period (Figure 20A). However in

PiSM, the theta power showed an anti-seizure characteristic as it gradually decreased during the pre-ictal period (Figure 20B).

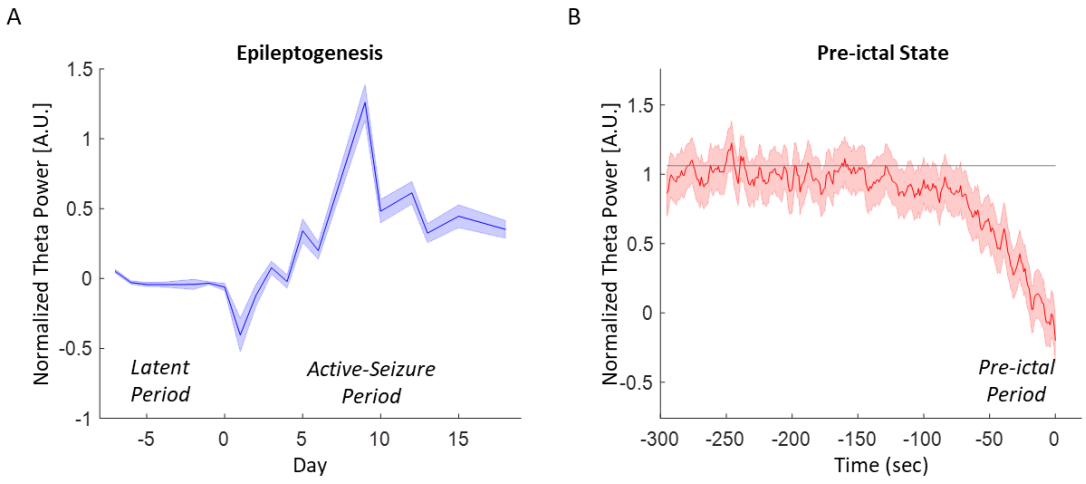

Figure 20. The hippocampal theta power (4-10Hz) during epileptogenesis (A) and the pre-ictal period (B). A. The theta power trace before and after the first seizure day (Day 0) with the confidence interval (shaded area). B. The theta power trace before the seizure onset (Time 0) with the confidence interval (shaded area). The averaged theta power during the inter-ictal period is indicated by the black line.

4.4 Discussion

The data-driven models were constructed to describe neural states during the progress of epileptogenesis and the pre-ictal period in TeNT rats. In addition, by using a feature reduction technique we identified informative neural features. First, EGM which is a linear regression model was able to predict a day relative to the first seizure. The output of EGM during the active-seizure period was clearly different from the active-seizure period, so a long-term susceptibility of seizures can be inferred by the model output. Second, PiSM was able to detect the different behaviors of neural features during the pre-ictal period compared to the inter-ictal period. Therefore, the output of PiSM indicates a short-term seizure susceptibility.

The output of the models can play a surrogate role in investigating the stimulation effect for developing the seizure treatment with neuromodulation. Finding the effective stimulation parameters is the key part of optimizing the treatment. However, it requires a huge amount of time and resources to explore the vast parameter space. Examining the effect on the surrogate instead of the epileptic symptom can save a tremendous amount of time to find effective stimulation parameters. The models were constructed to estimate a susceptibility of seizures, so modulating the model output is expected to change the neural state of the seizure susceptibility. A causality test is required to test if modulating the model output is causal to the epileptic symptom change. The data-driven model can be used for epilepsy treatment only when the causality exists.

A contradictory relationship between the hippocampal theta power and the seizure susceptibility encourages to examine the effect of the theta power modulation via external brain stimulation. In previous studies, Sedigh-Sarvestani-et-al[31] reported an anti-seizure characteristic of the theta power whereas the opposite was observed by Colom-et-al[102] and Desai-et-al[30]. Our results agreed with the literatures by showing both anti- and pro-seizure characteristics of hippocampal theta power (Figure 20). The theta power showed a pro-seizure characteristic in EGM whereas it showed the opposite characteristic in PiSM. Testing the effect of artificially increased theta power via external brain stimulation on seizure can validate the use of the theta power as a surrogate as well as can provide a better understanding of the theta power in epilepsy.

CHAPTER 5. MODULATION OF HIPPOCAMPAL EPILEPTIC NEURAL STATES VIA MEDIAL SEPTUM OPTOGENETIC STIMULATION

5.1 Introduction

Stimulation parameters which successfully suppressed seizures in both human epilepsy patients and animal models of epilepsy were not consistent, were rather various according to the previous studies. In human patients, both 130Hz biphasic pulses of electrical stimulation in the hippocampus[103] and much slower 5Hz bipolar electrical stimulation in the fornix[104] suppressed seizures. An optogenetic stimulation with constant light in the hippocampal GABAergic neurons[105] and 130Hz light in the dentate gyrus GABAergic neurons[106] suppressed seizures in the rodent kainic acid model. These results suggest that there does not exist one ideal stimulation parameter for the seizure suppression but potentially depends on the stimulation target, subject-specific anatomical or pathological characteristic and so on.

A selection of stimulation parameters is important to improve the stimulation effectiveness for epilepsy treatment as different parameters can induce different effects. However, testing a set of stimulation parameters requires a lot of time and resources. An effective stimulation parameter set found in one subject may not be generalizable across the subjects due to the variability of the stimulation effect between subjects[107–109]. Moreover, a natural or pathological neural state transition can yield a change of stimulation effect within the same subject[110–112]. In the previous chapter, we constructed data-driven

models which can be used as a surrogate of the epileptic symptom. Looking at the effect of stimulation on the surrogates rather than the epileptic symptom can save time and resources. However, the parameter space is still vast to find the optimal set in a short time.

In this chapter, I developed an effective way to modulate a neural feature or neural state model by applying the optimization platform introduced in chapter 3. A few modifications were required for applying the optimization for epileptic rats as they show frequent ictal discharges which hides the effect of the stimulation. In the first experiment, the medial septum (MS) optogenetic stimulation parameters for increasing the hippocampal theta power was optimized. Second, MS optogenetic stimulation parameter was optimized for effectively inducing the anti-seizure state by regulating the output of the pre-ictal state model (PiSM, Chapter 5). The subject-specific optimal stimulation parameter found by the optimizer can improve the effectiveness of the stimulation by solving an issue of variability in stimulation effects between subjects.

5.2 Methods

5.2.1 Animal preparation

An adult male Sprague-Dawley rat underwent two surgical procedures as described in Laxpati-et-al[47]. All procedures were approved by the Emory University Institute for Animal Care and Use Committee. The first survival surgery was an injection of a viral vector (AAV5-hSyn-hChR2(H134R), 1.8µL of 10^{13} particles/mL) to transfect the neurons in MS. A second survival surgery was performed for the injection of TeNT and the implantation of the electrode into the hippocampus, and the implantation of the fiber optic ferrule into the MS. 10-15 ng of TeNT was injected into the dorsal hippocampus centered

at 3.50mm posterior and 2.80mm lateral to bregma using a pulled glass pipette attached to an injector. Five 2.0mm stainless steel screws were mounted on the skull for the structural support and to serve as the reference and ground for a multi electrode array (MEA). The 16-channel MEA (Tucker Davis Technologies, Alachua, FL), consisting of two rows of eight channels offset by 1mm, was advanced ventrally into the brain while single unit activity was observed from both the CA3 and CA1 regions of the hippocampus. After the MEA was placed in the desired location, the ferrule was driven into the MS. The craniotomy was sealed with dental acrylic to secure the electrode and the ferrule.

5.2.2 Inter-ictal spikes removal

A removal of inter-ictal spikes was required for measuring the stimulation effect on neural features in epileptic animals. Inter-ictal spikes (IISs) accompany a high amplitude local field potential (LFP) which affects a wide frequency band of power spectral density (PSD) and coherence. This can hinder identifying the effect of stimulation on the frequency domain neural features. IISs in LFPs were removed by thresholding the wide band PSD (1-30Hz). A sum of the PSD (1-30Hz) was calculated in 16-channel LFP by using a sliding window (0.5 second width and 0.1 second resolution), and a threshold value for each channel was decided as the following equation:

$$Threshold = 75\%\ percentile + 1.5 \times (75\%\ percentile - 25\%\ percentile) \quad (12)$$

Short LFP segments of which 1-30Hz PSD was above the threshold were classified as IIS. An example of IIS detection is shown in Figure 21. LFPs and their PSD during the

baseline (black) and the MS optogenetic stimulation (Figure 21 blue, nested pulse-train: 50I-5.2Hz-67.8Hz) are shown for before and after IIS removal. A huge power throughout the wide frequency band due to IIS was suppressed and the effect of the stimulation, peaks around 21, 30 and 67.8Hz in PSD, emerged after removing IISs.

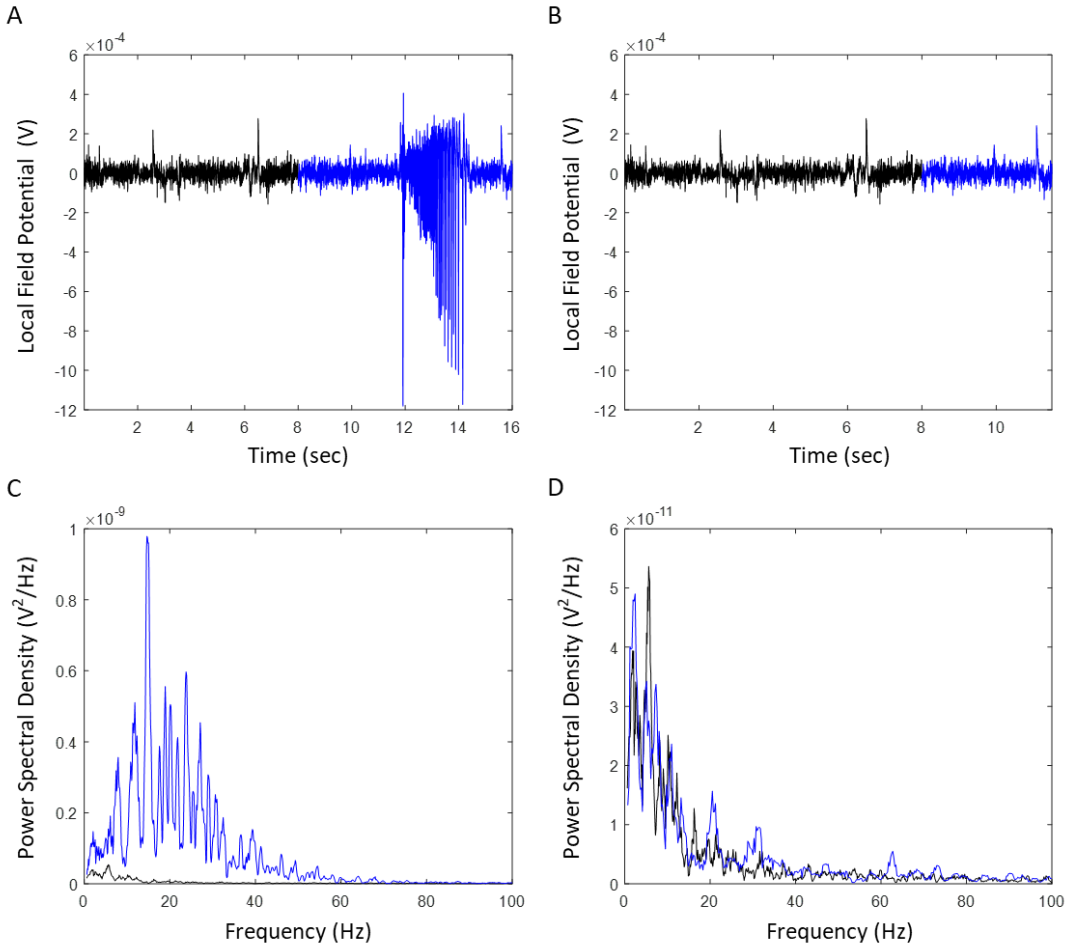

Figure 21. Inter-ictal spikes (IISs) removal. A-B. Hippocampal LFPs during the baseline (black) and stimulation (blue) before (A) and after (B) IISs were removed. C-D. PSD of the corresponding LFPs before (C) and after (D) IIS removal.

5.2.3 In vivo optimization for theta power

The optimal MS optogenetic stimulation parameter set for increasing the theta power was found by leveraging Bayesian optimization (BaO) when the rats were freely behaving. The *in vivo* BaO algorithm was implemented with Gaussian process (GP) model and UCB acquisition function (nu = 0.4, Equation 9) as described in Chapter 3. Two parameters of nested pulse-train (Figure 10A), a train-frequency and a pulse-frequency were optimized while an intensity (50I, 1I = 1mW/mm^2), a pulse-width (4ms) and a train-width (75ms) were fixed. Each optimization sample for testing a stimulation parameter set consists of 8 second baseline and 8 second stimulation. The theta power was calculated after inter-ictal spikes were removed from LFPs. If remained LFP after IIS removal was shorter than 3 second, the corresponding sample was abandoned and repeated. Then the objective function, the theta power change between baseline and the stimulation, was calculated and used for updating the GP model. The parameter space was explored with the random search for the first 10 samples, and then the intelligent search followed for next 30 samples. During the intelligent search, a next sample of the stimulation parameter set was selected by the acquisition function (UCB, Equation 9). Optimization was finished after the 40th sample, and the optimal parameter set was identified according to the GP model.

5.2.4 In vivo optimization for pre-ictal state model

The optimal stimulation parameter set for inducing anti-seizure neural state was found by leveraging BaO when the rats were freely behaving. The goal of the optimization was to increase the output of PiSM (PiSM score) where a high score indicates a neural state of less seizure likelihood (Chapter 4, Figure 18). The same optimization configuration with the theta power optimization was used. To reflect the natural oscillation of the PiSM score,

a new form of the objective function was designed. A baseline pattern of the PiSM score showed that the scores from two consecutive time window were negatively correlated (Figure 22A). Therefore, the PiSM score change between two windows was larger when the pre-stimulation score was negative and the score change was smaller when the pre-stimulation score was positive (Figure 22B). The state-dependency of the PiSM score can confuse the optimization process as it cannot distinguish between the stimulation effect and the natural oscillation. To solve this issue, the following equation (Equation 13) was used for calculating the objective function which can incorporate both pre-stimulation state and the stimulation effect. Two values were multiplied where the first one indicates the pre-stimulation score and the second one indicates the score change induced by the stimulation effect and the natural state oscillation. Both values were added by 1 to make them positive.

$$Objective\ Function = (1 + PiSM\ score1) \times (1 + PiSM\ score\ change) \quad (13)$$

The objective function was calculated and used for updating the GP model. The first 10 samples were for the random search, and then the intelligent search was performed for next 30 samples. During the intelligent search, a next sample of stimulation parameter set was selected by the acquisition function (UCB, Equation 9). Optimization was finished after the 40^{th} sample, and the optimal parameter set was identified according to the GP model.

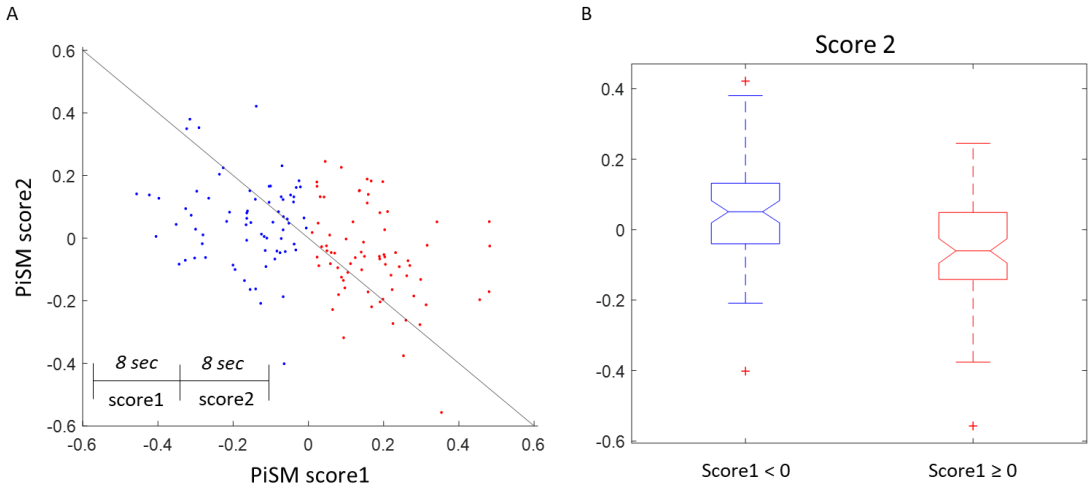

Figure 22. A natural oscillation of PiSM score. A. PiSM scores from two consecutive 8 second windows showed a negative relationship (Blue: score1 < 0 and red: score1 ≥ 0). B. A comparison of score2 between negative (blue) and positive (red) score1.

5.3 Results

5.3.1 Maximization of theta power

The optimal parameter set for increasing the theta power was found by testing 40 parameter sets through BaO. The series of the objective function, the theta power change, shows that the parameter sets tested during the intelligent search (11^{th}-40^{th}) induced a large theta power increase than the parameter sets tested during the random search (1^{st}-10^{th}, Figure 23A). An example of GP model shows that the effectiveness of the stimulation for increasing the theta power depends on selecting a right combination of a train-frequency and a pulse-frequency (Figure 23B). The optimal parameter was verified by comparing its effectiveness to sham and a sub-optimal parameter set. The parameter set which induced a zero or closest to zero theta power change was selected as the sub-optimal parameter set. Five different animals were tested, and each animal underwent 40 different trials for each parameter set (i.e. sham, optimal or sub-optimal). The optimal stimulation parameter set

induced the largest change (35.2% increase in average) from the baseline theta power (Figure 23C). Also, the level of theta power was highest when the optimal stimulation parameter set was applied compared to the sham or the sub-optimal parameter set (Figure 23D).

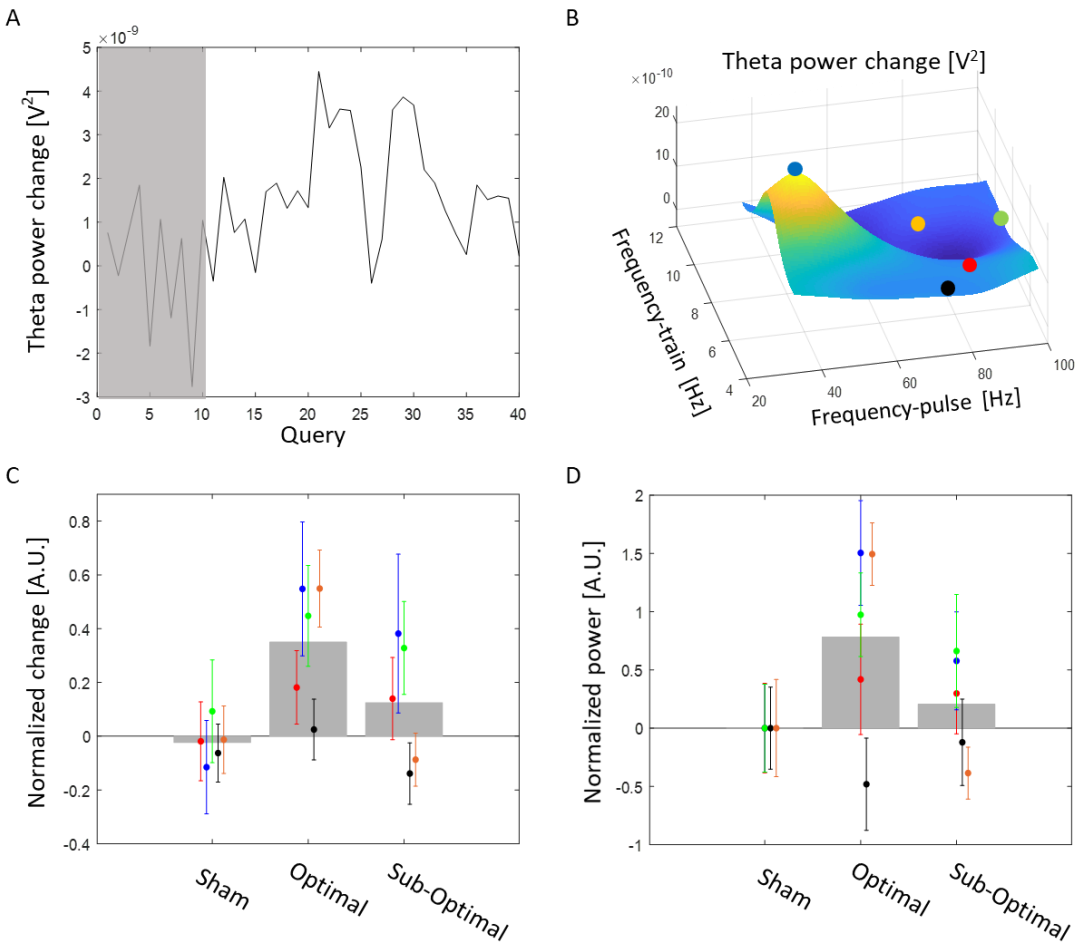

Figure 23. Stimulation parameter optimization for hippocampal theta power maximization. A. Theta power change for each sample (1st-10th: random search and 11th-40th: intelligent search). B. An example of GP model at the end of the optimization. The optimal parameters for 5 different animals are superimposed. C-D. A comparison of the theta power change (C) and the theta power (D) induced by sham, optimal and sub-optimal parameters in 5 different animals. Every dot and error bar represent a mean and the confidence interval of 40 trials.

5.3.2 Induction of anti-seizure neural state

The optimal parameter set for inducing the anti-seizure neural state is the one maximizes the PiSM score, and it was found by testing 40 parameter sets through BaO. The series of the objective function shows that the parameter sets tested during the intelligent search (11^{th}-40^{th}) induced a large PiSM score increase than the parameter sets tested during the random search (1^{st}-10^{th}, Figure 24A). An example of GP model shows that the effectiveness of stimulation for increasing the objective function depends on selecting a right combination of a frequency-train and a frequency-pulse (Figure 24B). The optimal parameter set was verified by comparing its effectiveness to sham and a sub-optimal parameter set. The parameter set which minimized the objective function (Equation 13) was selected as the sub-optimal parameter set. The optimization experiment was performed in five different animals, and two animals were tested in two days while the others were tested once. After optimization, the animal underwent 40 different trials for each parameter set (i.e. sham, optimal or sub-optimal). The optimal set induced the largest score increase (Figure 24C) and the highest score level (Figure 24D). In 3 different animals, the optimal stimulation parameter set increased the PiSM score. The optimal set increased PiSM score more than sham in 4 animals and than the sub-optimal sets in 3 animals. Also, the level of PiSM score was higher with the optimal set than the others in 3 different animals.

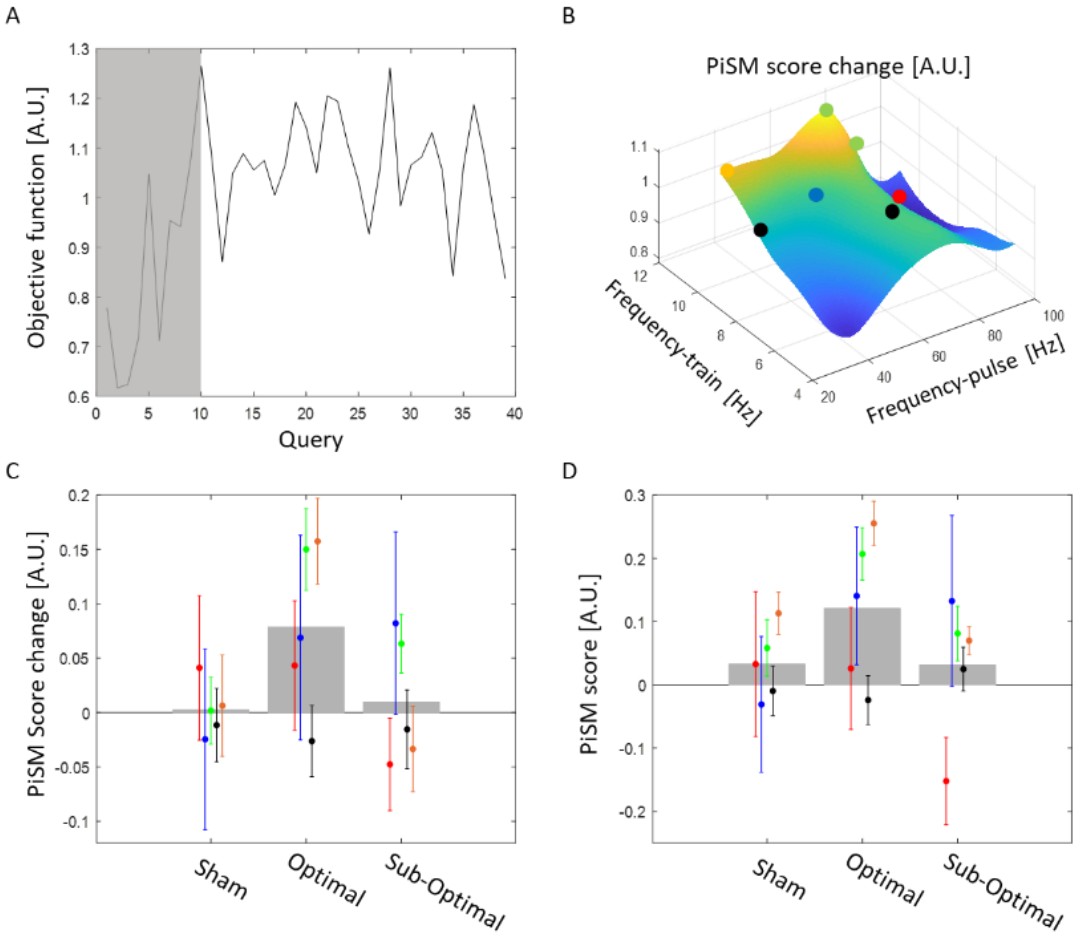

Figure 24. Stimulation parameter optimization for increasing PiSM score. A. Objective function described in Equation 13 for each sample (1st-10th: random search and 11th-40th: intelligent search). B. An example of GP model at the end of the optimization. The optimal parameters for 5 different animals (7 trials) are superimposed. C-D. A comparison of the PiSM score change (C) and the PiSM score level (D) induced by sham, optimal and sub-optimal parameters in 5 different animals. Every dot and error bar represent a mean and the confidence interval of 80 trials (green and black, 40 trials each for two different days) or 40 trials (others, one day).

5.3.3 State dependency of stimulation effect

The effectiveness of the optimal stimulation parameters for increasing the hippocampal theta power or the PiSM score depended on the pre-stimulation state (Figure 25). The theta power increase induced by sham, the optimal or the sub-optimal parameter

sets was compared between a high-theta and a low-theta pre-stimulation state (Figure 25A). The pre-stimulation theta power above its median was defined as a high-theta state and the one below its median was defined as a low-theta state. The amount of the increased theta power induced by the optimal stimulation parameter was much lower when the pre-stimulation power was high. The theta power decreased with sham or sub-optimal parameters when the pre-stimulation power was high. Similarly, the PiSM score increase induced by sham, the optimal or the sub-optimal parameter sets was compared between a high-PiSM and a low-PiSM pre-stimulation state (Figure 25B). The positive pre-stimulation PiSM score was defined as a high-PiSM state, and the negative one was defined as a low-PiSM state. The optimal stimulation parameters were able to increase the PiSM score when the pre-stimulation score was low but only maintained the score when the pre-stimulation score was high. Therefore, the optimal stimulation induced a transition from the pro-seizure state to the anti-seizure state and maintained the anti-seizure neural state. The sub-optimal parameters did not effectively increase or maintain the PiSM score than sham which showed the natural oscillation of the PiSM score.

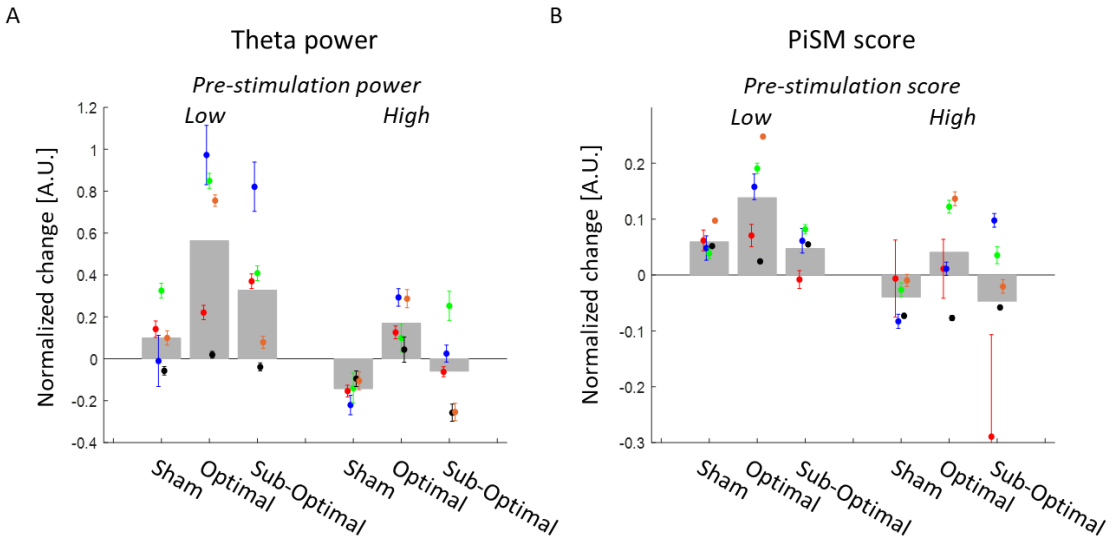

Figure 25. A state-dependency of the stimulation effect. The normalized change of the hippocampal theta power and the PiSM score was compared between a low and high pre-stimulation state. A. The theta power change when the pre-stimulation theta power was above (left) or below (right) the median. B. The PiSM score change when the pre-stimulation score was above (left) or below (right) zero.

5.4 Discussion

The *in vivo* BaO platform was modified to become suitable for epileptic animals where abnormal neural activities such as inter-ictal spikes emerge frequently. The modified BaO was applied to find the optimal MS optogenetic parameters which can effectively increase the theta power or induce anti-seizure neural state by increasing the PiSM score.

A variability in the stimulation effect was observed for both between subjects and within a subject. The variability between subjects was presented in two forms. First, the optimal parameter sets found by the optimization were spread across the entire parameter space (Figure 23B and Figure 24B). Second, the effectiveness of the optimal parameter sets was not consistent. The amount of increase in the theta power or the PiSM score induced by the optimal parameters was various across the animal (Figure 23C-D and Figure

24C-D). A high variability in the stimulation effect within a subject was observed during the multiple trials in the same day. Varying stimulation effects were observed when the identical stimulation parameter set (i.e. optimal or sub-optimal) was applied as indicated by the high confidence intervals of the theta power and the PiSM score modulation (Figure 23C-D and Figure 24C-D).

The high variability may originate from the state-dependency of the stimulation effect. The identical stimulation parameter set induced different effects depending on the pre-stimulation states (Figure 25). In addition, the state-dependency of the stimulation effect can potentially explain the low effectiveness of the optimal parameters observed in few subjects. The sub-optimal parameters were more effective for increasing the PiSM score than the optimal parameters in two animals when the pre-stimulation score was low (Figure 25, blue and black). This implies that the effective parameter set needs to be searched again if a state transition occurs.

The state-dependent Bayesian optimization (SDBaO) which incorporates the pre-stimulation state can improve the effectiveness of the stimulation. The SDBaO outperformed the standard Bayesian optimization by learning a state-dependent policy which selects the optimal stimulation parameters based on the pre-stimulation state (Connolly-et-al, *in press*). The modulation of the theta power and the PiSM score can be improved by applying the SDBaO. The variability in the stimulation effect and its state-dependency are already proven, and thus incorporating the pre-stimulation state will improve the stimulation effectiveness.

CHAPTER 6. VALIDATION OF DATA-DRIVEN APPROACH BY IDENTIFYING CAUSAL LINK BETWEEN MODULATION OF HIPPOCAMPAL NEURAL STATES AND SEIZURE CHARACTERISTICS

6.1 Introduction

Finding the effective stimulation parameters is the key part of optimizing the treatment[113–115]. It requires a large amount of time and resources to explore the vast parameter space. Examining the effect on the surrogates instead of directly on epileptic symptoms can save tremendous time to find effective stimulation parameters. In previous chapters, the data-driven model was constructed to describe a susceptibility of seizures. The optimization tool was demonstrated that it can find effective stimulation parameters to modulate a neural feature or the output of the data-driven model. The last step of the data-driven surrogate approach is to validate the surrogate neural state models by testing a causal relationship between epileptic symptom and the modulation of surrogates.

A few studies have shown that the modulation of neural features can affect the behavioral output or pathological symptoms[23,24,116]. Hultman-et-al constructed a neural state model and showed that an injection of chemical agent changed both output of the neural state model and the depression symptom[116]. Fuhrmann-et-al showed that modulation of the peak frequency in the hippocampal theta band power by delivering the MS optogenetic stimulation can control the locomotion speed[24]. Gangadharan-et-al also showed that the hippocampal theta power externally modulated via optogenetic stimulation

was correlated with a performance of exploration[23]. However, it still needs to be done to improve the efficacy of behavioral or pathological intervention by optimizing the stimulation parameters or finding more appropriate neural features in the wider space.

In this study, we tested and compared various stimulation strategies to find the optimal one as well as to investigate the causal relationship between neural feature modulation and the epileptic symptom (i.e. seizure). We tested three stimulation strategies including one conventional approach and two surrogate approaches. The conventional approach applied stimulation parameters selected empirically. The first surrogate approach applied the optimal parameter set to increase the hippocampal theta power, a well-known epileptic neural feature[30,31,102], and the second surrogate approach applied the optimal parameter set to induce an anti-seizure neural state. To induce the anti-seizure neural state, a susceptibility of seizures was inferred by the output of pre-ictal state model (PiSM) described in Chapter 4. The optimization for finding effective parameters was performed as described in Chapter 5. The therapeutic efficacy of these strategies was compared with the sham trials, and the optimal parameters to increase the theta power was most effective to suppress seizures.

6.2 Methods

6.2.1 Animal preparation

An adult male Sprague-Dawley rat underwent two surgical procedures as described in Laxpati-et-al [6]. All procedures were approved by the Emory University Institute for Animal Care and Use Committee. The first survival surgery was an injection of a viral vector (AAV5-hSyn-hChR2(H134R), 1.8μL of 10^{13} particles/mL) to transfect the neurons

in the medial septum (MS) as a part of another study. A second survival surgery was performed for the injection of TeNT and the implantation of the electrode into the hippocampus, and the implantation of the fiber optic ferrule into the MS. 10-15 ng of TeNT was injected into the dorsal hippocampus centered at 3.50mm posterior and 2.80mm lateral to bregma using a pulled glass pipette attached to an injector. Five 2.0mm stainless steel screws were mounted on the skull for the structural support and to serve as the reference and ground for a multi electrode array (MEA). The 16-channel MEA (Tucker Davis Technologies, Alachua, FL), consisting of two rows of eight channels offset by 1mm, was advanced ventrally into the brain while single unit activity was observed from both the CA3 and CA1 regions of the hippocampus. After the MEA was placed in the desired location, the ferrule was driven into the MS. The craniotomy was sealed with dental acrylic to secure the electrode and the ferrule.

6.2.2 Overview of causality test

Three different stimulation strategies were tested and compared with sham stimulation to evaluate the therapeutic effectiveness of the data-driven surrogate approach and the conventional approach. (1) 7Hz stimulation (Intensity: 50I, 1I = 1mW/mm^2, frequency: 7Hz and pulse-width: 10ms): the first stimulation strategy, as a part of the conventional approach, applied the stimulation parameter empirically selected based on the previous study that 7Hz pulsatile electrical stimulation in the hippocampus suppressed the seizures[30]. The data-driven surrogate approach was used for developing the second and third stimulation strategies. (2) Theta stimulation: the second strategy applied the optimal stimulation parameters to increase the hippocampal theta power which showed the anti-seizure characteristic during the pre-ictal period (Chapter 4). (3) PiSM stimulation: the

third strategy applied the optimal stimulation parameters to increase the output of pre-ictal state model (PiSM score) of which high score indicates the estimated anti-seizure neural state. (4) Sham stimulation: sham stimulation was performed by not applying the stimulation while keeping the other experimental setup the same. Each strategy was tested once in 5 different rats with a randomized order. Only one test was conducted per day, and the beginning time of the experiment was consistent to not be affected by the circadian rhythm.

A timeline for the experiment is shown in Figure 26. After a rat was connected to the headstage and the patch cable, the rat was given 15 minutes to habituate to the experimental space. Then the baseline recording was conducted for one hour. Next, *in vivo* optimization was performed to find the optimal parameter for theta power maximization or PiSM score regulation. Two strategies (Sham and 7Hz) did not require the optimization as their stimulation parameters were already decided (7Hz or no stimulation), but the optimization was still performed to control the potential residual stimulation effect during the optimization. A brief period (10 minutes) was given to washout the stimulation effect during the optimization. Then, the stimulation with 7Hz or the optimal parameter set was applied for one hour continuously. Lastly, one-hour recording was performed to test the post-stimulation effect.

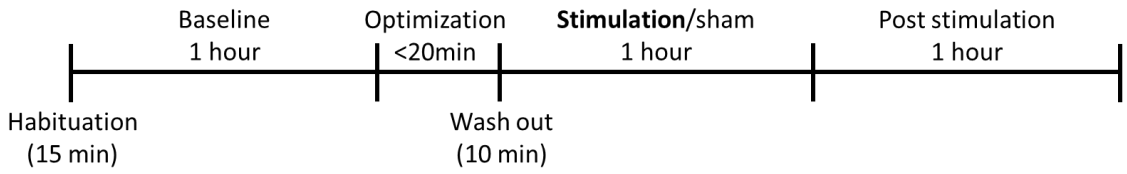

Figure 26. Experimental diagram for causality test. The seizures were detected for three phases – baseline, stimulation and post-stimulation.

6.2.3 In vivo optimization

In vivo Bayesian optimization described in Chapter 5 was performed to find the optimal parameters for the surrogate approaches. Two frequencies, a train-frequency and a pulse-frequency were optimized to effectively increase the hippocampal theta power or the PiSM score. The intensity (50I, 1I = 1mW/mm^2) and the pulse-widths (Train: 75ms and pulse: 4ms) were fixed.

6.2.4 Seizure detection and quantification

The seizures were detected with the low-frequency (3-300Hz) power thresholding method as described in Chapter 4. A time series of the wide band PSD was calculated from 3 second segments of the hippocampal LFP with the 1 second moving window. The thresholding value was calculated by the standard deviation of bottom 70% PSD values multiplied by 3, and a series of segments (>20 sec) with their PSD above the threshold was defined as a seizure (Figure 18A, Chapter 4). The video was used to confirm seizures to avoid false detection. After seizures were detected, the number of seizures and the total time of seizures were measured. If a seizure was trimmed due to the seizure onset or termination outside of the experimental window, it was counted as one seizure but the time spent only during the experiment was measured as a seizure length. If a seizure length is

not clearly measurable due to a disconnection between the headstage and the electrodes, the corresponding trial was not included for the analysis of the total time of seizures (indicated as * in **Table** 1-8).

6.2.5 Statistical test

A seizure frequency and total seizure time were calculated and used to find stimulation effects and compare the stimulation strategies. First, a paired t-test was conducted to investigate the stimulation effect during the stimulation and post-stimulation phases. Then, a three-way ANOVA with the model including the two-factor interactions was conducted to test the effects of multiple factors (i.e. experimental phase, stimulation strategies and animals). Lastly, Tukey's honest significant difference (HSD) criterion post hoc test was conducted to calculate adjusted p-values by reflecting the multiple comparisons. These three tests were performed again for the normalized seizure frequency and the normalized total seizure time. The seizure frequency and the seizure total time during the stimulation and post-stimulation phases were normalized to the one from the baseline phase (Equation 14, *S* is a seizure frequency or total seizure time). All statistical analyses were performed in MATLAB.

$$S_{normlized} = \frac{S_{stimulation/post} - S_{baseline}}{S_{baseline}} \quad (14)$$

6.3 Results

6.3.1 Seizure frequency

The number of seizures per hour (i.e. seizure frequency) was measured during baseline, stimulation and the post-stimulation phases to compare the effectiveness of the stimulation strategies (Table 2-Table 5). The P-values from the statistical analyses are shown in Table 6 and Table 7. The 3-way ANOVA test for the raw seizure frequency and the normalized seizure frequency showed that the stimulation strategy and the animal subject had effects on the seizure frequency (Table 6, α=0.05). The results of ANOVA can be interpreted as that each stimulation strategy induced different effects on the seizure frequency and the variability between subjects made the animal one of significant factors. The stimulation strategy to maximize the theta power (i.e. Theta stimulation) was the most promising method among the tested stimulation strategies to decrease the frequency of seizures (Figure 27). The number of seizures was decreased by 43% on average with Theta stimulation (Figure 27B). When Theta stimulation was applied, the number of seizures was decreased in 4 out of 5 animals while maintained in only 1 animal compared to the baseline (Table 4). This result was contrasted with Sham where the seizure frequency decreased in 2 animals, increased in 1 animal and unchanged in 2 animals (Table 2). The statistical significance, which was observed in the paired t-test between baseline and stimulation phases of Theta stimulation, was not observed anymore when the p-value was adjusted (Tukey's HSD) to consider the multiple comparisons (Table 7). A similar pattern was observed during the post-Theta stimulation phase. The seizure frequency was decreased about 30% compared to the baseline whereas the seizure frequency was increased by 17% during the post-Sham phase (Figure 27). The number of seizures was decreased in 3 animals and unchanged in the other 2 animals during the post-Theta phase compared to the baseline (Table 4). Meanwhile, this pattern of the decreased seizure number was not

observed in post-Sham phase where the number of seizures decreased in 1 animal and increased in other 2 animals compared to the baseline (Table 2). The other stimulation strategies did not decrease the seizure frequency more than Sham (Figure 27). A variability between trials was observed in the effect of 7Hz stimulation as the number of seizures maintained or increased in 2 animals respectively and decreased in the other animal compared to the baseline (Table 3). The optimal stimulation parameters to increase the PiSM score increased the seizure frequency during and after the stimulation (40% and 63% respectively) compared to the baseline (Figure 27B).

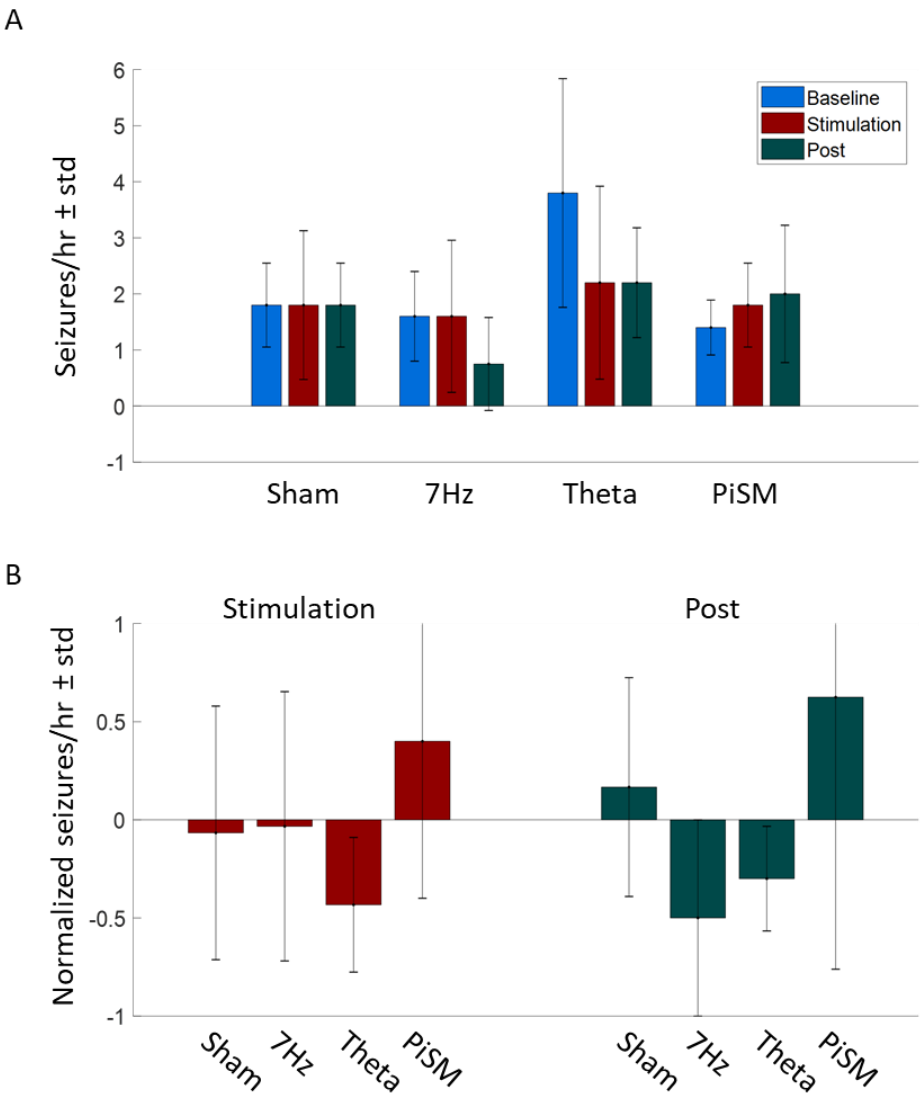

Figure 27. The number of seizures per hour (i.e. seizure frequency) to compare the effectiveness of the stimulation strategies. A. The raw seizure frequency with the standard deviation (error bar). B. The seizure frequency normalized to the baseline to identify the effect during and after the stimulation. The error bar indicates the standard deviation.

Table 2. The raw number of seizures for testing Sham

Number of seizures in 1 hour (normalized number): **Sham**

Rat ID	Session order	Baseline	Stimulation	Post
1	2	2 (0)	4 (1)	3 (0.5)
2	2	2 (0)	2 (0)	2 (0)
3	3	1 (0)	1 (0)	2 (1)
4	1	3 (0)	2 (-0.33)	1 (-0.67)
5	4	1 (0)	0 (-1)	1 (0)
	Mean ± std	1.8±0.75 (0±0)	1.8±1.33 (-0.07±0.65)	1.8±0.75 (0.17±0.56)

Table 3. The raw number of seizures for testing 7Hz stimulation

Number of seizures in 1 hour (normalized number): **7Hz**

Rat ID	Session order	Baseline	Stimulation	Post
1	1	3 (0)	4 (0.33)	*
2	3	1 (0)	2 (1)	0 (-1)
3	2	1 (0)	1 (0)	1 (0)
4	4	2 (0)	1 (-0.5)	2 (0)
5	3	1 (0)	0 (0)	0 (0)
	Mean ± std	1.6±0.8 (0±0)	1.6±1.36 (0.16±0.49)	0.75±0.83 (-0.25±0.43)

Table 4. The raw number of seizures for testing Theta stimulation

Number of seizures in 1 hour (normalized number): **Theta**

Rat ID	Session order	Baseline	Stimulation	Post
1	4	6 (0)	3 (-0.5)	4 (-0.33)
2	1	6 (0)	5 (-0.17)	2 (-0.67)
3	4	1 (0)	1 (0)	1 (0)

Table 4 continued

4	2	4 (0)	2 (-0.5)	2 (-0.5)
5	2	2 (0)	0 (-1)	2 (0)
	Mean ± std	3.8±2.04 (0±0)	2.2±1.72 (-0.43±0.34)	2.2±0.98 (-0.3±0.27)

Table 5. The raw number of seizures for testing PiSM stimulation

Number of seizures in 1 hour (normalized number): **PiSM**

Rat ID	Session order	Baseline	Stimulation	Post
1	3	1 (0)	3 (2)	4 (3)
2	4	2 (0)	2 (0)	2 (0)
3	1	1 (0)	1 (0)	1 (0)
4	3	2 (0)	2 (0)	1 (-0.5)
5	1	1 (0)	1 (0)	*
	Mean ± std	1.4±0.49 (0±0)	1.8±0.75 (2±1.22)	2.5±1.5 (0.63±1.39)

Table 6. Three-way ANOVA for the raw and normalized number of seizures

ANOVA: **Raw** number of seizures in 1 hour

Source	F	Prob>F
Experimental phase (baseline/stimulation/post stimulation)	0.92	0.4148
Stimulation strategy	6.53	0.0025
Animal	16.56	<0.0001
Experimental phase*Stimulation strategy	2.15	0.0874
Experimental phase*Animal	1.93	0.1065
Stimulation strategy*Animal	1.75	0.1241

ANOVA: **Normalized** number of seizures in 1 hour

Source	F	Prob>F
Experimental phase (baseline/stimulation/post stimulation)	0.18	0.6767
Stimulation strategy	5.49	0.0173
Animal	5.45	0.0136
Experimental phase*Stimulation strategy	0.74	0.5515
Experimental phase*Animal	1.78	0.2089
Stimulation strategy*Animal	2.58	0.0715

Table 7. P-values from paired t-test and Tukey's honset significant difference criterion post-hoc test.

Raw number of seizures in 1 hour			
Comparison		Raw P-value	Adjusted P-value
Sham-baseline	Sham-stimulation	1	1
Sham-baseline	Sham-post	1	1
Sham-stimulation	Sham-post	1	1
7Hz-baseline	7Hz-stimulation	1	1
7Hz-baseline	7Hz-post	0.1817	1
7Hz-stimulation	7Hz-post	0.7117	1
Theta-baseline	Theta-stimulation	0.0349	0.1249
Theta -baseline	Theta-post	0.0993	0.1249
Theta-stimulation	Theta-post	1	1
PiSM-baseline	PiSM-stimulation	0.3739	0.9995
PiSM-baseline	PiSM-post	0.6042	0.9916
PiSM-stimulation	PiSM-post	1	1
Normalized number of seizures in 1 hour			
Comparison		Raw P-value	Adjusted P-value
Sham-stimulation	7Hz-stimulation	0.9080	1
Sham-stimulation	Theta-stimulation	0.2688	0.9183
Sham-stimulation	PiSM-stimulation	0.1079	0.7863
Sham-post	7Hz-post	0.2560	0.7362
Sham-post	Theta-post	0.1148	0.7863
Sham-post	PiSM-post	0.6130	0.8049

6.3.2 Total seizure time

The total seizure time was calculated by measuring and summing the length of all seizures during the one-hour recording, and it was used to identify the effect of the stimulation strategies. The P-values from the statistical analyses are shown in Table 12 and Table 13. The 3-way ANOVA test for the raw total seizure time showed that the stimulation strategy had effects, and the same test for the normalized total seizure time showed that the animal subject had effects (Table 12, α=0.05). The results of ANOVA can be interpreted as that each stimulation strategy induced different effects on the seizure frequency and the variability between subjects made the animal one of significant factors. Similarly to the seizure frequency test results, there was a tendency of decreased total seizure time when

Theta stimulation was applied while it was not observed by the other stimulation strategies or Sham (Figure 28). First, the total seizure time during the stimulation phase in Sham trial showed zero average change resulted from an increase in 2 animals and a decrease in 3 other animals (Figure 28B, Table 8). Meanwhile, the total time of seizures decreased by 43% during Theta stimulation and 36% during the post-Theta stimulation phase (Figure 28B). It was observed that the total time was decreased in all five animals for both Theta stimulation and post-Theta stimulation compared to the baseline (Table 10). The statistical significance, which was observed in the paired t-test between baseline and stimulation phases of Theta stimulation, was not observed anymore when the p-value was adjusted (Tukey's HSD) to consider the multiple comparisons (Table 13). Again, a variability between subjects in the effect of 7Hz stimulation was observed. An increase of the total seizure time was observed in 2 different animals and a decrease was observed in 2 animals which resulted in 7% decrease overall (Table 9, Figure 28B). Although there were not many trials, the total time was decreased for all 3 animals during the post-7Hz stimulation phase (Table 9). PiSM stimulation worsened the epileptic symptom as the total time of seizures was increased for all animals, that had a clean recording without motion artifacts, during the stimulation (Table 11).

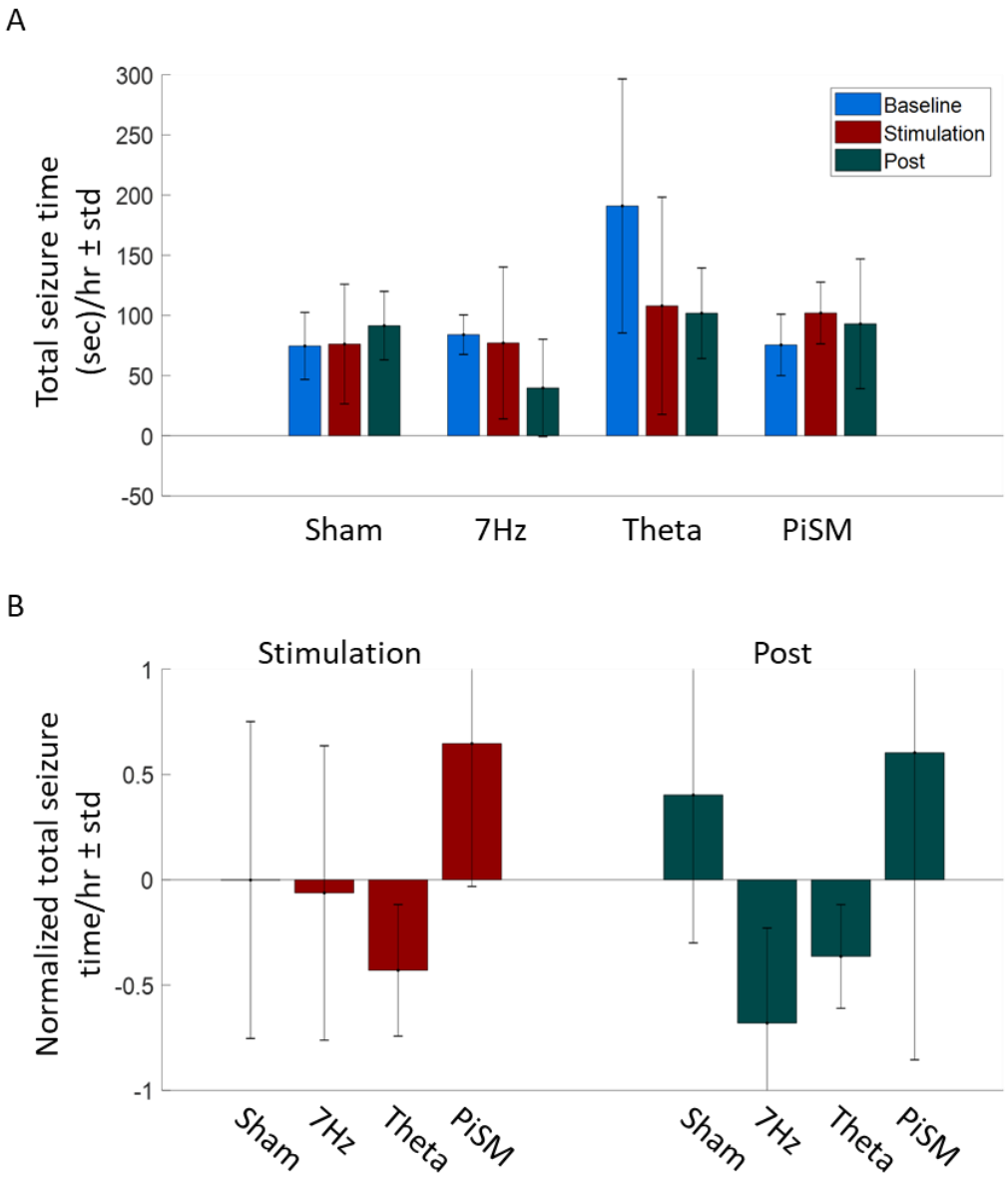

Figure 28. The total seizure time per hour to compare the effectiveness of the stimulation strategies. A. The total time of seizures per hour with the standard deviation (error bar). B. The total seizure time normalized to the baseline to identify the effect during and after the stimulation. The error bar indicates the standard deviation.

Table 8. Total seizure time for testing Sham.

Total seizure time in 1 hour (normalized time): **Sham**				
Rat ID	Session order	Baseline	Stimulation	Post
1	2	66 (0)	152 (1.3)	*
2	2	90 (0)	96 (0.07)	63 (-0.3)
3	3	57 (0)	56 (-0.02)	120 (1.11)
4	1	120 (0)	77 (-0.36)	*
5	4	40 (0)	0 (-1)	*
	Mean ± std	74.6±27.9 (0±0)	76.2±49.7 (0±0.75)	91.5±28.5 (0.41±0.71)

Table 9. Total seizure time for testing 7Hz stimulation.

Total seizure time in 1 hour (normalized time): **7Hz**				
Rat ID	Session order	Baseline	Stimulation	Post
1	1	100 (0)	173 (0.73)	*
2	3	57 (0)	84 (0.47)	0 (-1)
3	2	*	*	69 (*)
4	4	94 (0)	51 (-0.46)	90 (-0.04)
5	3	85 (0)	0 (-1)	0 (-1)
	Mean ± std	84±16.5 (0±0)	77±63 (-0.07±0.7)	39.8±40.4 (-0.68±0.45)

Table 10. Total seizure time for testing Theta stimulation.

Total seizure time in 1 hour (normalized time): **Theta**				
Rat ID	Session order	Baseline	Stimulation	Post
1	4	201 (0)	154 (-0.23)	117 (-0.42)
2	1	380 (0)	259 (-0.32)	111 (-0.71)

Table 10 continued

3	4	59 (0)	53 (-0.1)	52 (-0.12)
4	2	147 (0)	74 (-0.5)	70 (-0.52)
5	2	168 (0)	0 (-1)	159 (-0.05)
	Mean ± std	191±105.6 (0±0)	108±90.3 (-0.43±0.31)	101.8±37.6 (-0.36±0.25)

Table 11. Total seizure time for testing PiSM stimulation.

Total seizure time in 1 hour (normalized time): **PiSM**				
Session number	Rat ID	Baseline	Stimulation	Post
1	3	34 (0)	88 (1.6)	120 (2.53)
2	4	103 (0)	138 (0.34)	132 (0.28)
3	1	*	*	120 (*)
4	3	79 (0)	80 (0.01)	0 (-1)
5	1	86 (0)	*	*
	Mean ± std	75.5±25.5 (0±0)	102±25.7 (0.65±0.69)	93±53.9 (0.6±1.46)

Table 12. Three-way ANOVA for the raw and normalized number of seizures.

ANOVA: **Raw** total seizure time in 1 hour		
Source	F	Prob>F
Experimental phase (baseline/stimulation/post stimulation)	0.4	0.6752
Stimulation strategy	4.04	0.0289
Animal	2.82	0.0659
Experimental phase*Stimulation strategy	1.87	0.1574
Experimental phase*Animal	2.09	0.1093
Stimulation strategy*Animal	2.17	0.0845

ANOVA: **Normalized** total seizure time in 1 hour		
Source	F	Prob>F
Experimental phase (baseline/stimulation/post stimulation)	0.52	0.5043
Stimulation strategy	3.74	0.1108
Animal	7.48	0.0314
Experimental phase*Stimulation strategy	0.36	0.785
Experimental phase*Animal	1.08	0.4561
Stimulation strategy*Animal	1.43	0.3637

Table 13. P-values from paired t-test and Tukey's honset significant difference criterion post-hoc test.

Raw total seizure time in 1 hour			
Comparison		Raw P-value	Adjusted P-value
Sham-baseline	Sham-stimulation	0.9486	1
Sham-baseline	Sham-post	0.7578	0.9995
Sham-stimulation	Sham-post	0.8031	0.9996
7Hz-baseline	7Hz-stimulation	0.8572	1
7Hz-baseline	7Hz-post	0.1770	1
7Hz-stimulation	7Hz-post	0.7195	1
Theta-baseline	Theta-stimulation	0.0426	0.2351
Theta -baseline	Theta-post	0.1354	0.1693
Theta-stimulation	Theta-post	0.9058	1
PiSM-baseline	PiSM-stimulation	0.1926	1
PiSM-baseline	PiSM-post	0.8273	0.9987
PiSM-stimulation	PiSM-post	0.6390	1
Normalized total seizure time in 1 hour			
Comparison		Raw P-value	Adjusted P-value
Sham-stimulation	7Hz-stimulation	0.7655	1
Sham-stimulation	Theta-stimulation	0.2059	0.9056
Sham-stimulation	PiSM-stimulation	0.0097	1
Sham-post	7Hz-post	*	*
Sham-post	Theta-post	0.2952	0.7606
Sham-post	PiSM-post	*	*

6.4 Discussion

Two stimulation strategies by using the novel data-driven surrogate approach were applied to evaluate their therapeutic effectiveness. One strategy applied the optimal parameters to increase the hippocampal theta power (Theta stimulation) and the other strategy applied the optimal stimulation parameters to increase the output of PiSM (PiSM stimulation) for inducing the estimated anti-seizure neural state. An empirically selected parameter set as a conventional approach as well as sham stimulation were also tested for the comparison reason. Among them, only Theta stimulation showed a potential to be a novel method for suppressing the seizure as the frequency and the total seizure time during the stimulation decreased (4 and 5 out of 5 animals respectively, Table 4 and Table 10).

7Hz stimulation where the parameter set was empirically selected showed a high variability between subjects/trials as expected. PiSM stimulation did not suppress the seizure, so PiSM is not the desired surrogate for the data-driven approach.

In almost every animal, the optimal parameters to increase the hippocampal theta suppressed seizures by reducing the frequency and the total seizure time. In Chapter 4, the hippocampal theta showed two contradictory characteristics according to two neural state models. The hippocampal theta showed the pro-seizure characteristic during epileptogenesis whereas it showed the anti-seizure characteristic during the pre-ictal period. The result of suppressed seizures suggests that the increased hippocampal theta by MS optogenetic stimulation more likely represents the anti-seizure neural state.

PiSM stimulation did not suppress seizures, and there are two hypotheses which can explain the failure of PiSM stimulation. First, PiSM stimulation might have modulated some key neural features in the undesired way and resulted in inducing the pro-seizure state. As shown in Chapter 5, a combination of a few different neural features forms the output of PiSM. Therefore, it is possible that the modulation of PiSM output brought some features in the anti-seizure mode and the other features in the opposite mode. If one of the features in pro-seizure mode was the key, which is causal to seizures, the seizure susceptibility was likely to be promoted. The second potential hypothesis is that what high scores of PiSM represent is the pro-seizure neural state. PiSM was built by classifying neural features between the pre-ictal and inter-ictal periods, and the output of PiSM during the pre-ictal period was higher than during the inter-ictal period. If what PiSM describes is an effort of the brain to suppress the seizure, delivering the stimulation which increases the

output of PiSM likely suppressed the brain's activity to resist against a seizure. This possibly resulted in the increase of the seizure frequency and the total seizure time.

A few modifications can be considered to improve the effectiveness of the data-driven surrogate approach. The first is to develop more precise data-driven surrogate models for better describing the pathological neural states. PiSM is a linear classifier which is not able to describe complex behaviors of hippocampal neural features during the pre-ictal period. In addition, estimating the neural state may have suffered from a lack of information since only a limited feature set (i.e. power spectral density, coherence and phase coherence) was used to describe the neural state. A deep learning model such as a convolutional neural network is expected to better characterize the neural states with its ability to describe non-linear relationships and incorporate neural features from a wider space (e.g. time domain[117]). Second, the modulation of the neural state can be improved by leveraging state-dependent optimization. The state-dependency of MS optogenetic stimulation effect on the theta power or PiSM score was presented in Chapter 5. Given that a rat undergoes frequent natural state transitions, it is highly likely that the optimal stimulation parameter loses its effectiveness during the experiment. As explained in the Chapter 5 discussion, the state-dependent Bayesian optimization which incorporates the pre-stimulation state can improve the effectiveness of the stimulation. The state-dependent optimal parameter may effectively maintain the anti-seizure neural state or induce a transition from the pro- to anti-seizure state.

CHAPTER 7. CONCLUSIONS

7.1 Summary and conclusions

A novel data-driven approach for optimizing the neuromodulation more effectively and efficiently by investigating the stimulation effect on surrogate neural state models is presented. The conventional approach for preclinical studies requires a large amount of time and resources to find effective stimulation parameters and often fails due to the inter-subject variability in stimulation effect. To solve the listed limitations of the conventional approach, I implemented and demonstrated a variety of machine learning techniques to explore the stimulation effect, to describe the pathological neural states and to optimize the stimulation parameters. First, I have exhaustively explored the effect of exciting or inhibiting different neuronal subpopulations in the normal rat medial septum (MS) by using optogenetic stimulation. As a result, MS optogenetic stimulation using hSynapsin promoter (non-selective) in combination with Channelrhodopsin-2 was well suited for modulating electrophysiological activity of the hippocampus. Second, I demonstrated *in-vivo* Bayesian optimization (BaO) algorithm to quickly find the subject-specific optimal stimulation parameters to effectively modulate the hippocampal neural features. Third, I built data-driven neural state models to estimate a seizure susceptibility based on electrophysiological recordings. Two models were built to describe neural state transitions during epileptogenesis and pre-ictal period. The output of the model played a surrogate role by providing a metric which was regulated through MS optogenetic stimulation. Fourth, the BaO algorithm was modified to be applied for epileptic animals where abnormal activities (e.g. inter-ictal spikes) present. It was demonstrated that the hippocampal theta power and

the output of pre-ictal state model (PiSM) were effectively modulated with the optimal stimulation parameters found by the modified BaO algorithm. Lastly, I tested whether modulating the surrogate neural states affected the symptom of epilepsy (i.e. seizure). The treatment efficacy of a data-driven surrogate approach was compared to the stimulation with the empirically selected parameter. The subject specific stimulation parameters to maximize the hippocampal theta (4-10Hz) power was more effective than the empirically selected parameter (7Hz) for the seizure suppression. The optimal modulation of PiSM output for inducing the anti-seizure neural state did not suppress seizures. From the results of this thesis work viewed together, I conclude that the subject specific optimal parameters to modulate the surrogates for inducing the anti-seizure neural state is a potential novel neuromodulation method for epilepsy treatment.

The data-driven surrogate approach was developed by applying various machine learning and statistical techniques to improve the current neuromodulation technologies. There are two main advantages of the novel data-driven surrogate approach. First, it provides a new approach for preclinical study to save time and resources and minimize the side-effect. We demonstrated the effectiveness of Bayesian optimization in stimulation parameter search to modulate the neural state surrogates. By solving the issue that finding a stimulation parameter set from the enormous space with the limited time and resources, this approach can accelerate the process for developing a novel neuromodulation treatment. Second, it provides a chance to find the underlying mechanism of epilepsy by investigating the electrophysical activity in the hippocampus. Most of studies focus on either activity change induced by pathological symptom or brain stimulation. The data-driven surrogate approach, however, focuses on both by modulating the neural features which represents

the pathological neural state with the brain stimulation. Therefore, applying this approach will identify features from the electrophysiological recording as well as their causal relationship to the disease.

Data driven surrogate approach can be applied for not only epilepsy but also other diseases where brain signal recording and stimulation is performed. Therefore, this project will be a milestone which suggest the way to go for preclinical and clinical studies in neurology and psychiatry fields.

7.2 Alternative approaches and future direction

A few alternative methods can be considered to improve the therapeutic efficacy of the data-driven approach with MS optogenetic stimulation. First, it is needed to develop more precise data-driven surrogate models for better describing the pathological neural state. The pre-ictal state model (PiSM), a surrogate neural state model used for the seizure treatment, was a linear classifier which is not able to describe complex non-linear relationship between pre-ictal state and hippocampal neural features. In addition, estimating the neural state may have suffered from a lack of information since only a limited feature set (i.e. power spectral density, coherence and phase coherence) was used to describe the neural state. We expect to improve the ability to characterize the neural states by leveraging a deep learning model. A convolutional neural network (CNN) model is a feedforward neural network that implements parameter sharing facilitated by the convolution operations. The CNN model is an appropriate choice to use the time-domain LFP as an input as it can identify key temporal features in the pre-ictal period regardless of location within a given time window. In addition, the CNN model is well suited for the

multi-channel recording used in our experimental design by using a two-dimensional input (channel × LFP sample). Therefore, building the CNN model will provide a better estimation of pathological neural states by minimizing the loss of information in the hippocampal neural activities.

Second, a wider stimulation parameter space needs to be explored. Clear differences in the stimulation effect between single-frequency standard pulse and nested-pulse train were shown in Chapter 3. Therefore, extending the parameter space may enable an observation of new stimulation effects. Various patterns of the stimulation such as sinusoidal, Poisson or randomly distributed[118] pulse have not been tested yet. In addition to widening the stimulation parameter space, testing different neuronal subpopulation as a target of optogenetic stimulation needs to be considered. Applying excitation to MS neurons transfected with calcium/calmodulin-dependent protein kinase IIα (CamKIIα) promoter, which selectively transfects the glutamatergic neurons in MS[63,64], was also able to effectively modulate the hippocampal neural activities. As modulating different MS subpopulations is expected to induce different effects in the hippocampus, the new promoter may provide a better target to induce anti-seizure neural state in the hippocampus.

Third, it needs to be investigated whether a duration of the stimulation as another parameter can affect the effectiveness of stimulation for seizure treatment. In this project, we tested one-hour continuous stimulation to suppress seizures. However, a previous *in vitro* study showed that the effectiveness of optogenetic stimulation to suppress seizures significantly dropped after first 12 seconds of the stimulation[119]. In another *in vivo* study presented by Osawa-et-al a pattern of the causality between hippocampal regions was different after a few seconds of the stimulation from the beginning of the stimulation[120].

Desai-et-al also showed that intermittent electrical stimulation (2-minute on and 2-minute off) in the hippocampus was effective to suppress seizures[30]. Based on these previous studies, intermittent stimulation can improve the therapeutic efficacy by avoiding the decrease in the stimulation effectiveness. By optimizing a duration of stimulation on/off, intermittent stimulation may effectively induce anti-seizure neural state. In addition, a closed-loop approach which applies the stimulation only when a seizure is predicted can be an alternative to the current approach. Other studies suggested a habituation of the brain that the effect of neural stimulation may be cumulative, reaching maximum efficacy after a certain duration of stimulation delivered[10]. Although it is still not clearly identified, a long continuous stimulation may also induce a cognitive function deficit as a side effect[121–124]. A closed-loop approach can be a solution for these issues by applying the stimulation only when it is necessary. As responsive neural stimulation which delivers stimulation when a seizure is detected already presented successful cases, an improved closed-loop approach with the seizure prediction is expected to provide a better outcome.

It is needed to interpret the mechanism of treatment by investigating which neuronal pathway in the septo-hippocampal circuit is involved in the seizure suppression as a response to MS optogenetic stimulation. Given the complex anatomical connections in the septo-hippocampal circuit, it is extremely hard to predict the travel path of the neuronal activity induced by MS optogenetic stimulation. In addition, the selection of stimulation parameters may affect a pathway of neuronal signaling. The post-mortem immunohistological analyses can provide a method to identify which neuronal subpopulations are affected by the MS optogenetic stimulation. This study will help to

understand the underlying mechanisms of disease treatment through the neuromodulation as well as the functional pathway of the septo-hippocampal circuit.

REFERENCES

1. M. J. England, C. T. Liverman, A. M. Schultz and L. M. Strawbridge, Epilepsy across the spectrum: Promoting health and understanding. A summary of the Institute of Medicine report, *Epilepsy Behav.* **25** (2012) 266–276.

2. C. B. Josephson, J. Dykeman, K. M. Fiest, X. Liu, R. M. Sadler, N. Jette and S. Wiebe, Systematic review and meta-analysis of standard vs selective temporal lobe epilepsy surgery., *Neurology* **80** (2013) 1669–76.

3. G. L. Morris and W. M. Mueller, Long-term treatment with vagus nerve stimulation in patients with refractory epilepsy. The Vagus Nerve Stimulation Study Group E01-E05., *Neurology* (1999).

4. M. J. Morrell, Responsive cortical stimulation for the treatment of medically intractable partial epilepsy, *Neurology* (2011).

5. R. Fisher et al., Electrical stimulation of the anterior nucleus of thalamus for treatment of refractory epilepsy, *Epilepsia* **51** (2010) 899–908.

6. P. Kwan and M. J. Brodie, Early identification of refractory epilepsy., *N. Engl. J. Med.* (2000).

7. J. T. Willie, N. G. Laxpati, D. L. Drane, A. Gowda, C. Appin, C. Hao, D. J. Brat, S. L. Helmers, A. Saindane, S. G. Nour and R. E. Gross, Real-time magnetic resonance-guided stereotactic laser amygdalohippocampotomy for mesial temporal lobe epilepsy, *Neurosurgery* (2014).

8. R. E. Gross, M. A. Stern, J. T. Willie, R. E. Fasano, A. M. Saindane, B. P. Soares, N. P. Pedersen and D. L. Drane, Stereotactic laser amygdalohippocampotomy for mesial temporal lobe epilepsy, *Ann. Neurol.* (2018).

9. E. M. S. Sherman, S. Wiebe, T. B. Fay-McClymont, J. Tellez-Zenteno, A. Metcalfe, L. Hernandez-Ronquillo, W. J. Hader and N. Jetté, Neuropsychological outcomes after epilepsy surgery: Systematic review and pooled estimates, *Epilepsia* (2011).

10. N. G. Laxpati, W. S. Kasoff and R. E. Gross, Deep brain stimulation for the treatment of epilepsy: circuits, targets, and trials., *Neurotherapeutics* (2014).

11. C. Helmstaedter, S. Richter, S. Röske, F. Oltmanns, J. Schramm and T. N. Lehmann, Differential effects of temporal pole resection with amygdalohippocampectomy

versus selective amygdalohippocampectomy on material-specific memory in patients with mesial temporal lobe epilepsy, *Epilepsia* **49** (2008) 88–97.

12. C. C. McIntyre, C. R. Butson, C. B. Maks and A. M. Noecker, Optimizing deep brain stimulation parameter selection with detailed models of the electrode-tissue interface, *Annu. Int. Conf. IEEE Eng. Med. Biol. - Proc.* (2006) 893–895.

13. L. V. Colom, A. García-Hernández, M. T. Castañeda, M. G. Perez-Cordova and E. R. Garrido-Sanabria, Septo-Hippocampal Networks in Chronically Epileptic Rats: Potential Antiepileptic Effects of Theta Rhythm Generation, *J. Neurophysiol.* **95** (2006) 3645–3653.

14. P. Boon, R. Raedt, V. de Herdt, T. Wyckhuys and K. Vonck, Electrical Stimulation for the Treatment of Epilepsy, *Neurotherapeutics* **6** (2009) 218–227.

15. T. L. Skarpaas and M. J. Morrell, Intracranial Stimulation Therapy for Epilepsy, *Neurotherapeutics* **6** (2009) 238–243.

16. B. C. Lega, C. H. Halpern, J. L. Jaggi and G. H. Baltuch, Deep brain stimulation in the treatment of refractory epilepsy: Update on current data and future directions, *Neurobiol. Dis.* **38** (2010) 354–360.

17. S. Miocinovic, Computational Analysis of Subthalamic Nucleus and Lenticular Fasciculus Activation During Therapeutic Deep Brain Stimulation, *J. Neurophysiol.* **96** (2006) 1569–1580.

18. M. Lafreniere-Roula, W. D. Hutchison, A. M. Lozano, M. Hodaie and J. O. Dostrovsky, Microstimulation-induced inhibition as a tool to aid targeting the ventral border of the subthalamic nucleus, *J. Neurosurg.* **111** (2009) 724–728.

19. A. M. Aravanis, L. P. Wang, F. Zhang, L. A. Meltzer, M. Z. Mogri, M. B. Schneider and K. Deisseroth, An optical neural interface: in vivo control of rodent motor cortex with integrated fiberoptic and optogenetic technology., *J. Neural Eng.* **4** (2007).

20. V. Gradinaru, M. Mogri, K. R. Thompson, J. M. Henderson and K. Deisseroth, Optical Deconstruciton of Parkinsonian Neural Circuitry, *Science (80-.).* **324** (2009) 2005–2008.

21. A. V. Kravitz, B. S. Freeze, P. R. L. Parker, K. Kay, M. T. Thwin, K. Deisseroth and A. C. Kreitzer, Regulation of parkinsonian motor behaviours by optogenetic control of basal ganglia circuitry, *Nature* **466** (2010) 622–626.

22. O. Yizhar, L. E. Fenno, T. J. Davidson, M. Mogri and K. Deisseroth, Optogenetics

in Neural Systems, *Neuron* **71** (2011) 9–34.

23. G. Gangadharan, J. Shin, S.-W. Kim, A. Kim, A. Paydar, D.-S. Kim, T. Miyazaki, M. Watanabe, Y. Yanagawa, J. Kim, Y.-S. Kim, D. Kim and H.-S. Shin, Medial septal GABAergic projection neurons promote object exploration behavior and type 2 theta rhythm, *Proc. Natl. Acad. Sci.* **113** (2016) 6550–6555.

24. F. Fuhrmann, D. Justus, L. Sosulina, H. Kaneko, T. Beutel, D. Friedrichs, S. Schoch, M. K. Schwarz, M. Fuhrmann and S. Remy, Locomotion, Theta Oscillations, and the Speed-Correlated Firing of Hippocampal Neurons Are Controlled by a Medial Septal Glutamatergic Circuit, *Neuron* **86** (2015) 1253–1264.

25. M. Vandecasteele, V. Varga, A. Berényi, E. Papp, P. Barthó, L. Venance, T. F. Freund and G. Buzsáki, Optogenetic activation of septal cholinergic neurons suppresses sharp wave ripples and enhances theta oscillations in the hippocampus, *Proc. Natl. Acad. Sci.* **111** (2014) 13535–13540.

26. K. Hunka, O. Suchowersky, S. Wood, L. Derwent and Z. H. T. Kiss, Nursing time to program and assess deep brain stimulators in movement disorder patients., *J. Neurosci. Nurs.* (2005).

27. J. M. Van Buren, J. H. Wood, J. Oakley and F. Hambrecht, Preliminary evaluation of cerebellar stimulation by double-blind stimulation and biological criteria in the treatment of epilepsy, *J. Neurosurg.* (1978).

28. G. D. S. Wright, D. L. McLellan and J. G. Brice, A double-blind trial of chronic cerebellar stimulation in twelve patients with severe epilepsy, *J. Neurol. Neurosurg. Psychiatry* (1984).

29. C. C. McIntyre and W. M. Grill, Extracellular stimulation of central neurons: influence of stimulus waveform and frequency on neuronal output., *J. Neurophysiol.* (2002).

30. S. A. Desai, J. D. Rolston, C. E. McCracken, S. M. Potter and R. E. Gross, Asynchronous Distributed Multielectrode Microstimulation Reduces Seizures in the Dorsal Tetanus Toxin Model of Temporal Lobe Epilepsy, *Brain Stimul.* **9** (2016) 86–100.

31. M. Sedigh-Sarvestani, G. I. Thuku, S. Sunderam, A. Parkar, S. L. Weinstein, S. J. Schiff and B. J. Gluckman, Rapid Eye Movement Sleep and Hippocampal Theta Oscillations Precede Seizure Onset in the Tetanus Toxin Model of Temporal Lobe Epilepsy, *J. Neurosci.* **34** (2014) 1105–1114.

32. A. Bragin, C. L. Wilson, J. Almajano, I. Mody and J. Engel, High-frequency Oscillations after Status Epilepticus : Epileptogenesis and Seizure Genesis, **45** (2004) 1017–1023.

33. P. Salami, M. Lévesque, R. Benini, C. Behr, J. Gotman and M. Avoli, Neurobiology of Disease Dynamics of interictal spikes and high-frequency oscillations during epileptogenesis in temporal lobe epilepsy, *Neurobiol. Dis.* **67** (2014) 97–106.

34. J. Fell, B. P. Staresina, A. T. A. Do Lam, G. Widman, C. Helmstaedter, C. E. Elger and N. Axmacher, Memory modulation by weak synchronous deep brain stimulation: A pilot study, *Brain Stimul.* **6** (2013) 270–273.

35. C. Müller and S. Remy, Septo–hippocampal interaction, *Cell Tissue Res.* (2017) 1–11.

36. M. Frotscher and C. Léránth, Cholinergic innervation of the rat hippocampus as revealed by choline acetyltransferase immunocytochemistry: a combined light and electron microscopic study., *J. Comp. Neurol.* (1985).

37. T. Hajszan, M. Alreja and C. Leranth, Intrinsic vesicular glutamate transporter 2-immunoreactive input to septohippocampal parvalbumin-containing neurons: Novel glutamatergic local circuit cells, *Hippocampus* **14** (2004) 499–509.

38. J. Kiss, A. J. Patel and T. F. Freund, Distribution of septohippocampal neurons containing parvalbumin or choline acetyltransferase in the rat brain, *J. Comp. Neurol.* (1990).

39. J. Kiss, A. J. Patel, K. G. Baimbridge and T. F. Freund, Topographical localization of neurons containing parvalbumin and choline acetyltransferase in the medial septum-diagonal band region of the rat, *Neuroscience* (1990).

40. T. F. Freund and M. Antal, GABA-containing neurons in the septum control inhibitory interneurons in the hippocampus, *Nature* **336** (1988) 170–173.

41. T. F. Freund and G. Buzsáki, Interneurons of the hippocampus, *Hippocampus* **6** (1998) 347–470.

42. L. V. Colom, M. T. Castaneda, T. Reyna, S. Hernandez and E. Garrido-Sanabria, Characterization of medial septal glutamatergic neurons and their projection to the hippocampus, *Synapse* **58** (2005) 151–164.

43. F. Manseau, M. Danik and S. Williams, A functional glutamatergic neurone network in the medial septum and diagonal band area, *J. Physiol.* **566** (2005) 865–884.

44. Y. Sun, A. Q. Nguyen, J. P. Nguyen, L. Le, D. Saur, J. Choi, E. M. Callaway and X. Xu, Cell-type-specific circuit connectivity of hippocampal CA1 revealed through cre-dependent rabies tracing, *Cell Rep.* **7** (2014) 269–280.

45. M. Wu, T. Hajszan, C. Leranth and M. Alreja, Nicotine recruits a local glutamatergic circuit to excite septohippocampal GABAergic neurons, *Eur. J. Neurosci.* **18** (2003) 1155–1168.

46. P. R. Lewis, C. C. D. Shute and A. Silver, Confirmation from choline acetylase analyses of a massive cholinergic innervation to the rat hippocampus, *J. Physiol.* (1967).

47. N. G. Laxpati, B. Mahmoudi, C.-A. Gutekunst, J. P. Newman, R. Zeller-Townson and R. E. Gross, Real-time in vivo optogenetic neuromodulation and multielectrode electrophysiologic recording with NeuroRighter, *Front. Neuroeng.* **7** (2014).

48. B. J. Blumberg, S. P. Flynn, S. J. Barriere, P. R. Mouchati, R. C. Scott, G. L. Holmes and J. M. Barry, Efficacy of nonselective optogenetic control of the medial septum over hippocampal oscillations: the influence of speed and implications for cognitive enhancement, *Physiol. Rep.* **4** (2016) e13048.

49. F. Carpenter, N. Burgess and C. Barry, Modulating medial septal cholinergic activity reduces medial entorhinal theta frequency without affecting speed or grid coding, *Sci. Rep.* **7** (2017) 1–12.

50. P. Kaifosh, M. Lovett-Barron, G. F. Turi, T. R. Reardon and A. Losonczy, Septo-hippocampal GABAergic signaling across multiple modalities in awake mice, *Nat. Neurosci.* **16** (2013) 1182–1184.

51. J. Robinson, F. Manseau, G. Ducharme, B. Amilhon, E. Vigneault, S. El Mestikawy and S. Williams, Optogenetic Activation of Septal Glutamatergic Neurons Drive Hippocampal Theta Rhythms, *J. Neurosci.* **36** (2016) 3016–3023.

52. S.-E. Park, N. G. Laxpati, C.-A. Gutekunst, M. J. Connolly, J. Tung, K. Berglund, B. Mahmoudi and R. E. Gross, A Machine Learning Approach to Characterize the Modulation of the Hippocampal Rhythms Via Optogenetic Stimulation of the Medial Septum, *Int. J. Neural Syst.* **1950020** (2019) 1950020.

53. F. C. Morabito, M. Campolo, N. Mammone, M. Versaci, S. Franceschetti, F. Tagliavini, V. Sofia, D. Fatuzzo, A. Gambardella, A. Labate, L. Mumoli, G. G. Tripodi, S. Gasparini, V. Cianci, C. Sueri, E. Ferlazzo and U. Aguglia, Deep Learning Representation from Electroencephalography of Early-Stage Creutzfeldt-Jakob Disease and Features for Differentiation from Rapidly Progressive Dementia,

Int. J. Neural Syst. (2016).

54. A. Antoniades, L. Spyrou, D. Martin-Lopez, A. Valentin, G. Alarcon, S. Sanei and C. C. Took, Deep Neural Architectures for Mapping Scalp to Intracranial EEG, *Int. J. Neural Syst.* (2018).

55. N. Mammone, C. Ieracitano, H. Adeli, A. Bramanti and F. C. Morabito, Permutation Jaccard Distance-Based Hierarchical Clustering to Estimate EEG Network Density Modifications in MCI Subjects, *IEEE Trans. Neural Networks Learn. Syst.* (2018).

56. U. R. Acharya, S. L. Oh, Y. Hagiwara, J. H. Tan, H. Adeli and D. P. Subha, Automated EEG-based screening of depression using deep convolutional neural network, *Comput. Methods Programs Biomed.* (2018).

57. U. R. Acharya, S. L. Oh, Y. Hagiwara, J. H. Tan and H. Adeli, Deep convolutional neural network for the automated detection and diagnosis of seizure using EEG signals, *Comput. Biol. Med.* (2018).

58. L. V Colom, A. García-Hernández, M. T. Castañeda, M. G. Perez-Cordova and E. R. Garrido-Sanabria, Septo-hippocampal networks in chronically epileptic rats: potential antiepileptic effects of theta rhythm generation., *J. Neurophysiol.* **95** (2006) 3645–53.

59. R. Boyce, S. D. Glasgow and S. Williams, Causal evidence for the role of REM sleep theta rhythm in contextual memory consolidation, **352** (2016) 812–817.

60. F. Bender, M. Gorbati, M. C. Cadavieco, N. Denisova, X. Gao, C. Holman, T. Korotkova and A. Ponomarenko, Theta oscillations regulate the speed of locomotion via a hippocampus to lateral septum pathway, *Nat. Commun.* **6** (2015) 8521.

61. J. D. Rolston, A low-cost multielectrode system for data acquisition enabling real-time closed-loop processing with rapid recovery from stimulation artifacts, *Front. Neuroeng.* **2** (2009) 1–17.

62. J. D. Rolston, R. E. Gross and S. M. Potter, NeuroRighter: Closed-loop multielectrode stimulation and recording for freely moving animals and cell cultures, in *Proc. 31st Annu. Int. Conf. IEEE Eng. Med. Biol. Soc. Eng. Futur. Biomed. EMBC 2009* (2009).

63. J. L. Nathanson, Y. Yanagawa, K. Obata and E. M. Callaway, Preferential labeling of inhibitory and excitatory cortical neurons by endogenous tropism of adeno-associated virus and lentivirus vectors, *Neuroscience* **161** (2009) 441–450.

64. M. Chiruvella, The Use of Optogenetics for Cell-type Specific Activation in the Medial Septum (Emory University, 2015).

65. I. B. Witten, E. E. Steinberg, S. Y. Lee, T. J. Davidson, K. A. Zalocusky, M. Brodsky, O. Yizhar, S. L. Cho, S. Gong, C. Ramakrishnan, G. D. Stuber, K. M. Tye, P. H. Janak and K. Deisseroth, Recombinase-driver rat lines: Tools, techniques, and optogenetic application to dopamine-mediated reinforcement, *Neuron* **72** (2011) 721–733.

66. H. Bokil, P. Andrews, J. E. Kulkarni, S. Mehta and P. P. Mitra, Chronux: A platform for analyzing neural signals, *J. Neurosci. Methods* **192** (2010) 146–151.

67. H. Yu, C. Zhai and J. Han, Text classification from positive and unlabeled documents, *Proc. Twelfth Int. Conf. Inf. Knowl. Manag. - CIKM '03* (2003) 232.

68. H. Zou and T. Hastie, Regularization and variable selection via the elastic-net, *J. R. Stat. Soc.* **67** (2005) 301–320.

69. I. Rish, An empirical study of the naive Bayes classifier, *IJCAI 2001 Work. Empir. Methods Artif. Intell.* **22230** (2001) 41–46.

70. M. L. Zhang, J. M. Peña and V. Robles, Feature selection for multi-label naive Bayes classification, *Inf. Sci. (Ny).* **179** (2009) 3218–3229.

71. C. E. Rasmussen and C. K. I. Williams, Regression, *Gaussian Process. Mach. Learn.* (2006) Chapter 2.

72. S. Iliya and F. Neri, Towards Artificial Speech Therapy: A Neural System for Impaired Speech Segmentation, *Int. J. Neural Syst.* (2016).

73. W. H. Chen, S. H. Hsu and H. P. Shen, Application of SVM and ANN for intrusion detection, *Comput. Oper. Res.* (2005).

74. X. Y. Liu, J. Wu and Z. H. Zhou, Exploratory under-sampling for class-imbalance learning, in *Proc. - IEEE Int. Conf. Data Mining, ICDM* (2006).

75. C.-J. Hsieh, M. A. Sustik, I. S. Dhillon and P. Ravikumar, Sparse inverse covariance matrix estimation using quadratic approximation, *Adv. Neural …* (2011) 1–18.

76. F. Berkenkamp, A. Krause and A. P. Schoellig, Bayesian Optimization with Safety Constraints : Safe and Automatic Parameter Tuning in Robotics, (2015).

77. K. Nikolic, N. Grossman, M. S. Grubb, J. Burrone, C. Toumazou and P. Degenaar, Photocycles of channelrhodopsin-2, *Photochem. Photobiol.* **85** (2009) 400–411.

78. A. Pascale Simon, Firing Properties of Anatomically Identified Neurons in the Medial Septum of Anesthetized and Unanesthetized Restrained Rats, *J. Neurosci.* **26** (2006) 9038–9046.

79. C. Y. L. Huh, R. Goutagny and S. Williams, Glutamatergic Neurons of the Mouse Medial Septum and Diagonal Band of Broca Synaptically Drive Hippocampal Pyramidal Cells: Relevance for Hippocampal Theta Rhythm, *J. Neurosci.* **30** (2010) 15951–15961.

80. R. M. Yoder and K. C. H. Pang, Involvement of GABAergic and cholinergic medial septal neurons in hippocampal theta rhythm, *Hippocampus* **15** (2005) 381–392.

81. V. Villette, F. Poindessous-Jazat, A. Simon, C. Lena, E. Roullot, B. Bellessort, J. Epelbaum, P. Dutar and A. Stephan, Decreased Rhythmic GABAergic Septal Activity and Memory-Associated Oscillations after Hippocampal Amyloid- Pathology in the Rat, *J. Neurosci.* **30** (2010) 10991–11003.

82. L. A. Bell, K. A. Bell and A. R. McQuiston, Synaptic muscarinic response types in hippocampal CA1 interneurons depend on different levels of presynaptic activity and different muscarinic receptor subtypes, *Neuropharmacology* **73** (2013) 160–173.

83. K. Toth, T. F. Freund and R. Miles, Disinhibition of rat hippocampal pyramidal cells by GABAergic afferents from the septum\r, *J Physiol* **500** (1997) 463–474.

84. G. Buzsáki, Theta oscillations in the hippocampus, *Neuron* (2002).

85. J. Ma and L. W. S. Leung, Medial septum mediates the increase in post-ictal behaviors and hippocampal gamma waves after an electrically induced seizure, *Brain Res.* **833** (1999) 51–57.

86. P. B. Sederberg, A. Schulze-Bonhage, J. R. Madsen, E. B. Bromfield, D. C. McCarthy, A. Brandt, M. S. Tully and M. J. Kahana, Hippocampal and neocortical gamma oscillations predict memory formation in humans, *Cereb. Cortex* **17** (2007) 1190–1196.

87. M. K. van Vugt, A. Schulze-Bonhage, B. Litt, A. Brandt and M. J. Kahana, Hippocampal Gamma Oscillations Increase with Memory Load, *J. Neurosci.* **30** (2010) 2694–2699.

88. M. J. Connolly, R. E. Gross and B. Mahmoudi, The influence of the pre-stimulation neural state on the post-stimulation neural dynamics via distributed microstimulation of the hippocampus, *Proc. Annu. Int. Conf. IEEE Eng. Med. Biol.*

Soc. EMBS **2016**–**Octob** (2016) 1810–1813.

89. S.-E. Park, N. G. Laxpati, M. J. Connolly, B. Mahmoudi and R. E. Gross, Predicting the stimulation effectiveness using pre-stimulation neural states via optogenetic activation of the medial septum glutamatergic neurons modulating the hippocampal neural activity, in *2017 39th Annu. Int. Conf. IEEE Eng. Med. Biol. Soc.* (IEEE, 2017), pp. 2105–2108.

90. L. A. Ewell, L. Liang, C. Armstrong, I. Soltész, S. Leutgeb and J. K. Leutgeb, Brain State Is a Major Factor in Preseizure Hippocampal Network Activity and Influences Success of Seizure Intervention, *J. Neurosci.* (2015).

91. R. Lorenz, R. P. Monti, I. R. Violante, C. Anagnostopoulos, A. Aldo, G. Montana and R. Leech, The Automatic Neuroscientist : automated experimental design with real-time fMRI, *Neuroimage* **129** (2016) 1–22.

92. E. Brochu, V. M. Cora and N. De Freitas, A tutorial on Bayesian optimization of expensive cost functions, with application to active user modeling and hierarchical reinforcement learning, *Arxiv Prepr. ArXiv1012.2599* (2010) 1–49.

93. O. Mamad, H. M. McNamara, R. B. Reilly and M. Tsanov, Medial septum regulates the hippocampal spatial representation, *Front. Behav. Neurosci.* **9** (2015) 1–16.

94. C. Behr, M. Lévesque, T. Stroh and M. Avoli, Neurobiology of Disease Time-dependent evolution of seizures in a model of mesial temporal lobe epilepsy, *Neurobiol. Dis.* **106** (2017) 205–213.

95. A. J. Cadotte, T. B. DeMarse, T. H. Mareci, M. B. Parekh, S. S. Talathi, D. U. Hwang, W. L. Ditto, M. Ding and P. R. Carney, Granger causality relationships between local field potentials in an animal model of temporal lobe epilepsy, *J. Neurosci. Methods* **189** (2010) 121–129.

96. A. C. S. Broggini, I. M. Esteves, R. N. Romcy-Pereira, J. P. Leite and R. N. Leão, Pre-ictal increase in theta synchrony between the hippocampus and prefrontal cortex in a rat model of temporal lobe epilepsy, *Exp. Neurol.* (2016).

97. P. Britton, P. S. Whitton, L. J. Fowler and N. G. Bowery, Tetanus Toxin-Induced Effects on Extracellular Amino Acid Levels in Rat Hippocampus: An In Vivo Microdialysis Study, *J. Neurochem.* **67** (2002) 324–329.

98. M. Mainardi, M. Pietrasanta, E. Vannini, O. Rossetto and M. Caleo, Tetanus neurotoxin-induced epilepsy in mouse visual cortex, *Epilepsia* (2012).

99. J. G. R. JEFFERYS and M. C. WALKER, Tetanus Toxin Model of Focal Epilepsy, in *Model. Seizures Epilepsy* (Elsevier, 2006), pp. 407–414.

100. K. Sjöstrand and L. Clemmensen, Spasm: A matlab toolbox for sparse statistical modeling, *J. Stat. …* **VV** (2012).

101. B. Efron, T. Hastie, I. Johnstone and R. Tibshirani, Least Angle Regression, *Ann. Stat.* **32** (2004) 407–499.

102. A. García-Hernández, B. H. Bland, J. C. Facelli and L. V. Colom, Septo-hippocampal networks in chronic epilepsy, *Exp. Neurol.* **222** (2010) 86–92.

103. F. Velasco, J. D. Carrillo-Ruiz, F. Brito, M. Velasco, A. L. Velasco, I. Marquez and R. Davis, Double-blind, randomized controlled pilot study of bilateral cerebellar stimulation for treatment of intractable motor seizures, *Epilepsia* (2005).

104. M. Z. Koubeissi, E. Kahriman, T. U. Syed, J. Miller and D. M. Durand, Low-frequency electrical stimulation of a fiber tract in temporal lobe epilepsy, *Ann. Neurol.* (2013).

105. E. Krook-Magnuson, C. Armstrong, M. Oijala and I. Soltesz, On-demand optogenetic control of spontaneous seizures in temporal lobe epilepsy, *Nat. Commun.* **4** (2013) 1376–1378.

106. Y. Lu, C. Zhong, L. Wang, P. Wei, W. He, K. Huang, Y. Zhang, Y. Zhan, G. Feng and L. Wang, Corrigendum: Optogenetic dissection of ictal propagation in the hippocampal–entorhinal cortex structures, *Nat. Commun.* (2016).

107. A. Koy, M. Hellmich, K. A. M. Pauls, W. Marks, J. P. Lin, O. Fricke and L. Timmermann, Effects of deep brain stimulation in dyskinetic cerebral palsy: A meta-analysis, *Mov. Disord.* (2013).

108. S. E. Cooper, A. M. Noecker, H. Abboud, J. L. Vitek and C. C. McIntyre, Return of bradykinesia after subthalamic stimulation ceases: Relationship to electrode location, *Exp. Neurol.* (2011).

109. A. Karabanov, A. Thielscher and H. R. Siebner, Transcranial brain stimulation: Closing the loop between brain and stimulation, *Curr. Opin. Neurol.* (2016).

110. M. I. Hariz, P. Shamsgovara, F. Johansson, G. M. Hariz and H. Fodstad, Tolerance and tremor rebound following long-term chronic thalamic stimulation for Parkinsonian and essential tremor, in *Stereotact. Funct. Neurosurg.* (1999).

111. M. C. Rodriguez-Oroz et al., Bilateral deep brain stimulation in Parkinson's disease: A multicentre study with 4 years follow-up, *Brain* (2005).

112. A. Castrioto, A. M. Lozano, Y. Y. Poon, A. E. Lang, M. Fallis and E. Moro, Ten-year outcome of subthalamic stimulation in Parkinson disease: A blinded evaluation, *Arch. Neurol.* (2011).

113. P. Rajdev, M. Ward and P. Irazoqui, Effect of stimulus parameters in the treatment of seizures by electrical stimulation in the kainate animal model, *Int. J. Neural Syst.* (2011).

114. C. Wille, B. J. Steinhoff, D. M. Altenmüller, A. M. Staack, S. Bilic, G. Nikkhah and J. Vesper, Chronic high-frequency deep-brain stimulation in progressive myoclonic epilepsy in adulthood - Report of five cases, *Epilepsia* (2011).

115. C. Hamani, M. Hodaie, J. Chiang, M. del Campo, D. M. Andrade, D. Sherman, M. Mirski, L. E. Mello and A. M. Lozano, Deep brain stimulation of the anterior nucleus of the thalamus: Effects of electrical stimulation on pilocarpine-induced seizures and status epilepticus, *Epilepsy Res.* (2008).

116. R. Hultman, K. Ulrich, B. D. Sachs, C. Blount, D. E. Carlson, N. Ndubuizu, R. C. Bagot, E. M. Parise, M. A. T. Vu, N. M. Gallagher, J. Wang, A. J. Silva, K. Deisseroth, S. D. Mague, M. G. Caron, E. J. Nestler, L. Carin and K. Dzirasa, Brain-wide Electrical Spatiotemporal Dynamics Encode Depression Vulnerability, *Cell* **173** (2018) 166–180.e14.

117. M. Zhou, C. Tian, R. Cao, B. Wang, Y. Niu, T. Hu, H. Guo and J. Xiang, Epileptic seizure detection based on EEG signals and CNN, *Front. Neuroinform.* (2018).

118. D. T. Brocker, B. D. Swan, R. Q. So, D. A. Turner, R. E. Gross and W. M. Grill, Optimized temporal pattern of brain stimulation designed by computational evolution, *Sci. Transl. Med.* **9** (2017).

119. C. C. Chiang, T. P. Ladas, L. E. Gonzalez-Reyes and D. M. Durand, Seizure suppression by high frequency Optogenetic stimulation using in vitro and in vivo animal models of epilepsy, *Brain Stimul.* (2014).

120. S. I. Osawa, M. Iwasaki, R. Hosaka, Y. Matsuzaka, H. Tomita, T. Ishizuka, E. Sugano, E. Okumura, H. Yawo, N. Nakasato, T. Tominaga and H. Mushiake, Optogenetically Induced Seizure and the Longitudinal Hippocampal Network Dynamics, *PLoS One* **8** (2013).

121. V. Salanova et al., Long-term efficacy and safety of thalamic stimulation for drug-

resistant partial epilepsy, *Neurology* (2015).

122. M. E. Lacruz, A. Valentín, J. J. G. Seoane, R. G. Morris, R. P. Selway and G. Alarcón, Single pulse electrical stimulation of the hippocampus is sufficient to impair human episodic memory, *Neuroscience* (2010).

123. S. G. Coleshill, C. D. Binnie, R. G. Morris, G. Alarcón, W. Van Emde Boas, D. N. Velis, A. Simmons, C. E. Polkey, C. W. M. Van Veelen and P. C. Van Rijen, Material-Specific Recognition Memory Deficits Elicited by Unilateral Hippocampal Electrical Stimulation, *J. Neurosci.* (2004).

124. J. Jacobs et al., Direct Electrical Stimulation of the Human Entorhinal Region and Hippocampus Impairs Memory, *Neuron* **92** (2016) 983–990.